LOGISTICAL CONTROL OF IRON ORE STREAMS UNDER GEOLOGICAL AND MARKET UNCERTAINTY

Ghali Zbadi

Department of Mining and Materials Engineering
McGill University, Montreal, Quebec, Canada

A Thesis Submitted to McGill University
In Partial Fulfillment
of the Requirements for the Degree
of Master of Science (M. Sc.) in Mining Engineering (Thesis)

August 2024

COPYRIGHT © 2024 BY GHALI ZBADI

ACKNOWLEDGEMENTS

I am deeply grateful to my supervisor, Prof. Alessandro Navarra, whose exceptional guidance, steadfast support, and thoughtful feedback have been essential throughout my research and the writing of this thesis. His profound expertise and constant encouragement have significantly shaped my ideas and improved my work.

I would also like to extend my sincere thanks to all McGill technical and administrative staff. The resources and facilities provided were instrumental in allowing me to pursue my studies and complete this thesis. The institution's supportive environment made a tremendous difference in my academic journey. I am particularly appreciative of Barbara Hanley and Dr. Mathieu Brochu for their invaluable assistance and organizational skills which made my experience so much smoother.

I would like to share my gratitude to Dr. Maycon Athayde and Dr. Igor Cherubin of Quebec Iron Ore Inc. for their invaluable insights and industry knowledge, which have significantly contributed to the depth and quality of this thesis.

I am thankful to all my fellow members of the Mining System Dynamics Group. Your support and the shared experiences throughout our studies have been invaluable to my personal and academic growth.

To my family and friends, words cannot express how much your understanding, encouragement, and patience have meant to me during this challenging and rewarding time. Your unwavering support has been a beacon of motivation and strength.

Finally, my heartfelt thanks go to McGill University and the Department of Mining and Materials Engineering for the financial backing provided through the McGill International Master's Award and Graduate Excellence Award programs. Additionally, I appreciate the financial support received from Prof. Navarra, funded by the Natural Sciences and Engineering Research Council of Canada (NSERC). I also want to acknowledge the collaborative support from Stream Systems and McGill through the MITACS Accelerate internship program.

ABSTRACT

In recent years, the mining industry has been transformed by the advent of Industry 4.0 technologies, including the Industrial Internet of Things (IIoT) and automation. These advancements have brought significant improvements in efficiency and productivity (Rogers, Kahraman, Drews, Powell, Haight, Wang, Baxla & Sobalkar, 2019), yet mining still faces significant challenges. The iron ore sector continues to exemplify the industry's difficulties, grappling with declining ore grades, stringent environmental regulations, socio-economic issues, and volatile commodity prices. To sustain a competitive advantage throughout the entire value chain, iron mining companies must shift towards multiphase engineering methodologies that simultaneously optimize input and output streams. Within this context, Canadian iron ore producers must adapt their control strategies by establishing alternate operating modes that coordinate system-wide responses to changing feeds and market demand. In line with this imperative, Navarra et al. (2017) introduced a framework rooted in Discrete Rate Simulation (DRS) (a subtype of Discrete Event Simulation (DES)) and inventory theory. This framework has been developed to evaluate blending and stockpiling strategies under alternate modes of operation, aiming to mitigate processing plant feed uncertainty and can leverage simulation-based optimization techniques to enhance the competitiveness of mining operations.

While strategic approaches that align with the increasing adoption of mine-to-mill integration, which aims to optimize both mining and processing operations simultaneously, have become increasingly prevalent (Valery, Duffy, & Jankovic, 2019), there has been little research on modelling processing plant output streams and the interrelation between mill product quality and dynamic market demand. This challenge stems from the difficulty in acquiring representative data to accurately model various conditions, including production outputs, customer specifications, greenhouse gas emission allowances, dynamic spot prices and freight costs. This thesis addresses the necessity for developing decision-making tools tailored to logistical control across the entire iron ore value chain. It introduces an adaptation of Navarra et al.'s (2017) two-mode DRS framework contextualized for a Canadian iron ore operation with heterogeneous plant feed and a mathematical model to optimize iron ore product flows in the global market, by modelling primary ironmaking processes. As such, the proposed approach encompasses

management of stockpiling space and transportation networks in an integrated mine-to-mill-to-market approach. The mathematical model utilizes the tonnage of saleable products acquired from simulating production campaigns as its input. It then optimizes iron ore proportioning and distribution among customers based on diverse objectives, encompassing economic and environmental parameters.

RÉSUMÉ

Au cours de ces dernières années, l'industrie minière a été transformée par l'avènement des technologies de l'industrie 4.0, notamment l’Industrial Internet of Things (IIoT) et l'automatisation. Ces avancées ont permis d'améliorer considérablement l'efficacité et la productivité (Rogers, Kahraman, Drews, Powell, Haight, Wang, Baxla & Sobalkar, 2019), mais l'exploitation minière reste confrontée à d'importants défis. Le secteur du minerai de fer continue d'illustrer les difficultés de l'industrie, aux prises avec des teneurs en minerai en baisse, des réglementations environnementales strictes, des problèmes socio-économiques et la volatilité des prix des matières premières. Pour conserver un avantage concurrentiel tout au long de la chaîne de valeur, les sociétés d'extraction du fer doivent s'orienter vers des méthodologies d'ingénierie à phases multiples qui optimisent simultanément les flux d'entrée et de sortie. Dans ce contexte, les producteurs canadiens de minerai de fer doivent adapter leurs stratégies de contrôle en établissant des modes d'exploitation alternatifs qui coordonnent les réponses de l'ensemble du système à la variabilité des matières premières et de la demande du marché. Conformément à cet impératif, Navarra et al. (2017) ont introduit un cadre ancré dans la simulation des taux discrets (STD) (un sous-type de la simulation des événements discrets (SED)) et la théorie des inventaires. Ce cadre a été développé pour évaluer les stratégies de mélange et de stockage dans le cadre de modes d'exploitation alternatifs, visant à atténuer l'incertitude de l'approvisionnement de l'usine de traitement en minerai, et peut tirer parti des techniques d'optimisation basées sur la simulation pour améliorer la compétitivité des opérations minières.

Alors que les approches stratégiques qui s'alignent sur l'adoption croissante de l'intégration mine-usine, qui vise à optimiser simultanément les opérations d'extraction et de traitement, sont de plus en plus répandues (Valery, Duffy, & Jankovic, 2019), peu de recherches ont été menées sur la modélisation des flux de sortie des usines de traitement et sur l'interrelation entre la qualité des produits de l'usine et la demande dynamique du marché. Ce défi découle de la difficulté d'acquérir des données représentatives pour modéliser avec précision diverses conditions, y compris les sorties de production, les spécifications des clients, les quotas d'émission de gaz à effet de serre, les prix au comptant dynamiques et les coûts de transport. Cette thèse répond à la nécessité de développer des outils de prise de décision adaptés au contrôle logistique tout au long de la

chaîne de valeur du minerai de fer. Elle présente une adaptation du cadre DRS à deux modes de Navarra et al. (2017) contextualisé pour une exploitation canadienne de minerai de fer avec une alimentation hétérogène de l'usine et un modèle mathématique pour optimiser les flux de produits de minerai de fer sur le marché mondial, en modélisant les processus de fabrication de fer primaire. Ainsi, l'approche proposée englobe la gestion de l'espace de stockage et des réseaux de transport dans le cadre d'une approche intégrée de la mine à l'usine et au marché. Le modèle mathématique utilise comme données d'entrée le tonnage de produits vendables obtenu à partir de campagnes de production simulées. Il optimise ensuite le dosage et la distribution du minerai de fer entre les clients sur la base de divers objectifs, englobant des paramètres économiques et environnementaux

CONTRIBUTION OF AUTHORS

This thesis is the sole work of the author, who conceived the research idea, conducted all experiments, analyses, and literature review, and wrote the entire manuscript.

TABLE OF CONTENTS

LIST OF TABLES

LIST OF FIGURES

LIST OF ABBREVIATIONS

BF	Blast Furnace
BFS	Basic Feasible Solution
BOF	Basic Oxygen Furnace
CFR	Contract Of Affreightment
COA	Cost-of-Freight
DES	Digital Twin
DR	Direct Reduced Iron
DRI	Direct Reduction
DRS	Direct Shipping Ore
DSO	Discrete Event Simulation
DT	Discrete Rate Simulation
EAF	Economic Order Quantity
EOQ	Electric Arc Furnace
FOB	Free-On-Board
IIoT	Industrial Internet of Things

KPI	Key Performance Indicator
LP	Linear Programming
MC	Mersenne Twister
MOEA	Monte Carlo
MOLP	Multi-Objective Evolutionary Algorithm
MOOP	Multi-Objective Linear Programming
MT	Multi-Objective Optimization Problem
PO	Pareto Optimal
RQ	Reorder Quantity
SOLP	Single-Objective Linear Programming
VBA	Visual Basic for Applications

CHAPTER 1. INTRODUCTION

1.1 Background

The iron mining industry is intricately linked with the steelmaking sector, as iron ore constitutes the primary input to produce steel. Steelmakers prioritize consistency and reliability in their raw material sourcing. As a differentiated commodity, buyers place a premium on knowing that shipments consistently maintain uniform chemical and physical properties. This assurance of consistency and reliability is crucial for steelmakers to maintain the quality and efficiency of their steel production processes. Suppliers who can consistently deliver iron ore with predictable and standardized characteristics are highly valued, as they enable steelmakers to optimize their operations and produce high-quality steel products consistently. In the context of iron ore production, from the standpoint of an iron ore producer, it becomes crucial to leverage advanced modeling and forecasting tools, such as simulation technology. These tools enable producers to evaluate different control strategies to manage uncertain parameters, such as mill feed compositions, due to the inherently variable nature of mineral deposits, on plant performance. By stabilizing and enhancing plant performance, iron ore producers can maintain consistency and forecast saleable product output in terms of both tonnages and quality. The mill-to-market segment of the mining value chain is the focal point for revenue generation. Therefore, it is crucial for decision-makers in the iron mining industry to comprehend global market dynamics. This enables iron mining companies to ascertain their position relative to competitors in the supply of iron ore to customers. This thesis centers on the introduction of a novel decision-making tool, which leverages simulation and mathematical optimization techniques, specifically designed for the mill-to-market profile of the iron mining industry. In the following section, a brief overview of the global iron ore market, its trends and dynamics, is provided to offer context. Subsequently, the thesis objectives are delineated, along with an outline of the thesis structure.

1.1.1 Introduction to Iron Ore and Steelmaking

Steel emerged as a defining emblem of the second industrial revolution in the twentieth century, standing out more prominently than any other commodity. This alloy, a modified form of cast iron with reduced carbon content, possesses remarkable properties, notably a distinctive combination of hardness and tensile strength (Ghosh, & Chatterjee, 2008). The initial stages of steel manufacturing appeared resistant to the early attempts at mass production. However, a significant transformation took place in the latter part of the nineteenth century, driven by a series of innovative technological and metallurgical developments that opened new avenues for production. These pivotal advancements included the utilization of coking coal in blast furnaces to refine cast iron, the invention of the Bessemer Converter for de-carbonizing it, and the subsequent adoption of the more efficient open-hearth furnace (Chakrabarti, 2006). These collective breakthroughs, along with the more recent developments in direct reduction, have enabled the production of unprecedented volumes of steel, which inevitably led to a corresponding increase in iron mining projects worldwide. Today, steelmakers remain the predominant consumers of iron ore, as it is the primary input in the production of steel and accounts for approximately 98% of the iron mined worldwide (Yellishetty, Ranjith, & Tharumajah, 2010).

Iron is a very abundant mineral. It constitutes over 30% of the Earth's mass, with its elemental distribution ranging from approximately 5% in the Earth's crust to as high as 80% in the planet's core. Magnetite (Fe_3O_4), hematite (Fe_2O_3). and goethite ($FeO(OH)$) stand as the three most prevalent iron ore minerals, collectively constituting over 99% of the iron minerals found in globally traded seaborne iron ores in 2020 (Clout, & Manuel, 2015). Hematite, with its higher in situ iron content, typically requires a simpler beneficiation process, which is less energy-intensive, and less costly, while magnetite, with its lower in situ iron content, typically incurs higher production and beneficiation expenses. Hematite is therefore considered to be a Direct Shipping Ore (DSO) since it can be directly used as an input to the blast furnace process. Nevertheless, the increased beneficiation expenses of magnetite are balanced by the premium price it commands from steel mills due to the high iron content and minimal impurities of magnetite concentrates.

Iron ore minerals are situated within a diverse array of igneous, sedimentary, and metamorphic rock formations. For instance, igneous iron ores can be found in magnetite accumulations within mafic intrusions, or deposits of magmatic-hydrothermal origin. However, the majority of global iron ore production, stems from iron-rich cherty sedimentary rocks and their metamorphic or supergene derivatives, collectively referred to as "iron formations" (Government of Newfoundland & Labrador, 2012). Given the relative abundance of iron, its concentration in a deposit must reach a certain threshold to render mining economically feasible. The first iron deposits that were mined were near-surface geological formations containing hematite ores with grades over 60% known as Direct Shipping Ore (DSO) deposits. With depleting surface reserves, the iron mining industry has shifted towards lower grade projects. Nowadays, grades of around 25% serve as typical cut-off points for determining the viability of an operation. This is particularly relevant to the Canadian context as the Labrador Trough, which constitutes North America's primary iron ore mining district, has seen this gradual shift in the types of deposits mined. While high-grade hematite deposits mined in the early 1960s in the Schaefferville area boasted grades above 60% Fe, newer mines in the Southern through have lower grade ores (25-40% Fe) but produce high grade concentrates with additional beneficiation (Schiller, 2011).

Nowadays, the two most common steelmaking methods are the basic oxygen furnace (BOF) and the electric arc furnace (EAF). In the BOF process, molten iron from a blast furnace is transferred to the furnace vessel where it undergoes oxidation using a high-purity oxygen lance. This removes impurities such as carbon, silicon, and phosphorus, resulting in high-quality steel. The EAF process, on the other hand, relies on electric arcs generated between graphite electrodes and the scrap steel charge to melt and refine the steel. This method is highly flexible and can utilize various raw materials, including recycled scrap steel, direct reduced iron (DRI), and pig iron. Due to the usage of scrap steel in the EAF process, it is considered to have a lower carbon footprint end energy consumption (Ghosh, & Chatterjee, 2008).

1.1.2 Global Iron Ore Market

Figure 1.1.2-1 shows the global share of iron ore production and global imports (adapted from NRC, 2022). In 2022, the global production of iron ore was estimated to be 2,611 million tonnes, representing a slight decline from the 2,681 million tonnes produced in the previous year, 2021.

The global iron ore production is dominated by four countries: Australia, Brazil, India, and China, which collectively contribute 75% of the total output. Among these leading producers, Australia emerged as the dominant player, accounting for 34% of the global iron ore production, underscoring its pivotal role in the global iron ore market (NRC, 2022). The supply side of the iron ore market is dominated by three major Australian producers—FMG, BHP Billiton, and Rio Tinto—along with Brazilian mining giant Vale.

As discussed, most iron ore in the world is extracted in open-pit mines. It is then carried to dedicated ports by rail, and then shipped to steel plants around the world, mainly in Asia and Europe. China stands as the largest importer of iron ore, commanding approximately two-thirds of all global imports. Apart from China, several other countries also play a substantial role in the global iron ore trade. Notable importers include Japan, South Korea, India, Germany, and Switzerland, all of which contribute significantly to the demand for iron ore on the international market.

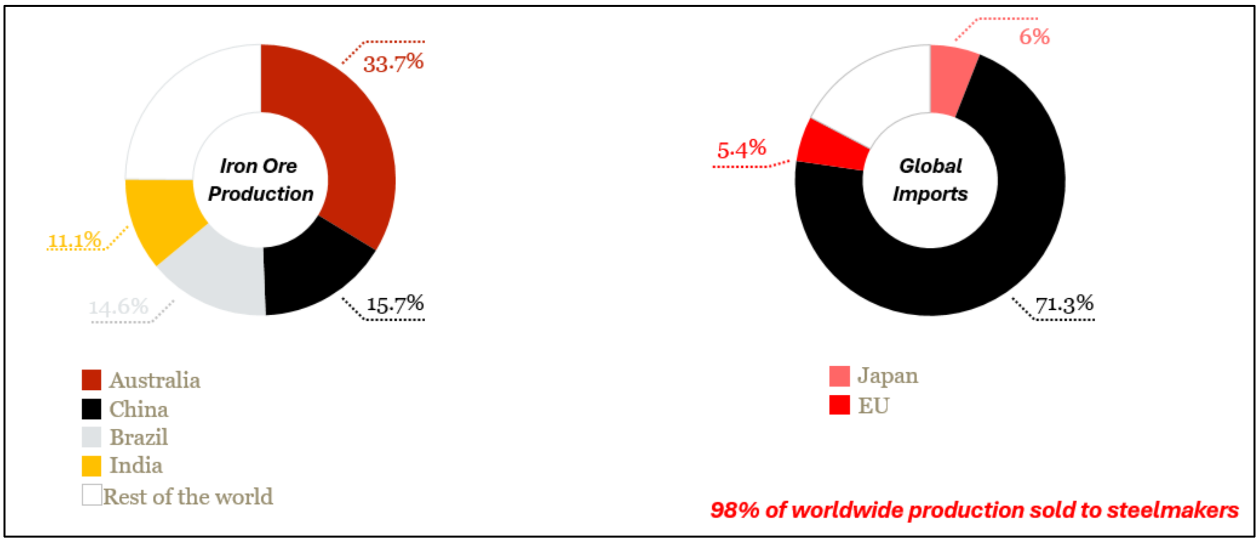

Figure 1.1.2-1 Global Share of Iron Production and Imports (adapted from NRC, 2022)

1.1.3 Iron Saleable Products

As previously discussed, hematite ores typically require less beneficiation than their magnetite counterparts. After crushing and screening, hematite ore is divided into “lump” and fine” fractions. Iron ore fines are responsible for 70% of global iron ore imports. To form a suitable feedstock for subsequent ironmaking, these fines must be agglomerated in a process called sintering, since they tend to smother furnaces during smelting. Sintering involves the application of high temperatures to the fines in the presence of binding fluxes. This process incurs additional costs for steel mills, leading to a premium for lump ore, which requires minimal processing. Magnetite ore, on the other hand, requires additional concentration to increase its commercial grade. Processing magnetite ore involves several steps, including crushing, screening, grinding, magnetic separation, and drying. Magnetite concentrates are pelletized at the processing plant, or directly by the customer, along with pellet-feed fines, to produce high-grade pellets which have ideal furnace properties since they are hard and of regular size and shape, which allows good permeability and gas flow.

1.1.4 Pricing Mechanisms and Market Dynamics

As the primary raw material for steelmaking, the interplay between supply and demand of iron ore is intricately tied to broader economic trends, with periods of robust economic expansion typically driving increased demand for steel and, consequently, iron ore. Conversely, economic downturns often result in reduced demand for steel, impacting the consumption of iron ore. Therefore, fluctuations in global economic conditions serve as a primary determinant of the supply and demand dynamics within the iron ore market. The iron ore market exhibits greater short-term price volatility compared to other commodity markets. This volatility stems from its reliance on spot transactions, which are trades conducted for immediate delivery and payment based on current market prices. In contrast, other markets primarily depend on long-term fixed-price contracts, where prices and delivery terms are agreed upon well in advance, providing stability and predictability. The predominance of spot transactions in the iron ore market leads to frequent price fluctuations, highlighting a key difference from base metal markets with long-term contracts (Jégourel, 2020). Figure 1.1.4-1 depicts short-term iron ore price fluctuations for a 40-day period (Fastmarkets, 2024).

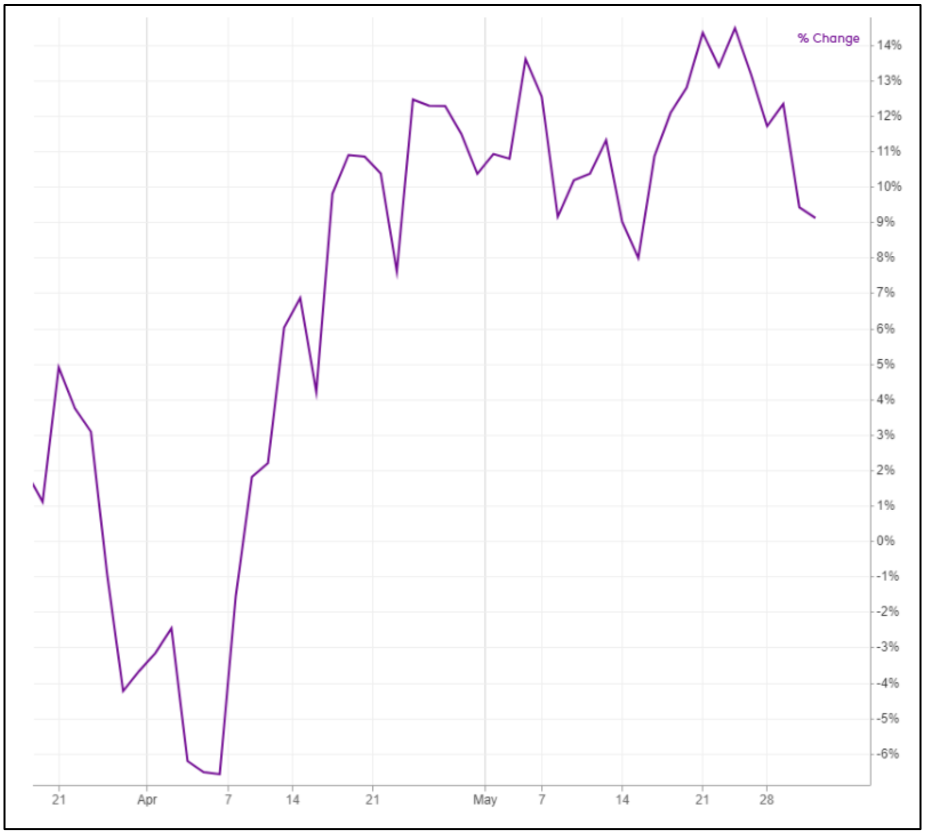

Figure 1.1.4-1 Short-Term Iron Ore Price Fluctuations (Fastmarkets, 2024)

Platts and Fastmarkets publish daily updates for their iron ore indices (P62, MB65), which give a reliable representation of the physical iron spot market price. These indices have strict standards on the grade of iron and weight percentage of deleterious elements and are used to price iron ore products. For example, Platts' P62 index is based on iron ore fines with 62% iron, 2.25% alumina, 4% silica and 0.09% phosphorus. Since a supplier's products rarely match price index specifications, normalizations are applied for iron grade differences. For instance, a cargo with specifications of 58% Fe will be normalized by dividing its price by 58 and then multiplying by 62 for normalization to P62 specifications. For deleterious elements, linear or non-linear value-in-use (VIU) differentials published by Platts and Fastmarkets help in assessing premia or penalties. Iron ore contracts are either on a free-on-board (FOB) or a cost-of-freight (CFR) basis. Under the FOB regime, the buyer is responsible for arranging shipping. The most used pricing basis for iron ore is CFR, where freight cost is included in the pricing. Freight costs adds another dimension of complexity to iron ore pricing, due to their dynamic nature. The Baltic Indices are published daily by the Baltic Exchange and provide standardized benchmark points for negotiating freight rates. The Capesize index is relevant to the iron mining industry since it refers to freight rates of 150,000-ton cargo carriers of iron ore and coal. Table 1.1.4-1 details the most relevant routes for freight cost calculations in the iron ore industry.

Table 1.1.4-1 Capesize Routes

Route	Vessel Size (dwt)	Cargo	Port of Origin	Port of Destination
c_2	160,000	Iron Ore	Tubarao (Brazil)	Rotterdam (Netherlands)
c_3	150,000	Iron Ore	Tubarao (Brazil)	Baoshan/Qingdao (China)
c_5	150,000	Iron Ore	Dampier (Australia)	Baoshan/Qingdao (China)

Iron ore is priced (in \$/t) using the formulas in equations (1.1.4-1) and (1.1.4-2) in a cost-of-freight (CFR) and free-on-board (FOB) basis respectively.

$$Price\ Index + VIU + Premium/Discount = CFR\ Price \qquad (1.1.4-1)$$

$$Price\ Index + VIU + Premium/Discount - Freight = FOB\ Price \qquad (1.1.4-2)$$

The quality of iron ore is a critical determinant of its price, similar to other extractive or renewable resources. However, it is important to note that differentiation strategies based on quality or geographical origin are currently ineffective in the long term. Iron ore, being a commodity, experiences price fluctuations driven by demand shocks, whether positive or negative. These fluctuations affect the market uniformly, with little to no differentiated impact on price based on the quality or origin of the iron ore. This inherent characteristic of commodities underscores the challenge in leveraging quality or origin as a sustainable competitive advantage in the iron ore market.

1.2 Research Objectives

The following key points define the main objective of this thesis.

i. Develop a platform for generic Discrete Rate Simulation (DRS) on Visual Basic for Applications (VBA) with real-time visualizations.
ii. Contextualize the DRS framework with model specific parameters and variables to represent and iron milling operation.
iii. Build a mathematical model for the main metallurgical processes involved in ironmaking using material balances and logistical considerations.
iv. Develop a platform on VBA for automatically setting model constraints based on user input and solving it.
v. Demonstrate the use of the novel decision-making tool in different contexts.

1.3 Thesis Outline

i. Chapter 1 serves as an introduction to the thesis, providing insight into its motivation and offering an overview of the global iron ore market. It delves into the primary producers and customers within the market, elucidates prevailing trends, dynamics, and key market drivers shaping the industry landscape.
ii. Chapter 2 offers an exhaustive literature review encompassing pertinent subjects related to conventional iron and steelmaking processes. It also explores Discrete Event Simulation (DES) applications specifically within the mining industry context. Additionally, this chapter delves into mathematical optimization models representing various decision problems encountered throughout the ironmaking value chain.
iii. Chapter 3 furnishes a comprehensive overview of Discrete Event Simulation (DES) frameworks. Initially, it introduces the fundamental paradigm of Monte Carlo (MC) simulation and elucidates its relevance to the reorder quanity (RQ) problem. Additionally, this chapter investigates the interconnection between the RQ problem and mine-to-mill control strategies for ore blending. Moreover, it delves into the application

of mathematical optimization techniques aimed at enhancing mine-to-mill DES frameworks.

iv. Chapter 4 presents a case study of the integration of a Discrete Rate Simulation (DRS) framework for stabilizing plant performance under heterogeneous and variable feeds with a mathematical optimization model for saleable product sales on the global iron market. The flexibility of the mathematical model is showcased through different examples involving competing objectives.

v. Chapter 5 summarizes the thesis findings and outlines potential directions for future work.

CHAPTER 2. LITERATURE REVIEW

This chapter presents a literature review of relevant topics pertaining to conventional iron and steelmaking processes, Discrete Event Simulation (DES) applications in the mining industry and mathematical optimization models representing different decision problems in the ironmaking value chain. The review is organized as follows:

i. Section 2.1 delves into traditional ironmaking processes, including the Blast Furnace (BF) and Direct Reduction (DR), providing a brief historical overview, outlining their inputs and outputs, and discussing the chemical reactions involved. Following this, the section continues with a discussion on steelmaking, encompassing the Basic Oxygen Furnace (BOF) and the Electric Arc Furnace (EAF), and addressing the environmental impact of these processes.

ii. Section 2.2 covers pertinent literature concerning the utilization of Discrete Event Simulation (DES) frameworks within mining contexts. It examines the development of Digital Twin (DT) technology through DES, in the context of Industry 4.0 advancements. The concept of alternate modes of operation, which coordinate system-wide responses to variability, is introduced and contextualized within DES frameworks.

iii. Section 2.3 presents previous endeavors in applying mathematical optimization techniques within the ironmaking industry with a focus on sintering plants, blast furnaces and integrated DRI-BF steel plants.

2.1 Iron and Steel Metallurgical Routes

2.1.1 Ironmaking

Ironmaking represents the first step to obtain steelmaking raw materials. Traditionally, hot metal generated from blast furnaces and steel scrap constituted the primary feed materials for steelmaking, with a typical composition ratio of 75% hot metal to 25% scrap (Yang, Raipala, & Holappa, 2014). The BF process has continually evolved, maintaining its relative low cost and dominance as the main iron generator, as it nowadays accounts for over 91% of the total global iron production from ores (World Steel Association, 2023). The iron and steel industry stands as one of the most energy-intensive in the world and holds the title of the largest coal consumer in the industrial sector (Energy Information Administration, 2016), due to the widespread use of metallurgical coke in blast furnaces. Recent trends in the ironmaking industry show a gradual shift from coal-fired furnaces to electric arc furnaces (EAFs) amidst growing environmental concerns. Furthermore, constraints on coking coal availability and the inflexibility of blast furnace operations, necessitating coking and sintering plants, have spurred the pursuit of alternative ironmaking processes, notably gas-based Direct Reduction (DR) (Ramakgala & Danha, 2019).

2.1.1.1 Blast Furnace (BF)

The principal objective of the iron blast furnace is the smelting of iron-bearing raw materials to yield a liquid crude iron. Upon liquefaction, this crude iron is referred to as hot metal, while upon solidification it is referred to as pig iron (Isnugroho & Birawidha, 2018). In addition to iron ores and agglomerates, the BF charge typically includes metallurgical coke as a reducing agent and heat source, although alternatives such as fuel oil, conventional oil, coal tar (Pustejovska, Jursova, Brozova & Sousek, 2013) and pulverized coal (Shen, Yu, Austin & Zulli, 2012) have also been used in the industry, and limestone and dolomite as fluxing agents.

The blast furnace is a continuously operating shaft furnace that functions as a closed counter-current reactor and heat exchanger (Yongyi, Hegui, Keng, Jianliang & Kuangdi, 2023). The burden is loaded through top charging equipment in alternating layers and descends the furnace under the influence of gravity. Simultaneously, preheated air is blown into the furnace from the tuyeres via bustle pipes and air feeders, initiating a reaction with coke within the burden, resulting in the generation of carbon monoxide (Make, Bo & Kuangdi, 2023). This gas ascends within the furnace and reduces the iron oxides contained in the burden. Irreducible impurities in the iron ore (CaO, SiO_2, Al_2O_3, MnO, MgO…) combine with fluxes to form slag. Eventually, the iron and slag, are periodically discharged from the notches at the furnace's base. Top gas and flue dust are also generated during the BF process (Yang et al., 2014). Figure 2.1.1.1-1 depicts the inputs and outputs of the BF process.

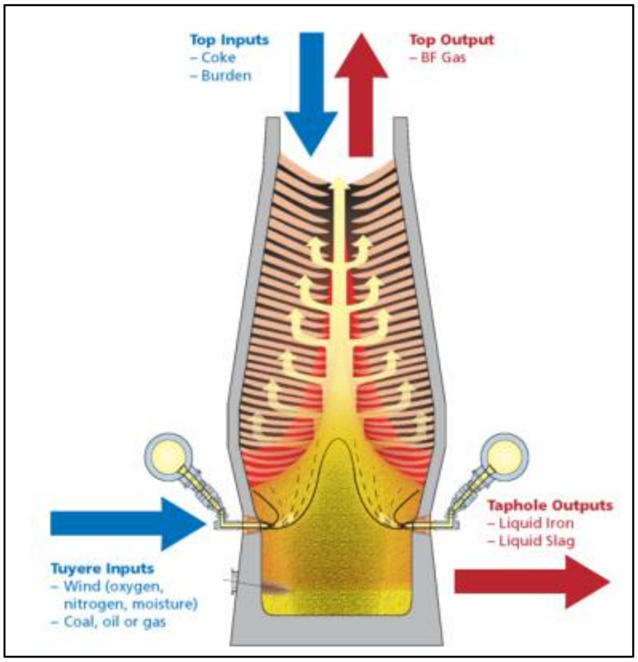

Figure 2.1.1.1-1 Inputs and Outputs of the BF Process (Geerdes, Chaigneau & Lingiardi, 2020)

The temperature profile and chemical reactions within a blast furnace are intricately interconnected. The ironmaking process within the furnace is characterized by heat and mass transfer, resulting in distinct zones delineated by the physical and chemical states of the feed materials and temperature (Kumar, Agrawal, Kumar & Kumar, 2023). The ferrous burden is charged mainly as hematite (Fe_2O_3) and magnetite (Fe_3O_4). The oxides are reduced to wustite (FeO) by reacting with carbon monoxide (CO) at temperatures between 600 and 900 °C. The wustite is further indirectly reduced by carbon monoxide as a gas-solid reaction at temperatures between 900 to 1100 °C. The carbon dioxide (CO_2) generated from the latter reduction undergoes the Boudouard reaction with coke (carbon), resulting in the production of carbon monoxide

(Geerdes et al., 2020). Figure 2.1.1.1-2 illustrates the chemical reactions and the temperature profile in a blast furnace (da Silva Guimarães, Borges & Arbex, 2020).

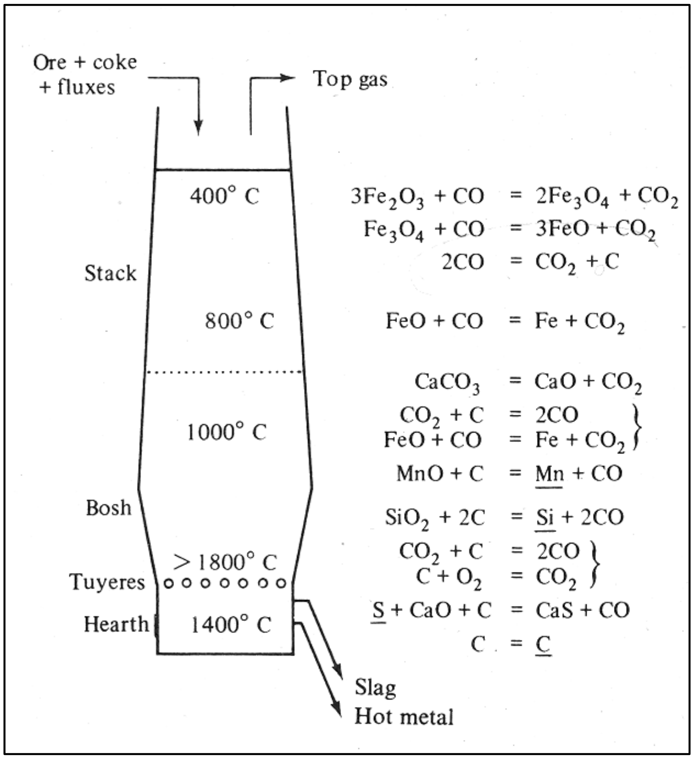

Figure 2.1.1.1-2 Blast Furnace Chemical Reactions and Temperature Profile (da Silva Guimarães et al., 2020)

Hot metal generated from blast furnaces typically contains approximately 94.5% iron (Fe), complemented by around 4.5% carbon (C), 0.4–0.6% silicon and 0.05–0.13% phosphorus, contingent upon the chemical composition of the burden materials. The rest of the hot metal is constituted of sulfur, manganese, and titanium among other diverse elements.

Concerning slag, its predominant components, comprising approximately 96% of its volume, encompass Al_2O_3 (8–20%), MgO (6–12%), SiO_2 (28–38%), and CaO (34–42%) (Geerdes et al., 2020).

2.1.1.2 Direct Reduction (DR)

The blast furnace (BF) process is termed an indirect reduction method for iron production owing to its multi-step reaction sequence. This contrasts with direct reduction (DR), which is defined as the direct conversion of iron ore to metallic iron in the solid-state, in a single step (Battle, Srivastava, Kopfle, Hunter, & McClelland, 2024). The early 20th century saw the beginnings of developments in iron direct reduction technology, culminating in significant advancements with the introduction of the HYL® Process in Mexico during the 1950s. This momentum continued to grow with the global adoption of the MIDREX® Process in the 1970s (Lüngen, & Schmöle, 2022).

Direct Reduction processes predominantly use iron ore pellets with occasional additions of lump ore (Muwanguzi, Wy, Karasev, Byaruhanga, & Jönsson, 2013). In DR, the typical reductants that convert iron oxides to metallic iron are carbon or hydrogen. Unlike in conventional blast furnace technology, these reductants function at lower temperatures and facilitate solid-solid or solid-gas reactions. As none of the components are melted, slag formation does not occur, leading to impurities being transported with the Direct Reduced Iron (DRI) to the steelmaking furnace (Battle et al, 2024). As such, the iron ore load needs to be highly processed to remove impurities to a greater extent, before being fed to the DRI furnace.

DRI presents a range of technology options, including both coal-based and gas-based processes. Gas-based direct reduction remains the primary method, while coal-based technologies have gained commercial traction, notably in India (Nduagu, Yadav, Bhardwaj, Elango, Biswas, Banerjee, & Rajagopalan, 2022). The most widely used feedstock for producing reducing gas in Direct Reduction processes is natural gas. Conventional natural gas-based direct reduction using the MIDREX® Process occurs within a shaft furnace, as illustrated in Figure 2.1.1.2-1 (Béchara, Hamadeh, Mirgaux, & Patisson, 2018). Natural gas undergoes reforming to produce carbon monoxide (CO) and hydrogen (H_2), with methane being the primary source of both CO and H_2. Reducing gas is introduced into the shaft and ascends against the flow of the iron ore. The discharged top gas undergoes purification, with a majority directed to the reformer along with natural gas to produce additional reducing gas. The Direct Reduced Iron (DRI) obtained from the process typically comprises 90–94% Fe, 2–2.5% C, 1–8% SiO2, 0.3–0.7% Al2O3, 0.8–1.4% CaO, alongside trace amounts of other minor elements (Battle et al., 2024). Since natural gas-based DR processes eliminate the need for metallurgical coke and operate at much lower temperatures than blast furnaces, DRI represents an improvement in energy consumption and emissions (Sohn, 2019).

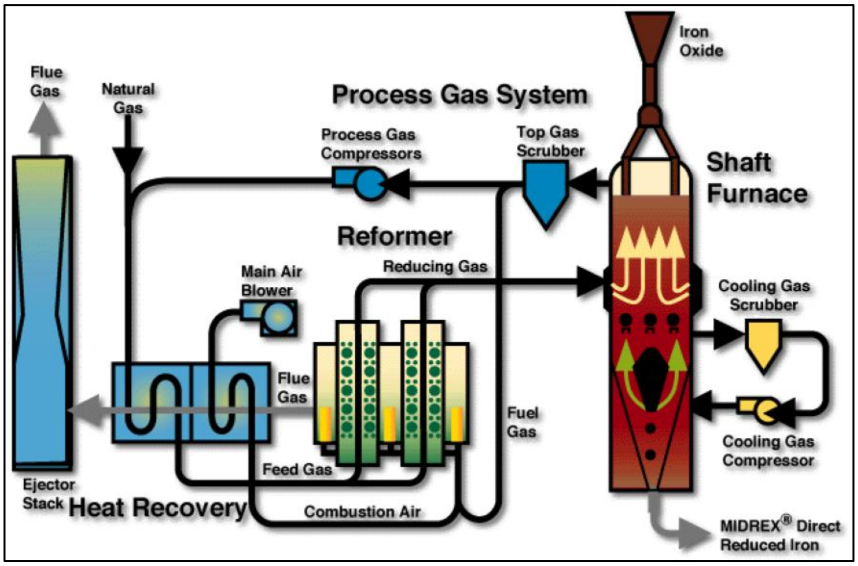

Figure 2.1.1.2-1 MIDREX® Process (Béchara et al., 2018)

2.1.2 Steelmaking

Steelmaking involves the production of steel from iron ore and/or scrap. During this process, impurities including nitrogen, silicon, phosphorus, sulfur, and excess carbon are eliminated from the hot metal and Direct Reduced Iron (DRI). Presently, two major steelmaking processes dominate the industry landscape. The more prevalent method is the Basic Oxygen Furnace (BOF), which relies on hot metal from blast furnaces and scrap. It accounts for 70% of worldwide steel production (World Steel Association, 2023). Conversely, the electric arc process, while less common, is well-suited for producing steel from high-quality industrial scrap or DRI (Williams, 1983).

2.1.2.1 Basic Oxygen Furnace (BOF)

The Basic Oxygen Furnace (BOF) is a pivotal technology in modern steelmaking, introduced in the 1950s to replace the open-hearth process (Ghosh, & Chatterjee, 2008). In the BOF process, pure oxygen is blown through a top lance onto the molten pig iron and steel scrap. This results in a carbon monoxide-rich gas phase, alongside a metal phase and a slag phase containing impurities such as carbon, silicon, phosphorus, and manganese. Fluxes are added for optimal operating conditions, such as limestone for slag formation and iron monosilicide for temperature control (De Vos, Bellemans, Vercruyssen, & Verbeken, 2019). Figure 2.1.2.1-1 shows a schematic representation of the BOF process (Yildirim, & Prezzi, 2011).

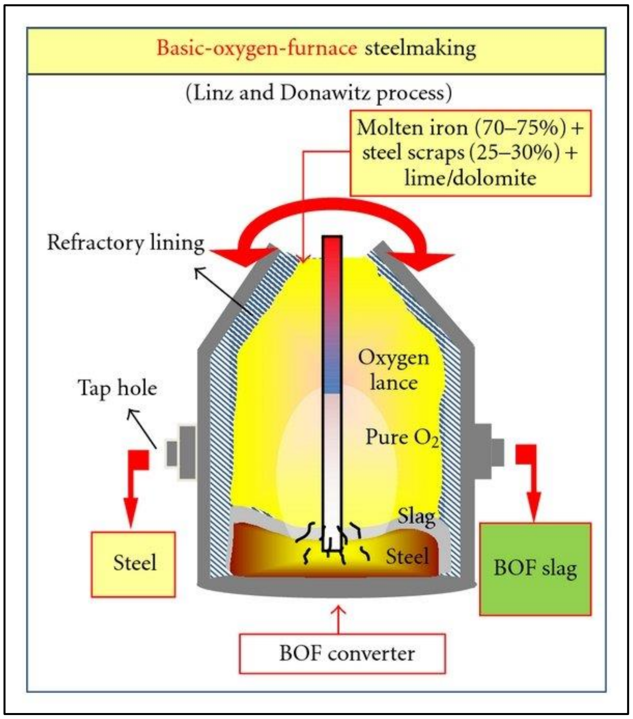

Figure 2.1.2.1-1 Schematic Representation of the BOF Process (Yildirim et al., 2011)

Despite its efficiency and cost-effectiveness, the BOF process significantly impacts the environment, primarily through CO_2 emissions (Madhavan, Brooks, Rhamdhani, & Bordignon, 2022). Efforts to mitigate these impacts focus on carbon capture and storage, as well as recycling carbon-rich waste materials to replace fossil fuels in the steelmaking process (Qian, Li, Hao, Yu, & Hu, 2024).

2.1.2.2 Electric Arc Furnace (EAF)

Introduced in the late 19th century, the Electric Arc Furnace (EAF) process involves generating high temperatures through electric arcs between graphite electrodes and the metal charge, which primarily consists of scrap steel. The EAF process can also accommodate direct reduced iron (DRI) as an input. During the operation, the electric arcs melt the charge, creating a molten metal bath and a slag phase that absorbs impurities such as sulfur and phosphorus. The primary outputs are steel and slag. The EAF process is environmentally advantageous compared to the Basic Oxygen Furnace (BOF) due to its lower CO_2 emissions, primarily because it relies heavily on recycled scrap metal rather than raw materials derived from iron ore. A standard EAF design is shown on Figure 2.1.2.2-1 (Madias, 2024).

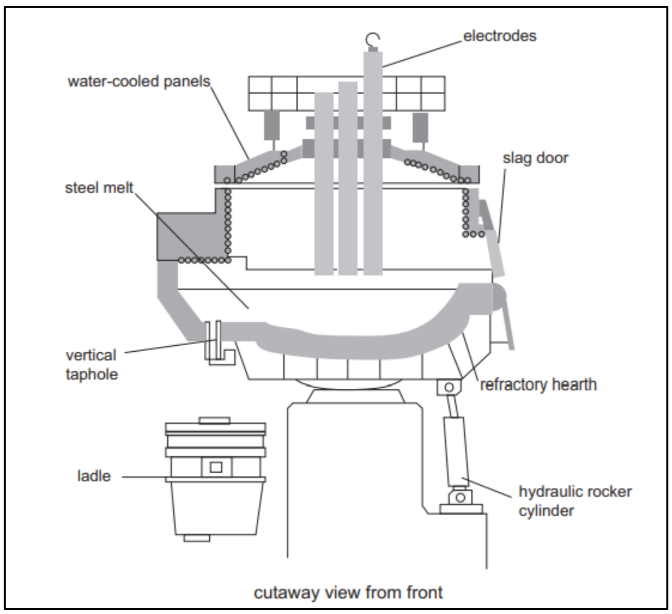

Figure 2.1.2.2-1 Standard EAF Design (Madias, 2024)

2.2 DES Frameworks and Applications in Mining Projects

In the last decades, the “intelligent” networking of machines and processes spearheaded by advancements in digital and information technologies have led to the emergence of network-based, self-regulating systems known as Industry 4.0 (Ivanov, Dolgui, Das, & Sokolov, 2019). These improvements are revolutionizing the competitive landscape and fostering the development of versatile "intelligent" enterprises that leverage simulation during the development, deployment, and execution of their strategies to gain a competitive edge (Agalianos, Ponis, Aretoulaki, Plakas, & Efthymiou, 2020). Discrete Event Simulation (DES) models the real world quantitatively, simulating dynamics on an event-by-event basis and interactions between critical process parameters in response to random variations (Eduard, & Ming, 2010). As a form of Monte Carlo simulation, DES effectively captures the stochastic nature of real-world processes (Lawson, & Leemis, 2008), which is of particular interest to the mining industry due to the natural variability of orebodies.

Discrete Event Simulation (DES) frameworks have found various applications in the mining industry. Salama et al. (2014) use DES to compare two different haulage units using production targets as Key Performance Indicators (KPIs). Tabesh et al. (2011) simulate a continuous iron ore milling process using a DES framework with batching for one hour’s worth of feed material to evaluate the quality of the output concentrate and the operational bottlenecks caused by machine failure interactions. Runciman et al. (1999) employ DES to evaluate underground development mining systems in terms of advance footage obtained over a 30-day period.

2.2.1 Digital Twins via Discrete Event Simulation

In the recent years, digital twins have emerged as powerful computational intelligence tools that simulate the comprehensive physical and functional aspects of integrated processes or systems (Wilson, Mercier, Patarachao, & Navarra, 2021). Leveraging the most advanced and up to date information models, digital twins quantify causal relationships between key variables and parameters and aim to mimic the operational life of a system. Recent technological advancements, particularly in connectivity, data storage, and the Industrial Internet of Things (IIoT), have further expanded the utility of digital twins and enabled closed-loop analytics (Eyring, Hoyt, Tenny, Domike, & Hovanski, 2022). Digital Twin technology when coupled with DES is particularly effective for designing and testing alternative operational policies and evaluating trade-offs throughout all lifecycle phases of engineering projects (Wilson et al., 2021).

In the mining industry, DES-based Digital Twins have been developed to optimize equipment maintenance (Savolainen, & Urbani, 2021) and to mitigate operational risk factors, such as ore stockouts, in the extractive processing of bitumen deposits (Wilson et al, 2021).

2.2.2 *Alternate Modes of Operation*

The particularity of mining is the uncertainty on the supply side due to geological variability. This may be managed by alternating between operational modes (Navarra, Alvarez, Rojas, Menzies, Pax & Waters, 2019). Operational modes in complex systems are defined based on system-wide metrics rather than local metrics that only pertain to isolated unit operations and are characterized by separate operational policies (Wilson et al., 2021). The operational decision to switch between modes is triggered by the crossing of a critical threshold (Navarra, Grammatikopoulos, & Waters, 2018).

There have been extensive studies on the application of the two-mode mining system model using DES for the mitigation of ore stockouts for heterogenous mill feeds. Wilson et al. (2021) integrate a predictive Partial Least Squares (PLS) regression model into a DES Digital Twin of a bitumen processing plant accepting low fine and high fine ore, to stabilize feed balances and evaluate stockout risk. Saldaña et al. (2019) optimize the mineral recovery of a copper heap leaching plant accepting oxides and sulfides through alternating modes of operation. Wilson et al. (2021b) balance stockpile levels against cement production rates for a tailings deposit, constituted of 2 types of ore and waste, undergoing secondary mining.

2.3 Optimization Models in the Ironmaking Industry

Optimization models offer a robust mathematical foundation for rigorous decision-making in engineering projects. In the mining and mineral processing industry, these models have been developed and applied to various critical areas. For instance, they are used in production scheduling (Dimitrakopoulos & Ramazan, 2008), optimizing cut-off grade policies (Khan & Asad, 2020), fleet selection (Santelices, Pascual, Lüer-Villagra, Mac Cawley, & Galar, 2017), and optimizing the profit generated by a lead-zinc concentrator (Navarra, Rafiei, & Waters, 2017).

Building on the successful application of Operations Research (OR) methods in mining and mineral processing, the ironmaking industry also leverages these models to optimize its complex and interconnected unit operations, such as sintering, pelletizing, coke preparation and various other processes. Liu et al. (2016) employ a linear program to optimize sinter proportioning, aiming to minimize energy consumption. Through their analysis, they find that Carajas and Chengchao ore, along with limestone, exert the most significant influence on energy consumption. Dai (2021) uses Chicken Swarm Optimization-Genetic Algorithm (CSO-GA), which is a biologically inspired meta-heuristic, to optimize the batching process of a sintering operation with the objective to minimize costs and sulfur emissions. Fabian (1967) expresses the blast furnace production process in terms of a material mass balance with thermochemical metallurgical constraints. The model can obtain a minimum cost selection of input materials. Huiti et al. (2013) evaluate the replacement of BF grade pellets with DRI using simplified mathematical models of the different operations in an integrated steel plant. The authors develop a non-linear optimization model to minimize steel production costs and find that DRI could replace BF grade pellets if the former is produced with a renewable reductant.

CHAPTER 3. FOUNDATIONS

Variability is a fundamental characteristic of mining systems, influencing every aspect of geological structures, features, and processes. Geological heterogeneity is governed by lithological boundaries, alteration zones, and the spatial distribution of grades, among other critical attributes. As a result, this variability can cause fluctuations in the quality of feed to mineral processing plants, posing a significant challenge for maintaining optimal operations, since the efficiency of a processing plant relies heavily on the consistency of its feed (Navara et al., 2019). This precaution is especially crucial when expanding mining projects into new geological domains, where there's the potential for encountering slightly or drastically different ore types. Such variations may necessitate a more sophisticated processing plant, a need that can be addressed by incorporating additional modes of operation. Indeed, feed variability is managed through blending practices, with different modes of operation imposing specific proportions of various ores to manage stockouts. This strategic approach is akin to inventory management issues in other industries, such as the reorder quantity (RQ) problem. The anticipation of variations in stockpile levels and the coordinated response of the integrated mining and mineral processing system to geological variations provide an excellent context for simulation.

This chapter provides an overview of Discrete Event Simulation (DES) frameworks by first introducing the overarching paradigm of Monte Carlo (MC) simulation and explores the connection between the RQ problem and mine-to-mill control strategies for ore blending. Furthermore, it delves into mathematical optimization techniques that can enhance mine-to-mill DES frameworks. This research exemplifies such augmentation by integrating mill-to-market operations through mathematical programming representations of global commodity markets by accounting for raw material blending and logistical factors.

3.1 Discrete Event Simulation

3.1.1 The Monte Carlo Paradigm

The Monte Carlo (MC) Paradigm is a class of simulation techniques that rely on repeated random sampling of probability distributions to model and analyze the behavior of complex systems and processes. Interactions in a system can be quantified through mathematical models that have a set of input parameters being fed to mathematical functions to produce outputs. The uncertainty in input parameters necessitates shifting from deterministic models to approaches that quantify risk based on these parameters, which is the main motivation of MC methods. While best-case and worst-case scenarios of a classic what-if analysis can aid in assessing the risk of a model relative to its input parameters, they come with significant disadvantages. These include the improbability of all input variables reaching their best or worst outcomes simultaneously, the challenge of accurately determining these extreme cases, and the computational expense involved in storing the results of numerous experiments (Raychaudhuri, 2008). Conversely, Monte Carlo simulation enables decision-makers to systematically explore the full spectrum of risk associated with each uncertain input variable. In Monte Carlo simulation, each input parameter to a model is either given a deterministic value, or it is assigned a statistical distribution. For each uncertain input variable, random samples are drawn from these distributions to assign values to the input variables. For each set of input parameters, a corresponding set of output parameters is obtained, each representing a specific outcome scenario of the simulation run. Multiple simulation runs generate numerous output values. Statistical analysis can then be performed on these output values and risk profiles can be graphed to inform decision-making processes. Figure 3.1.1-1 (Chen, Molina-Cristóbal, Guenov, Datta, & Riaz, 2019) illustrates the general framework of simulation techniques pertaining to the Monte Carlo Paradigm. The next sections dive into the different steps of MC simulation methods.

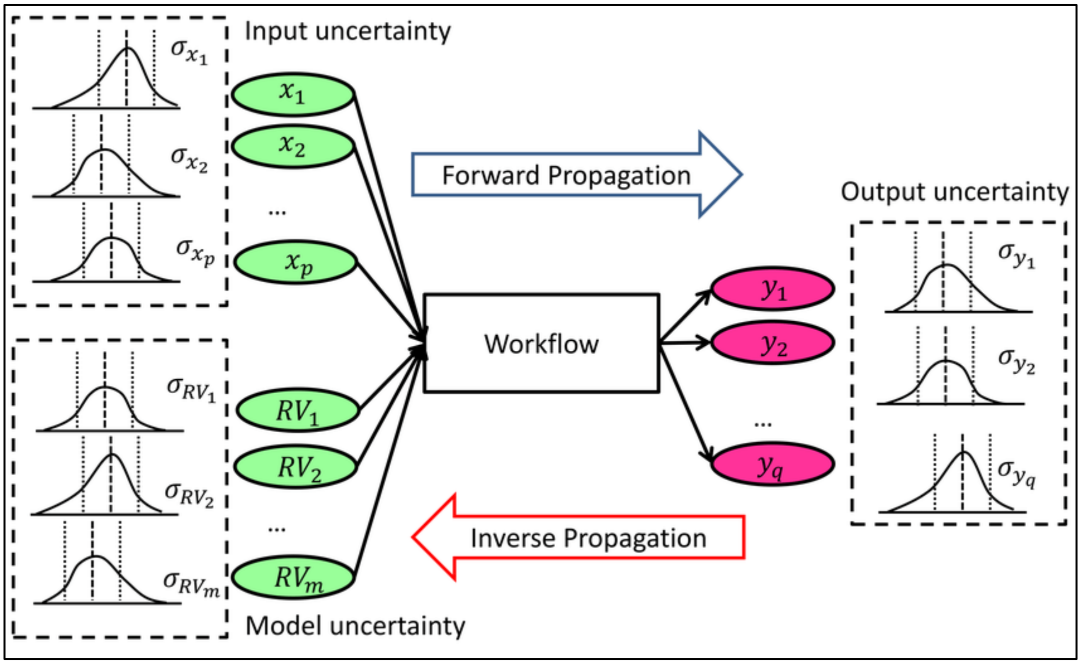

Figure 3.1.1-1 Uncertainty Propagation, the Idea Behind MC Simulation (Chen et al., 2019)

3.1.1.1 Identifying Underlying Distributions

Input parameters can be subject to uncertainty for various reasons. The principle behind identifying an underlying distribution for a stochastic parameter is to use historical data and fit a probability distribution with numerical methods. The fundamental property of probability distributions is that it can be uniquely identified using its parameters. As such, the fitting procedure is a matter of find the parameters of a probability distribution. Multiple methods for distribution fitting have been identified in the literature (Hašek, & Schenk, 1991). Among these, Maximum Likelihood Estimation (MLE) is the most popular. In MLE, given a dataset of observed values, the task is to infer the parameters of the underlying distribution by assuming that all observed data is independent and identically distributed. The likelihood of obtaining a sample $x_1, \ldots x_n$ from a probability density (or mass, for a discrete distribution) function f with parameter vector $\boldsymbol{\theta}$, is

$$\mathcal{L}(\boldsymbol{\theta}) = f_{\boldsymbol{\theta}}(x_1, \ldots x_n | \boldsymbol{\theta}) \qquad (3.1.1.1 - 1)$$

Given the independence of the observations, equation (3.1.1.1-1) can be rewritten as

$$\mathcal{L}(\boldsymbol{\theta}) = \prod_{i=1}^{n} f_{\boldsymbol{\theta}}(x_i|\boldsymbol{\theta}) \qquad (3.1.1.1-2)$$

To conveniently optimize equation $(3.1.1.1-2)$, it is first transformed to a linear sum by taking the logarithm. The log-likelihood function $\mathcal{L}\mathcal{L}(\boldsymbol{\theta})$ is

$$\mathcal{L}\mathcal{L}(\boldsymbol{\theta}) = \sum_{i=1}^{n} \ln f_{\boldsymbol{\theta}}(x_i|\boldsymbol{\theta}) \qquad (3.1.1.1-3)$$

By maximizing equation $(3.1.1.1-3)$, the underlying probability density (mass) function can be found.

3.1.1.2 Random Number Generation

After identifying the underlying distributions, one must sample them to generate values for the stochastic parameters. Generating random numbers for use in simulations is a well-studied area, with numerous methods discussed in the literature (L'Ecuyer, 2012). The most common method involves using Pseudorandom Number Generators (PRNGs) to produce uniformly distributed numbers, which can then be transformed into the desired distribution through a function that maps the uniform distribution to the target distribution. Most PRNGs involve recurrence relations and modular arithmetic to generate a sequence of numbers. This sequence is not truly random since it depends on its initial value, called the seed value.

The present work makes use of Excel's RAND function to generate uniformly distributed numbers. Excel's built-in PRNG is based on the Mersenne Twister (MT) algorithm (Matsumoto, & Nishimura, 1998). The MT algorithm generates word vectors, which are w-dimensional row vectors in $\mathbb{Z}/2\mathbb{Z} = \{0,1\}$ for machine word size w. The algorithm revolves around the following linear recurrence

$$\boldsymbol{x}_{k+n} \coloneqq \boldsymbol{x}_{k+m} \oplus \left(\boldsymbol{x}_k^u \middle| \boldsymbol{x}_{k+1}^l\right)\boldsymbol{A} \qquad (3.1.1.2-1)$$

$$1 \leq m < n, \qquad k = 0,1,\ldots$$

where $\boldsymbol{x}_{k+n}$ and $\boldsymbol{x}_{k+m}$ are word vectors, n is the degree of recurrence, $\boldsymbol{x}_k^u$ is the upper $w-r$ bits of $\boldsymbol{x}_k$ and $\boldsymbol{x}_{k+1}^l$ the lower r bits of $\boldsymbol{x}_{k+1}$ for a number r such that $0 \leq r < w-1$ and $\boldsymbol{A}$ is $w \times w$ constant matrix with entries in $\mathbb{Z}/2\mathbb{Z}$. Here $\oplus$ is the XOR operator (bitwise addition modulo two), and $\left(\boldsymbol{x}_k^u \middle| \boldsymbol{x}_{k+1}^l\right)$ refers to a concatenation of bit vectors. During initialization ($k=0$), word vectors $\boldsymbol{x}_0, \boldsymbol{x}_1, \dots, \boldsymbol{x}_{n-1}$ are given as seeds and $\boldsymbol{x}_n$ is generated by the algorithm. The MT algorithm generates values in the range $(0, 2^w - 1)$. To obtain uniformly distributed numbers in $(0,1)$, the numbers are divided by $2^w - 1$.

After generating uniformly distributed random numbers, inverse transform sampling is performed to obtain random numbers that follow the distribution of choice. On Excel, this is done using the F.INV function where F is a placeholder for the cumulative distribution function that needs to be inverted.

3.1.1.3 Output Analysis

Monte Carlo simulations are run multiple times, with each iteration representing a different equiprobable scenario. The collection of outputs approximates the distribution of possible system behaviors (Órdenes, Toro, Quelopana, & Navarra, 2022). The set of outputs can be analyzed with various statistical measures such as the mean, median, standard deviation, variance, skewness, kurtosis and percentiles (Raychaudhuri, 2008), and overall system performance can be assessed using so-called Key Performance Indicators (KPI).

3.1.2 Discrete Event/Rate Simulation (DES/DRS)

Discrete Event Simulation (DES) is a computer-based method for simulating dynamic systems that experience changes at discrete points in time. DES considers discrete time steps $T_1 < T_2 < T_3 < \cdots$ with the assumption that the system state does not change or follows a deterministic path between time steps T_i and T_{i+1}. At each discrete time step T_i, an event triggers a system state change. DES is part of the Monte Carlo Paradigm, as it leverages random sampling and statistical modelling to introduce variability and quantify uncertainty in the simulation outcomes, by using RNG to determine the time between events, but also the value of stochastic variables.

Due to the static system assumption of DES, it is unable to capture continuous dynamics with a great accuracy. Indeed, when modelling a continuous system with discrete events, a batch size must be chosen to represent material flow as a single item, therefore dividing the flow into single entities. Although continuous simulation addresses the need to batch material flow, inadequate timesteps can lead to significant precision errors since state change events can occur between timesteps. Discrete Rate Simulation (DRS) has been developed to tackle these challenges. DRS is a subtype of DES which combines the discrete event-based timing of classic DES models with continuous dynamics to calculate material flow over a system. In DRS, events are scheduled and stored in a list so that the system knows when to calculate a new set of rates and determines the appropriate flow for each modelled stream. These events are defined as threshold crossing events. The system state is parametrized by piece-wise continuous variables in the form of level-rate pairs (L_i, r_i) where $i = 1, \dots, n$ is the index of the i-th continuous state variable. At each discrete time step T_i, levels are updated as follows

$$L_i \coloneqq L_i + (T_i - T_{i-1})r_i \qquad (3.1.2 - 1)$$

whereas rates r_i are updated with model-specific formulas.

Figure 3.1.2-1 (Damiron, & Krahl, 2014) shows a comparison of the simulation of a tank filling and emptying at different rates with DES, DRS and continuous simulation. DES and continuous simulation suffer from characteristic imprecisions at capturing the “full” and “empty” thresholds due to the batching process and an inadequate timestep respectively, while DRS does not breach those thresholds.

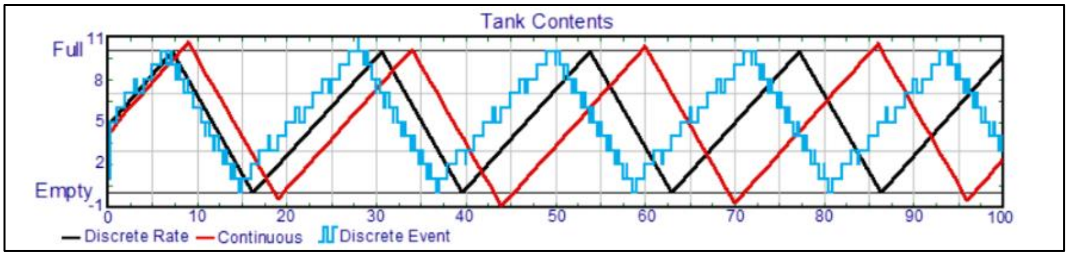

Figure 3.1.2-1 Comparison of Discrete Rate, Discrete Event and Continuous Simulation (Damiron, & Krahl, 2014)

3.1.3 The RQ Model in Inventory Theory

Inventory management is crucial for companies to meet customer demand promptly. To achieve this, they often maintain stock that is ready for sale, or further processing. In the mining industry, for instance, blended ore stockpiles serve as mill feeders to ensure a constant supply and act as buffers during mine shutdowns (Jupp, Howard, & Everett, 2013). Inventory Theory provides a framework for determining the rules that management can follow to minimize the costs associated with maintaining inventory while satisfying customer demand.

The Economic Order Quantity (EOQ) model is a fundamental concept within Inventory Theory. It aims to identify the optimal order size Q and timing, represented by the crossing of the inventory level corresponding to the reorder point R, to avoid stockouts. Since resupplies are not instantaneous, the period between placing a reorder and the arrival of order quantity Q is known as the lead time L. The EOQ model is deterministic, hence it assumes constant demand Q, constant consumption rate r and lead time L, as well as repetitive ordering (Winstin & Goldberg, 2004). The optimal value of R is determined using equation (3.1.3-1)

$$R = rL \qquad (3.1.3-1)$$

Figure 3.1.3-1 shows the optimal reorder point R for a deterministic EOQ model.

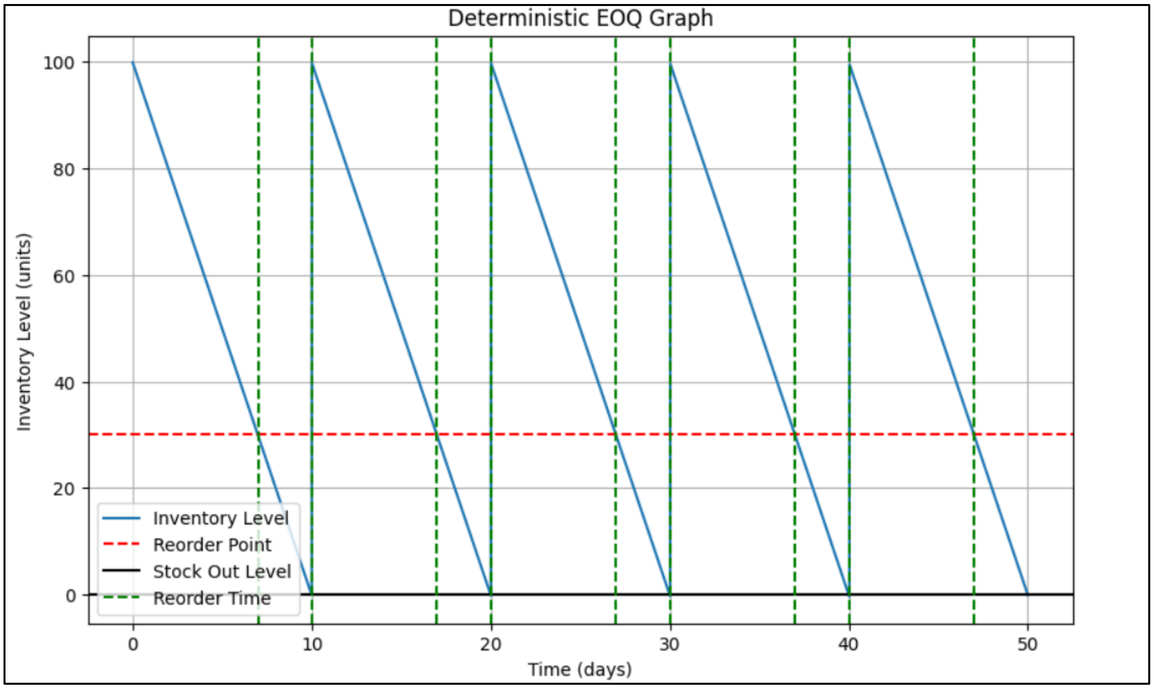

Figure 3.1.1.3-1 Optimal Reorder Point for a Deterministic EOQ Model

In various industries, demand fluctuations can occur due to seasonality, leading to an irregular demand pattern. In the mining industry, mill feeds are relatively constant, while uncertainty is usually encountered at the level of ore supply to stockpiles, due to geological variability (Navarra et al, 2019), which affects consumption rates. This irregularity means that the constant demand and consumption rate assumptions, essential for the effectiveness of EOQ models, cannot be applied, necessitating alternative approaches to inventory management. Figure 3.1.3-2 illustrates the ineffective translation of a deterministically optimized reorder point *R* in a stochastic demand scenario, causing stockouts.

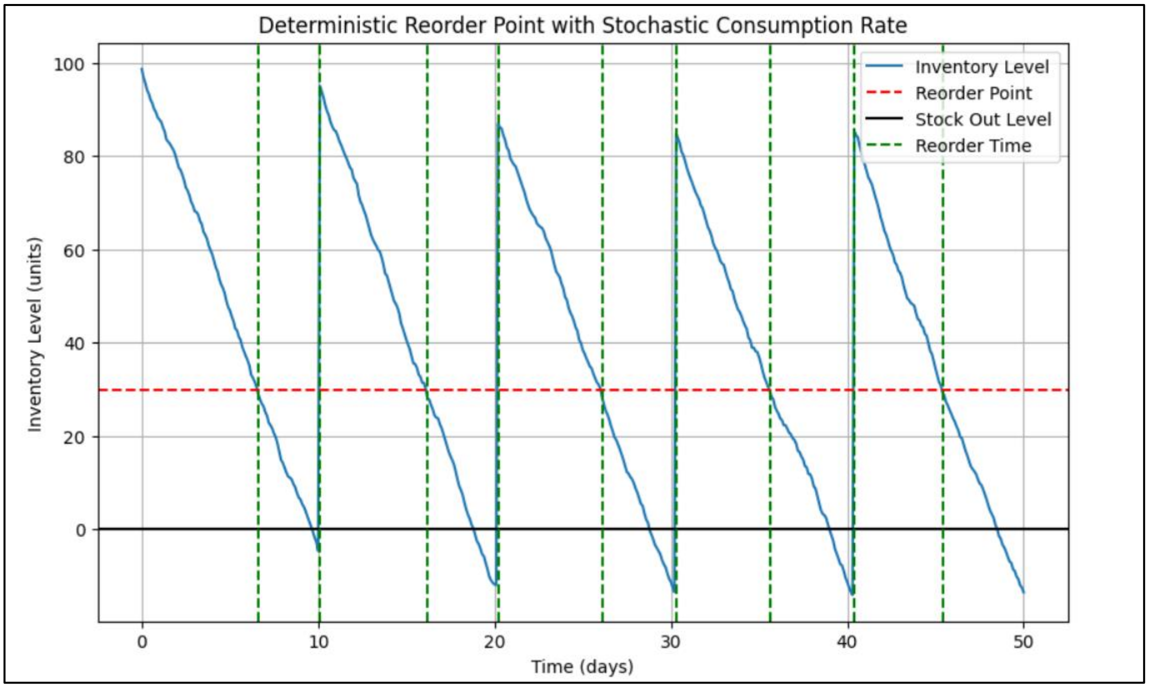

Figure 3.1.1.3-2 Deterministic Reorder Point with Stochastic Consumption Rate

The Reorder Quantity (RQ) model is an extension of the EOQ model that accounts for uncertain parameters (demand, lead time, consumption rate), adding complexity to the decision-making process (Winstin et al., 2004). The RQ model aims determine quantities R and Q to mitigate stockout risks. Figure 3.1.3-3 shows that by raising the reorder point, stockouts are prevented. However, this implies increased holding and storage costs. The impact of quantities R and Q on operational performance can be profound. The optimization of these values is crucial to maintain acceptable stockout risk while minimizing auxiliary costs associated with material inventory.

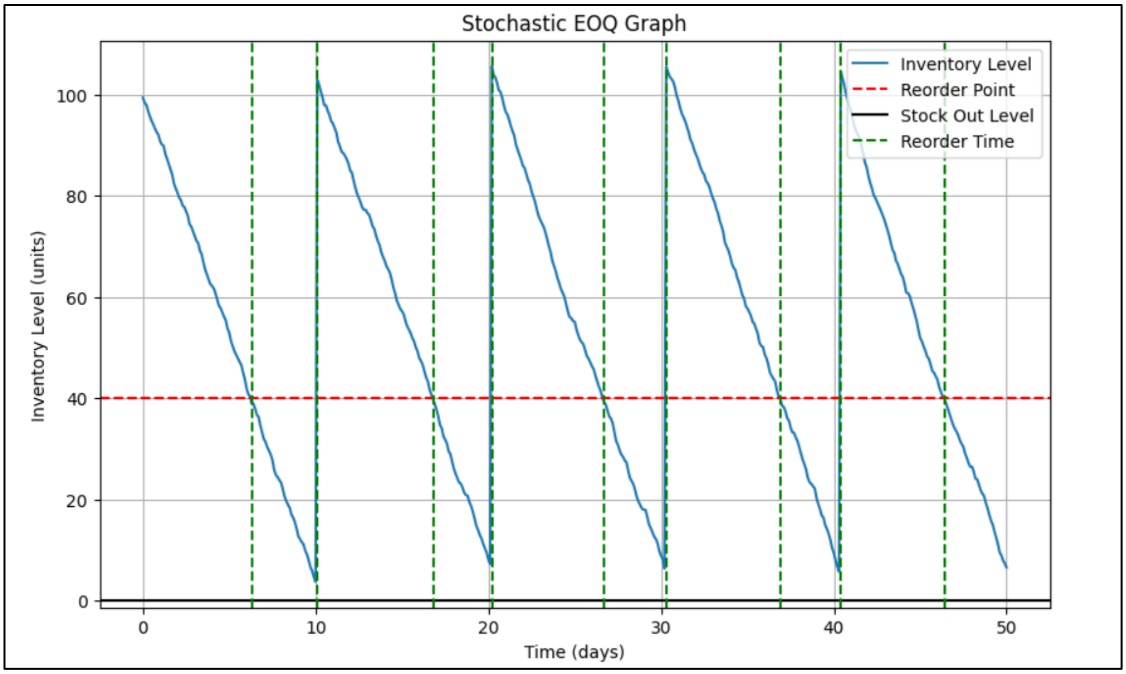

Figure 3.1.1.3-3 Raising the Reorder Point to Mitigate Stockout Risk

The operational efficacy of a system operating within a specified Reorder Quantity (RQ) framework can be thoroughly evaluated through Key Performance Indicators (KPIs), which facilitate the analysis of various permutations of R and Q values. Discrete Event Simulation (DES) emerges as an ideal tool for modeling extended periods of operational activity with their associated stockout and replenishing events, under different R and Q scenarios.

3.1.4 Discrete Event Framework Development

Navara et al. (2019) develop a generic DES/DRS framework, based on the RQ problem from Inventory Theory to balance stockout risk due to geological uncertainty with other KPIs, such as throughput, for mines with heterogenous ore types. In the framework, stockpile levels are equivalent to inventory levels from the RQ problem. The main difference with the original problem is that instead of considering replenishments at discrete time steps that instantly increase the inventory level by quantity Q, the framework distinguishes between two modes: a consumption mode that is profitable in the short-term, but unsustainable due to frequent stockouts, and a comparatively less profitable replenishment mode. Reorder quantity Q is replaced with L_{max}, an upper bound on the stockpile size, due to operational and economic constraints, and reorder point

R becomes L_{crit}, the critical level at which an operational mode change is triggered. Figure 3.1.4-1 illustrates the two modes. Here L_{crit} is raised as in Figure 3.1.3-3 to prevent stockouts at the expense of a higher L_{max}.

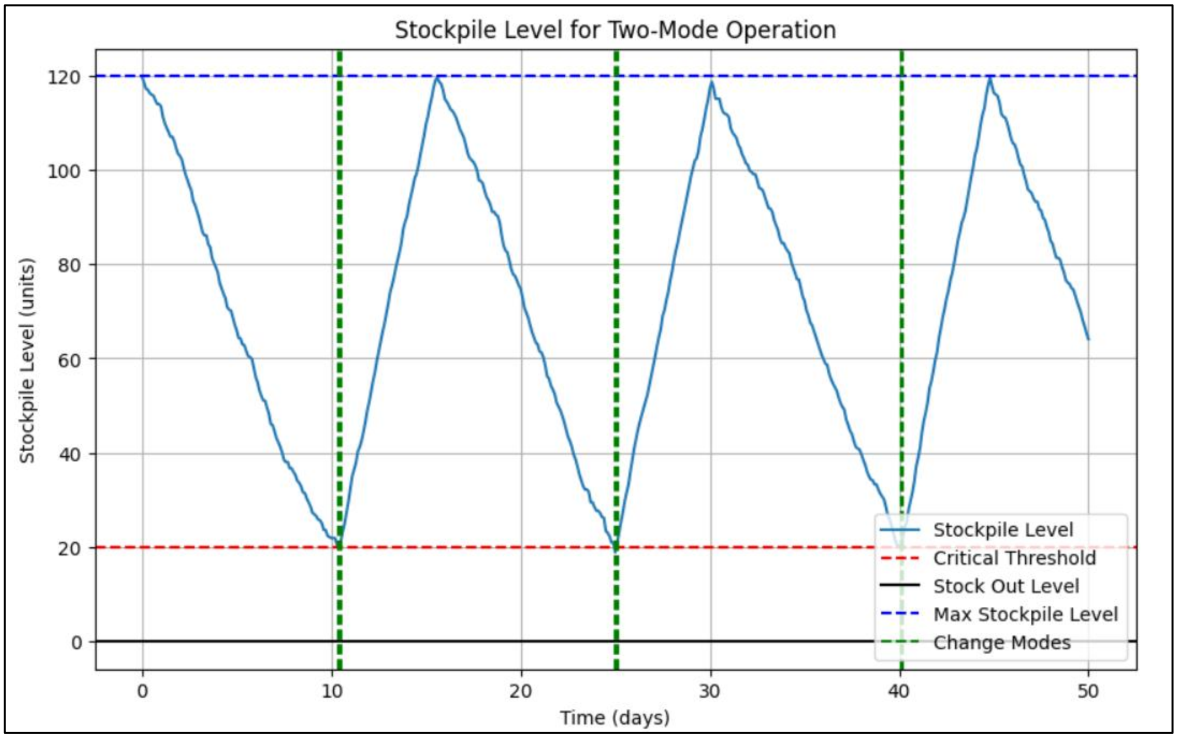

Figure 3.1.4-1 Stockpile Level for Two-Mode Operation

To manage geological variation, Navarra et al.'s framework uses alternating operational modes which affect the configuration of an ore concentrator. In its simplest form, the framework considers two ore types, Ore 1 and Ore 2 which are blended and processed either in Mode A or Mode B. Each mode is associated with a milling rate r_A and r_B, and different weight fractions of the two ore types, w_{1A}, w_{2A} and w_{1B}, w_{2B}, for Mode A and Mode B respectively, in the blended mill feed. The weight fractions of Ore 1 and Ore 2 in the deposit are given by w_{1D} and w_{2D}. Mode A is more productive than Mode B but cannot be applied indefinitely since $w_{2A} > w_{2D}$. Hence, once a critical Ore 2 stockpile level $L_{crit,Ore2}$ is crossed, a mode change is triggered to allow its replenishment. Due to geological variability, a previously well-selected $L_{crit,Ore2}$ level can still fail at preventing a stockout. As such, contingency modes which serve as less-productive auxiliary modes to Modes A and B are also defined. Mode A contingency is associated with milling rate

r_{ACont} and ore fractions w_{1ACont} and w_{2ACont}. Similarly, Mode B contingency has milling rate r_{BCont} and ore fractions w_{1BCont} and w_{2ACont}. The contingency segments allow the buildup of ore suffering from a stockout by only processing the other ore type.

The DES/DRS framework readapts concepts from the RQ problem to analyze concentrator tactics amidst geological uncertainty and optimize operational parameters with the help of simulation. Multiple operational scenarios can be simulated and compared to one another using KPIs. The framework is generalizable and flexible in modelling complex mining systems involving ore supply problems and has been applied to a variety of contexts across the value chain (Wilson et al., 2021, Órdenes et al., 2022, Navarra et al., 2021). While prior research has predominantly concentrated on incorporating quantitative methodologies into DES/DRS frameworks at the input stage, the present work shifts the focus towards integrating the framework's output to an optimization model.

3.1.5 Algorithmic Implementation

Figure 3.1.5-1 is a diagram of the algorithmic implementation of a generic DRS framework. The algorithm was implemented for the present work on Visual Basic for Applications (VBA), and macro-enabled Excel sheets.

The first step in the algorithm is the initialization of model-specific values for levels, timers and discretely dynamical and categorical variables, and the starting mode of operation represented by the rate configuration number. The simulation clock and the time increment used to update levels are set to zero and the model-specific rate formulas are translated from strings to numerical values. The assignment addresses that call onto Excel's Random Number Generator (RNG) to introduce stochastic parameters are also translated. After the initialization of the state variables, the duration until the next threshold crossing is defined as the minimum of all potential threshold crossing events among all levels and timers. The critical level or timer is determined, as well as the direction of the crossing event (positive or negative). The simulation clock is then advanced using the duration until threshold crossing. The time increment between two threshold crossing events can be used to update levels using equation (3.1.2-1). The characterization of the threshold crossing event, namely the direction and the type of the crossing variable, determine the assignment address that assigns new values to levels, timers, discretely dynamical numerical variables and categorical variables, based on deterministic formulas, or Excel's built-in RNG. The algorithm checks if the terminating condition is met. If it is, the algorithm ends and returns output statistics and graphs for the simulation. Otherwise, it characterizes the next mode of operation by updating the rate configuration number.

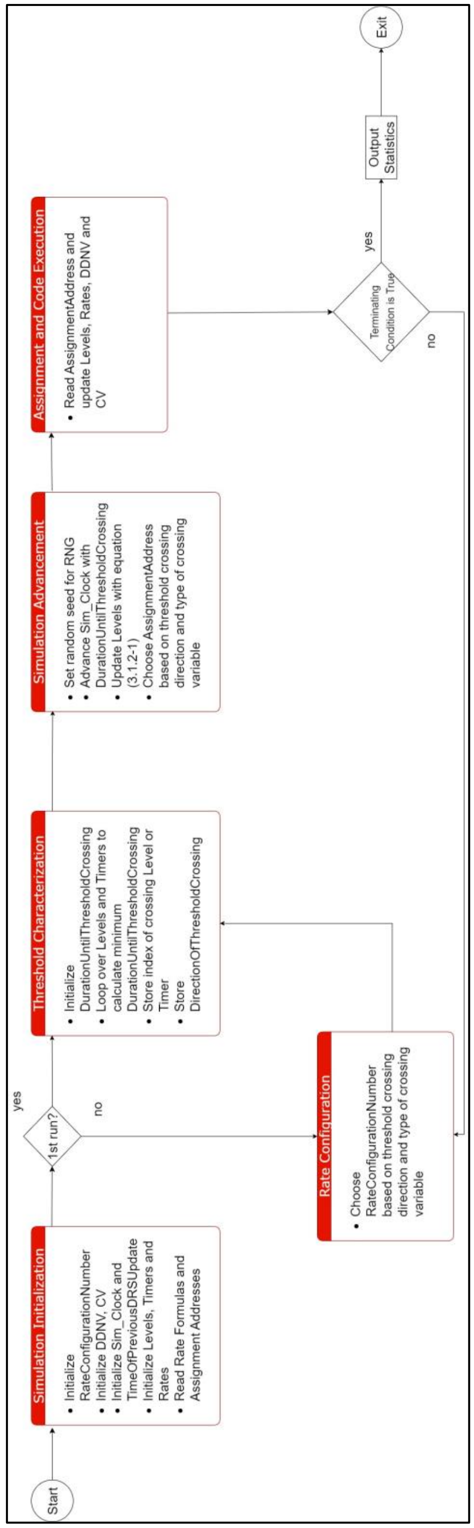

Figure 3.1.5-1 Algorithmic Implementation of DRS Framework

3.2 Multi-Objective Optimization

Balancing competing goals is a common challenge in fields such as engineering, economics, agriculture, aviation, and healthcare (Gunantara, 2018). Much of engineering research involves optimizing several goals simultaneously. For instance, in the design phase of a new vehicle, a company might aim to balance costs with performance. This could involve selecting materials that are both affordable and durable, ensuring the vehicle is cost-effective while still meeting safety and reliability standards. The challenge of optimizing multiple goals that may not align is the central topic of multi-objective optimization (MOO). Due to the often-conflicting nature of objectives, MOO problems rarely have a single optimal solution and will most often have a set of trade-off solutions, which will be compared to each other using the concept of Pareto optimality. An informed decision-maker is thus presented with a representative set of solutions that fulfill Pareto criteria and must choose the most suitable design based on industry knowledge and preferences. The following sections explore multi-objective linear programming (MOLP) concepts by first introducing single-objective linear optimization, which serves as the foundation for traditional algorithms for MOLP problems. This is followed by a discussion of different methods to solve MOLP problems.

3.2.1 Single-Objective Linear Programming

3.2.1.1 <u>Overview of Linear Programming</u>

Linear Programming (LP) addresses the challenge of optimizing a linear objective function while adhering to linear equality and inequality constraints on the decision variables. It is a special case of a general constrained optimization problem. The standard form of the LP can be posed as

$$\begin{aligned} &Minimize \quad \boldsymbol{c}^T\boldsymbol{x} = z \\ &Subject\ to \quad \boldsymbol{Ax} = \boldsymbol{b}, \quad \boldsymbol{A} : m \times n,\ \ m \le n \qquad (3.2.1.1-1) \\ &\boldsymbol{x} \ge 0. \end{aligned}$$

where

$$\boldsymbol{c} = \begin{pmatrix} c_1 \\ \vdots \\ c_n \end{pmatrix}, \boldsymbol{b} = \begin{pmatrix} b_1 \\ \vdots \\ b_n \end{pmatrix}, \boldsymbol{x} = \begin{pmatrix} x_1 \\ \vdots \\ x_n \end{pmatrix} \in \mathbb{R}^n,$$

are two given column vectors and the vector of decision variables respectively, and $\boldsymbol{A}$ an $m \times n$ matrix. The function $z : \boldsymbol{x} \to \boldsymbol{c}^T\boldsymbol{x}$ whose value is to be minimized is called the objective function. Every maximization problem $\max(\boldsymbol{c}^T\boldsymbol{x})$ can be transformed into a minimization problem $-\min(-\boldsymbol{c}^T\boldsymbol{x})$.

In other words, linear programming is equivalent to maximizing or minimizing a linear function of the form $\sum_{i=1}^{n} c_i x_i$ over all $\boldsymbol{x}$ in a polyhedron $P \subseteq \mathbb{R}^n$ defined as $P = \{\boldsymbol{x} \in \mathbb{R}^n : \boldsymbol{Ax} = \boldsymbol{b}, \boldsymbol{x} \geq 0\}$ (P is termed a polytope if it is bounded). Any $\boldsymbol{x}$ satisfying $\boldsymbol{Ax} = \boldsymbol{b}$ is said to be feasible. If there are no such $\boldsymbol{x}$, the linear program is said to be unfeasible. If the solution can be made arbitrarily small (in the case of a minimization problem, arbitrarily large otherwise), the linear program is said to be unbounded. An optimal solution is a feasible solution $\overline{\boldsymbol{x}}$ such that $\boldsymbol{c}^T\boldsymbol{x} \geq \boldsymbol{c}^T\overline{\boldsymbol{x}}$ for all feasible $\boldsymbol{x}$, $\boldsymbol{c}^T\overline{\boldsymbol{x}}$ is termed the optimal value of the program.

Let $\boldsymbol{B}$ be a square matrix formed by m linearly independent columns of matrix $\boldsymbol{A}$ ($rank(A) = m$), if the columns of $\boldsymbol{A}$ are reordered such that the columns of $\boldsymbol{B}$ appear first, the following relation holds

$$\boldsymbol{A} = [\boldsymbol{B}, \boldsymbol{N}] \qquad (3.2.1.1-2)$$

where $\boldsymbol{N}$ is an $m \times (n-m)$ of the remaining columns of $\boldsymbol{A}$. Recall that $\boldsymbol{Ax} = \boldsymbol{b}$. Since the columns of the square matrix $\boldsymbol{B}$ are linearly independent, it is invertible, and the following equation can always be solved.

$$\boldsymbol{Bx_b} = \boldsymbol{b} \qquad (3.2.1.1-3)$$

Going back to the original equation, if $\boldsymbol{x}$ is an n-vector such that its first m-components $x_1, \ldots, x_m$ form vector $\boldsymbol{x_b}$ and its remaining components are 0 ($\boldsymbol{x} = [\boldsymbol{x_b}^{\boldsymbol{T}}, \boldsymbol{0}^{\boldsymbol{T}}]^T$), then $\boldsymbol{x}$ is a basic solution to $\boldsymbol{Ax} = \boldsymbol{b}$ with respect to basis $\boldsymbol{B}$. The components of $\boldsymbol{x_b}$ are termed the basic variables. If one or more basic variables is zero, the basic solution is degenerate. If solution $\boldsymbol{x}$ is also feasible, then it is referred to as basic feasible solution (BFS) (or degenerate basic feasible solution in case of zero basic variables). Basic feasible solutions (BFS) have a paramount importance in solving LPs (Chong, & Zak, 2013).

Theorem 3.1 ***(Fundamental Theorem of Linear Programming)***

Given a linear program in standard form:

1. *If there exists a feasible solution* $\boldsymbol{x}$ *(i.e.,* $\boldsymbol{Ax} = \boldsymbol{b}, \boldsymbol{x} \geq 0$), *then there exists a basic feasible solution.*
2. *If there exists an optimal feasible solution* $\overline{\boldsymbol{x}}$ *(i.e.,* $\boldsymbol{c}^T\boldsymbol{x} \geq \boldsymbol{c}^T\overline{\boldsymbol{x}}$ for all feasible $\boldsymbol{x}$*), then there exists an optimal basic feasible solution.*

Theorem 3.1 shows that to solve a LP, it suffices to search over all basic feasible solutions (BFS). The number of basic feasible solutions (BFS) is finite since for matrix $\boldsymbol{A} : m \times n$ with $rank(A) = m,$ the total number of basic solutions is at most

$$\binom{n}{m} = \frac{n!}{m!\,(n-m)!} \qquad (3.2.1.1-4)$$

The geometric interpretation of Theorem 3.1 is the basis for the simplex method that will be covered in the next section.

Definition 3.1 ***(Convex Sets)***

A set $S \subset \mathbb{R}^n$ *is defined as convex if for all* $\boldsymbol{x}, \boldsymbol{y} \in S$ *and all* $\lambda \in (0,1)$,

$$\lambda\boldsymbol{x} + (1-\lambda)\boldsymbol{y} \in S \qquad (3.2.1.1-5)$$

Theorem 3.2 ***(Set of Feasible Solutions is Convex)***

The set of points satisfying $\boldsymbol{Ax} = \boldsymbol{b}, \boldsymbol{x} \geq \boldsymbol{0}$ *is convex.*

Proof. Suppose $\boldsymbol{x}$ and $\boldsymbol{y}$ satisfy the constraints and $\lambda \in (0,1)$. Let $\boldsymbol{w} = \lambda\boldsymbol{x} + (1-\lambda)\boldsymbol{y}$.

Then

$$\boldsymbol{Aw} = \boldsymbol{A}[\lambda\boldsymbol{x} + (1-\lambda)\boldsymbol{y}] = \lambda\boldsymbol{Ax} + (1-\lambda)\boldsymbol{Ay}$$

$$= [\lambda + (1 - \lambda)]\boldsymbol{b}$$

$$= \boldsymbol{b} \qquad (3.2.1.1 - 6)$$

and $\boldsymbol{w} \geq \lambda\boldsymbol{0} + (1 - \lambda)\boldsymbol{0} = \boldsymbol{0}$, hence $\boldsymbol{w} \in S$.

Definition 3.2 ***(Extreme points)***

A point $\boldsymbol{x}$ in a convex set S is an extreme point of S if there are no two distinct points $\boldsymbol{x_1}, \boldsymbol{x_2} \in S$ and $\lambda \in (0,1)$ such that $\boldsymbol{x} = \lambda\boldsymbol{x_1} + (1 - \lambda)\boldsymbol{x_2}$. In other words, an extreme point $\boldsymbol{x}$ is not in the interior of any line segment lying in S.

Theorem 3.3 ***(Set of Feasible Solutions is Convex)***

If an LP has an optimal solution, then it has an optimal solution at an extreme point of the feasible set.

From Theorems 3.1, 3.2, and 3.3, it follows that the set of extreme points of the convex polytope $P = \{\boldsymbol{x} \in \mathbb{R}^n : \boldsymbol{Ax} = \boldsymbol{b}, \boldsymbol{x} \geq 0\}$ is equal to the set of basic feasible solutions (BFS) to $\boldsymbol{Ax} = \boldsymbol{b}, \boldsymbol{x} \geq 0$. Therefore, to solve an LP it suffices to examine the extreme points of the constraint set.

3.2.1.2 The Simplex Algorithm

The core principle of the simplex algorithm is to transition from one basic feasible solution (BFS)to another, improving the objective value at each iteration, until an optimal basic feasible solution (BFS) is reached. Geometrically, this corresponds to visiting the vertices of the convex polytope defined by the LP, as depicted on Figure 3.2.1.2-1 (Leal-Taixé, 2014).

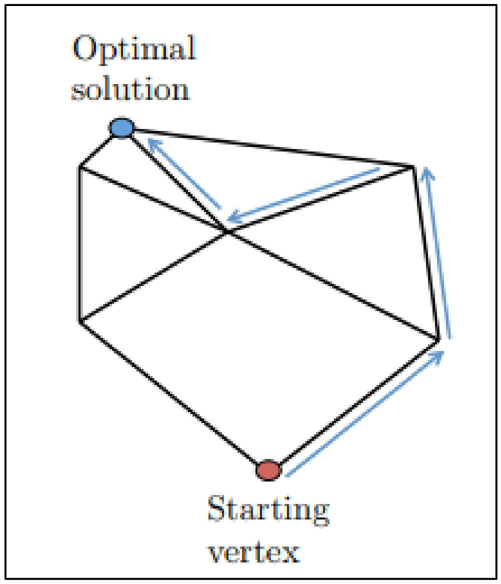

Figure 3.2.1.2-1 Representation of the Simplex Algorithm (Leal-Taixé, 2014)

A concept that is fundamental to the simplex method is reduced cost.

Definition 3.3 ***(Reduced Cost)***

Let $\boldsymbol{A} = [\boldsymbol{B}, \boldsymbol{N}]$ be a partition of matrix $\boldsymbol{A}$, with $\boldsymbol{B}$ a matrix of basic variables and $\boldsymbol{N}$ a matrix of non-basic variables. The objective function can be written as $\boldsymbol{c}_{\boldsymbol{B}}^{T}\boldsymbol{x}_{\boldsymbol{b}} + \boldsymbol{c}_{\boldsymbol{N}}^{T}\boldsymbol{x}_{\boldsymbol{N}}$. Given that $\boldsymbol{Ax} = \boldsymbol{b}$, which can be rewritten as $\boldsymbol{B}\boldsymbol{x}_{\boldsymbol{b}} + \boldsymbol{N}\boldsymbol{x}_{\boldsymbol{N}} = \boldsymbol{b}$, it follows that

$$\boldsymbol{x}_{\boldsymbol{b}} = \boldsymbol{B}^{-1}\boldsymbol{b} - \boldsymbol{B}^{-1}\boldsymbol{N}\boldsymbol{x}_{\boldsymbol{N}} \qquad (3.2.1.2-1)$$

Replacing $\boldsymbol{x}_{\boldsymbol{b}}$ in $\boldsymbol{c}_{\boldsymbol{B}}^{T}\boldsymbol{x}_{\boldsymbol{b}} + \boldsymbol{c}_{\boldsymbol{N}}^{T}\boldsymbol{x}_{\boldsymbol{N}}$, the objective function becomes $\boldsymbol{c}_{\boldsymbol{B}}^{T}\boldsymbol{B}^{-1}\boldsymbol{b} + (\boldsymbol{c}_{\boldsymbol{N}}^{T} - \boldsymbol{c}_{\boldsymbol{B}}^{T}\boldsymbol{B}^{-1}\boldsymbol{N})\boldsymbol{x}_{\boldsymbol{N}}$, where vector

$$\hat{\boldsymbol{c}}_{\boldsymbol{N}}^{T} = (\boldsymbol{c}_{\boldsymbol{N}}^{T} - \boldsymbol{c}_{\boldsymbol{B}}^{T}\boldsymbol{B}^{-1}\boldsymbol{N}) \qquad (3.2.1.2-2)$$

is called the reduced cost. Each $\hat{c}_j$, for j=1,…,n, is the per unit change of the objective function when increasing the corresponding non-basic variable x_j.

Building on the concept of reduced cost, each iteration of the simplex algorithm undergoes the following steps

1. *Initialization.* Pick a BFS.
2. *Pricing.* Examine the vector of reduced costs, if $\forall\, j \in N,\ \hat{c}_j \geq 0$, the simplex algorithm terminates and declares the current BFS as optimal. Otherwise, choose non-basic variable x_e with $\hat{c}_e < 0$ such that

$$e = arg\min_{j} \hat{c}_e \qquad (3.2.1.2-3)$$

   The objective function will decrease if x_e is increased.
3. *Ratio test.* Since variable x_e is increased from its previous value of 0, it is no longer non-basic, and is said to enter the basis $\boldsymbol{B}$ at the next iteration. Increasing the value of x_e leads to a change in the value of the basic variables quantified by $\Delta \boldsymbol{x_b} = -\Delta x_e \boldsymbol{B}^{-1}\boldsymbol{a}_e$. The first basic variable to reach a value of 0 after an increase of Δx_e is termed the leaving variable, as it leaves the basis at the next iteration. The index l of the leaving variable is determined by the ratio test, as follows

$$l = arg\min_{i} \left(\frac{\hat{b}_i}{\hat{a}_{ie}}\right), \hat{a}_{ie} > 0 \qquad (3.2.1.2-4)$$

   If no basic variable ever reaches 0 despite an arbitrarily large increase of Δx_e, the simplex algorithm stops and declares the LP unbounded. If $x_l = 0$, no improvement in the objective function is possible and the BFS is called degenerate.
4. *Update BFS.* x_e replaces x_l in the basic partition to yield a BFS. The objective function is guaranteed to decrease by $\Delta(\boldsymbol{c}^T\boldsymbol{x}) = \hat{c}_e \times \frac{\hat{b}_l}{\hat{a}_{le}}$, unless there is degeneracy.

As stated in step 1, the simplex algorithm must start at a BFS. If an initial BFS is not known, it is found by applying the simplex algorithm on a relaxed problem based on the original LP with the introduction of artificial variables. This is commonly referred to as Phase I, while Phase II involves finding, if it exists, an optimal BFS. The relaxed LP is defined as

$$\begin{aligned} &Minimize \quad \boldsymbol{c}^T\boldsymbol{x} = z \\ &Subject\ to \quad \boldsymbol{Ax} + \boldsymbol{u} = \boldsymbol{b}, \qquad \boldsymbol{A} : m \times n,\ \ m \leq n \qquad (3.2.1.2-5) \\ &\boldsymbol{x}, \boldsymbol{u} \geq 0. \end{aligned}$$

by introducing slack variables $u_1, u_2, \dots, u_m$. If all slack variables are forced to be 0, then the solution of equation (3.2.1.2-5) is equivalent to the solution of equation (3.2.1.1-1). To obtain a BFS for the original LP, the auxiliary problem is posed as follows with a modified objective function

$$Minimize \quad \mathbf{1}_m^T \boldsymbol{u} = z'$$

$$Subject\ to \qquad \boldsymbol{Ax} + \boldsymbol{Iu} = \boldsymbol{b}, \qquad \boldsymbol{A} : m \times n, \;\; m \le n \qquad (3.2.1.2-6)$$

$$\boldsymbol{x}, \boldsymbol{u} \ge 0.$$

The auxiliary LP_{aux} is solved, if it has an optimal value of 0, then the original LP is feasible, and a feasible basis can be constructed. The set $\boldsymbol{B} = \{1, \dots, m\}$ is a basis of LP_{aux} with basic solution $(\overline{\boldsymbol{x}}, \overline{\boldsymbol{u}})$, with $\overline{\boldsymbol{x}} = \boldsymbol{0}$ and $\overline{\boldsymbol{u}} = \boldsymbol{b}$, if the RHS of equation (3.2.1.2-6) is assumed to be positive (in the case that some components are $\boldsymbol{b}$ are negative, the associated constraint is multiplied by -1). However, the basic initial solution $(\overline{\boldsymbol{x}}, \overline{\boldsymbol{u}})$ is not necessarily feasible. The trick is to perform pivot operations to exchange entering and leaving variables in the basis to make said solution feasible for LP_{aux}.

Algorithm 3.2.1.1 shows the pseudocode of Phase I of the simplex algorithm.

Algorithm 3.2.1.1 Simplex Initialization

Input:

$A \in R^{m \times n}$ - Coefficient matrix of size $m \times n$

$b \in R^{m}$ - Right-hand side vector of size m

$c \in R^{n}$ - Cost vector of size n

Output:

BFS - Basic Feasible Solution (initial)

flag - Status flag (feasible, unbounded, infeasible)

$B \in R^{m \times m}$ - Basis matrix

$N \in R^{m \times (n-m)}$ - Non-basis matrix

if $x_j = 0 \ \forall j \in N$ is a BFS **then** ▷ Is the initial basic solution feasible?

  return $(B, N, A, b, c, \text{flag} = \text{feasible})$

else

  Set up LP_{aux} with slack form (B, N, A, b, c, u)

  $(B, N, A, b, c, u) \leftarrow PIVOT$(B, N, A, b, c, u, l, 0) ▷ Perform pivot operation on identified leaving and entering variables to make basic solution feasible for LP_{aux}

  Perform simplex iterations on LP_{aux} until an optimal solution $\overline{x}_0$ is found

  if $\overline{x}_0 = 0$ **then**

    if $\overline{x}_0$ is basic **then**

      Perform a pivot operation to make it non-basic

      Delete all x_0 terms from the constraints and restore LP

      Replace all basic variables in the objective function of LP with

      RHS constraints

      return modified slack form

    end if

  else

    return unfeasible

  end if

end if

Algorithm 3.2.1-1 Simplex Initialization

The pseudocode of Phase II is shown in Algorithm 3.2.1.2.

Algorithm 3.2.1.2 Simplex Algorithm

Input:
$A \in R^{m \times n}$ - Coefficient matrix of size $m \times n$
$b \in R^m$ - Right-hand side vector of size m
$c \in R^n$ - Cost vector of size n
Output:
Optimal solution - $(\overline{x}_1, \overline{x}_2, \ldots, \overline{x}_n)$

Call Simplex Initialization ▷ Obtain a BFS to LP
Let $\phi \in R^n$ be a vector that stores results of the ratio test
while some index $j \in N$ has $c_j < 0$ **do**
  choose an index $e \in N$ for which $c_e < 0$
  for each index $i \in B$ **do** ▷ Ratio test
    if $a_{i,e} > 0$ **then**
      $\phi_i \leftarrow \frac{b_i}{a_{i,e}}$
    else
      $\phi_i \leftarrow \infty$
    end if
  end for
  $l \leftarrow \arg\min_i \left(\frac{\hat{b}_i}{\hat{a}_{ie}}\right)$, where $\hat{a}_{ie} > 0$
  if $\phi_l = \infty$ **then**
    return "unbounded"
  else
    $(B, N, A, b, c, u) \leftarrow \text{PIVOT}(B, n, A, b, c, u, \phi, l, e)$ ▷ Exchange entering and leaving variables
  end if
end while
for $i = 1$ to n **do**
  if $i \in B$ **then**
    $\overline{x}_i \leftarrow b_i$
  else
    $\overline{x}_i \leftarrow 0$
  end if
end for
return $(\overline{x}_1, \overline{x}_2, \ldots, \overline{x}_n)$

Algorithm 3.2.1-2 Simplex Algorithm

3.2.2 Multi-Objective Linear Programming

3.2.2.1 <u>General Formulation</u>

The general Multi-Objective Linear Programming (MOLP) problem in standard form for a vector of objective functions $\boldsymbol{F}(\boldsymbol{x}) = (\,(\boldsymbol{c}^1)^T\boldsymbol{x}, (\boldsymbol{c}^2)^T\boldsymbol{x}, \ldots, (\boldsymbol{c}^k)^T\boldsymbol{x})^{\boldsymbol{T}}$is

$$Minimize \quad \boldsymbol{F}(\boldsymbol{x})$$

$$Subject\ to \qquad \boldsymbol{Ax} = \boldsymbol{b}, \qquad \boldsymbol{A} : m \times n,\ \ m \le n \qquad (3.2.2.1-1)$$

$$\boldsymbol{x} \ge 0.$$

where $\boldsymbol{c}^i$ is an n-dimensional vector for $i = 1, \ldots, k$, corresponding to the cost vector of objective i. The vector function $\boldsymbol{F}(\boldsymbol{x}) : \mathbb{R}^n \to \mathbb{R}^k$ for $k \ge 2$ contains multiple objectives. The minimization in equation (3.2.2.1-1) is understood to be component-wise for each linear objective function $\left(\boldsymbol{c}^i\right)^T\boldsymbol{x}$ for $i = 1, \ldots, k$. Since the components of $\boldsymbol{F}(\boldsymbol{x})$ often describe various goals, it is likely that the scale and units used are different. To make the objective functions comparable, the components of matrix $\boldsymbol{C}$ of size $k \times n$, that contains the k cost vectors ($\boldsymbol{C} = (\,(\boldsymbol{c}^1)^T\boldsymbol{x}, (\boldsymbol{c}^2)^T\boldsymbol{x}, \ldots, (\boldsymbol{c}^k)^T\boldsymbol{x})$) can be normalized.

$$\widetilde{\boldsymbol{c}_j^i} = \frac{\boldsymbol{c}_j^i}{\left(\sum_j \left(\boldsymbol{c}_j^i\right)^2\right)^{1/2}} \qquad (3.2.2.1-2)$$

where $\boldsymbol{c}_j^i$ is the j-th coefficient of the k-th objective function, and $\widetilde{\boldsymbol{c}_j^i}$ its normalized form. Through normalization, the objective functions become tangential to the unit sphere and are hence commensurate. The feasible set in decision space is a polyhedron $X = \{\boldsymbol{x} \in \mathbb{R}^n :\ \boldsymbol{Ax} = \boldsymbol{b}, \boldsymbol{x} \ge 0\}$, while the feasible set in objective space is defined as $Y = \{\boldsymbol{Cx} : \boldsymbol{x} \in X\}$. Figure 3.2.2.1-1 (Denysiuk, 2013) illustrates the mapping between feasible and objective space for a bi-objective optimization problem (BOOP) .

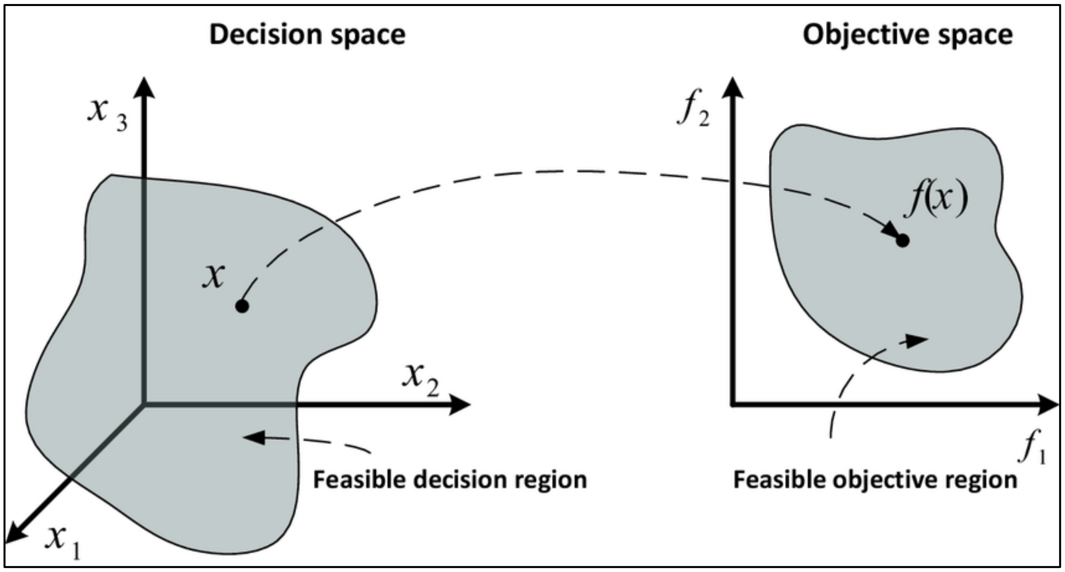

Figure 3.2.2.1-1 Mapping from Decision Space to Objective Space for a BOOP (Denisyuk, 2013)

3.2.2.2 Dominance Criterion and Pareto Optimal Set

In the realm of single-objective optimization problems, a solution is preferred by a decision maker over others through the comparison of their respective objective function values. Conversely, within the domain of multi-objective optimization problems (MOOP), the assessment of solution quality is predicated upon the principle of dominance, wherein multiple solutions may coexist as equally favorable alternatives for a given problem instance. A solution for which no improvement in the value of an objective function is possible without diminishing (increasing in case of a minimization) the value of one or more other objective functions in $\boldsymbol{F}(\boldsymbol{x})$, is called non-dominated, or Pareto Optimal.

Let $\bar{\boldsymbol{x}}^i$ denote the optimal solution to the single-objective LP for objective function $\left(\boldsymbol{c}^i\right)^T \boldsymbol{x}$. The vector of single-objective optimal solutions $\bar{\boldsymbol{x}}$ does not necessarily coincide with the optimal solution to equation (3.2.2.1-1), since the objective functions can be inherently conflicting (maximizing performance while minimizing expenditure).

Definition 3.4 ***(Non-Dominated Solution)***

A feasible solution $\dot{\boldsymbol{x}}$ to equation (3.2.2.1-1) is said to be non-dominated if and only if

$$\left(\boldsymbol{c}^i\right)^T \boldsymbol{x} \geq \left(\boldsymbol{c}^i\right)^T \dot{\boldsymbol{x}} \quad i = 1, \dots, k$$

$$\exists s: (\boldsymbol{c}^s)^T \boldsymbol{x} > (\boldsymbol{c}^s)^T \dot{\boldsymbol{x}} \quad 1 \leq s \leq k \qquad (3.2.2.2-1)$$

$$\forall \boldsymbol{x} \in X = \{\boldsymbol{x} \in \mathbb{R}^n : \boldsymbol{A}\boldsymbol{x} = \boldsymbol{b}, \boldsymbol{x} \geq 0\}$$

In other words, solution $\dot{\boldsymbol{x}}$ is no worse than $\boldsymbol{x}$ in all objectives and strictly better than $\boldsymbol{x}$ in at least one objective, for all feasible $\boldsymbol{x}$.

Symbolically, dominance is represented by equation (3.2.2.2-2), where feasible solution $\boldsymbol{x_1}$ dominates feasible solution $\boldsymbol{x_2}$

$$\boldsymbol{x_1} \succ \boldsymbol{x_2} \qquad (3.2.2.2-2)$$

The concept of dominance is illustrated on Figure 3.2.2.2-1. Solution A dominates solution C. Solutions A and B are non-dominated when considering the set of solutions $\{A, B, C\}$.

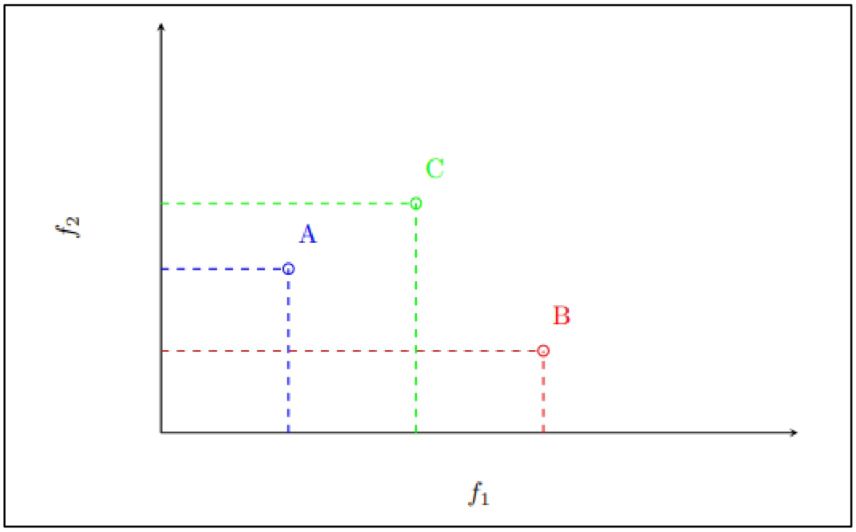

Figure 3.2.2.2-1 Solution Dominance for a Standard Form BOOP

Definition 3.5 ***(Pareto Optimal Set)***

The Pareto Optimal Set X_{PO} *is defined as the set of non-dominated solutions in decision space*

$$X_{PO} = \{\boldsymbol{x}_i \in X : \boldsymbol{x}_i \nprec \boldsymbol{x}, \boldsymbol{x} \in X\} \qquad (3.2.2.2-3)$$

While the previous definitions considered all $\boldsymbol{x} \in X$ to establish the Pareto Optimality of a solution, one can define a locally Pareto Optimal solution $\dot{\boldsymbol{x}}_{loc}$ as a non-dominated feasible solution in an open neighborhood $H(\dot{\boldsymbol{x}}_{loc}) \in \mathbb{R}^n$ of $\dot{\boldsymbol{x}}_{loc}$.

3.2.2.3 Pareto Optimal Front

The set of all Pareto Optimal outcomes is called the Pareto Front.

Definition 3.6 ***(Pareto Front)***

Let $X_{PO} = \{\boldsymbol{x}_i \in X : \boldsymbol{x}_i \nprec \boldsymbol{x}, \boldsymbol{x} \in X\}$ *represent the Pareto Optimal Set. The Pareto Front is is defined as*

$$X_{PF} = \{\boldsymbol{C}\boldsymbol{x}_i, \boldsymbol{x}_i \in X_{PO}\} \qquad (3.2.2.3-1)$$

The Pareto Optimal Front is the result of the mapping of the non-dominated solutions from decision space to objective space, as depicted in Figure 3.2.2.3-1 (Gkiotsalitis, 2023).

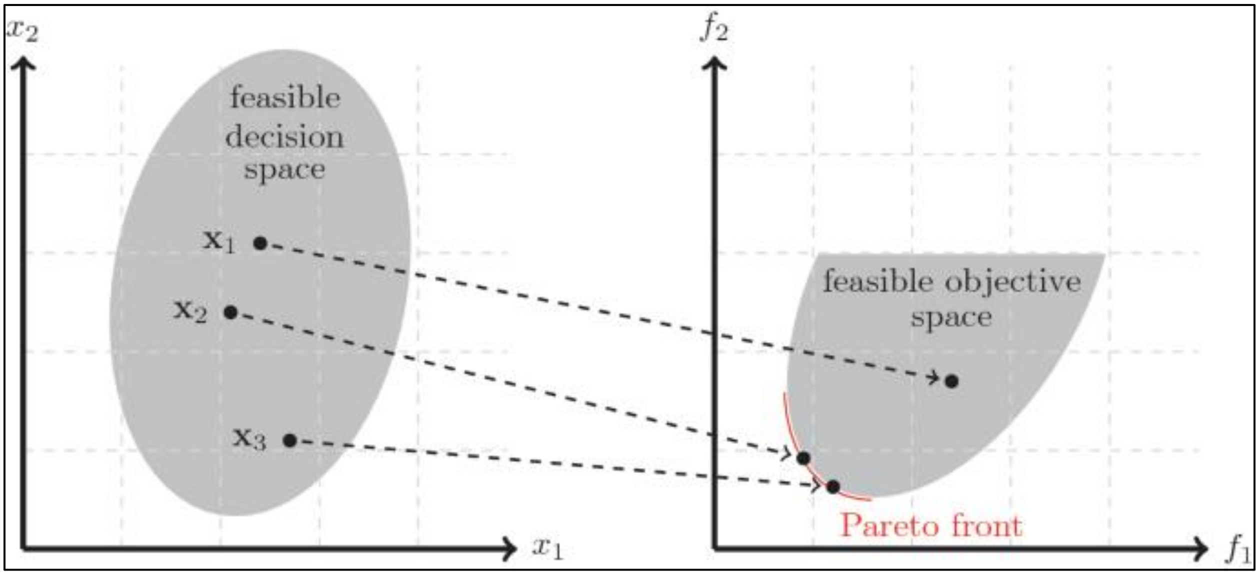

Figure 3.2.2.3-1 Construction of the Pareto Front from Non-Dominated Solutions (Gkiotsalitis, 2023)

The primary objective of MOOP revolves around identifying or approximating an exhaustive or representative set of Pareto Optimal solutions. In the case of bi-objective and triple objective optimization problems, the Pareto Front can be visualized in 2D or 3D space and represents a trade-off curve for the decision-maker.

The Pareto Optimal Front is not necessarily continuous, although it always occurs at the borders of the feasible region in objective space. This relates to the previously introduced concept of locally and globally Pareto Optimal solutions. Figure 3.2.2.3-2 (Kusch, 2020) depicts a discontinuous Pareto Optimal Front (solid black line) and locally Pareto Optimal solutions (black dots). The section depicted with grey dots is the boundary of the concave feasible region where no locally or globally Pareto Optimal solutions can be found.

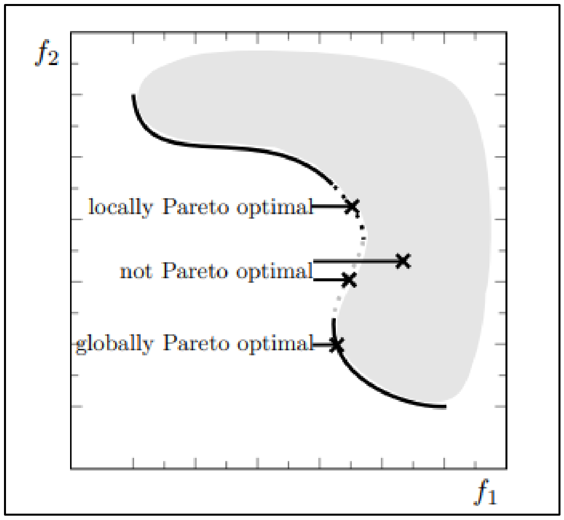

Figure 3.2.2.3-2 Local and Global Pareto Optimal Solutions (Kusch, 2020)

When implementing the solution of a MOOP in a process, it is often unfeasible to attain the optimal solution with arbitrary precision. The more sensitive an optimal solution is to variable variations in its neighborhood, the more impact it will have on the implemented solution. As such, a decision-maker might favor robust solutions. Different definitions of robustness exist in the literature (Deb, & Gupta, 2005), but they all involve evaluating an agglomerate of points around solutions to examine their sensitivity. Figure 3.2.2.3-3 (Deb et al., 2005) shows the comparison of two-Pareto Optimal solutions A and B, small variations in the value of B in decision space have a large impact when mapped on objective space. Hence, it is possible to conclude that Pareto Optimal solution A is “more robust” than solution B.

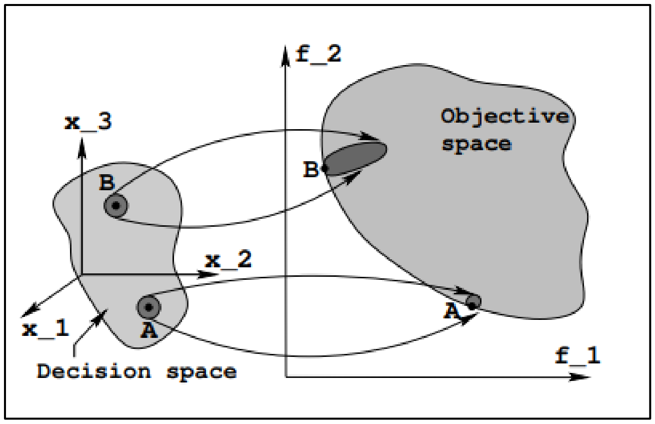

Figure 3.2.2.3-3 Comparison of the Robustness of two-Pareto Optimal Solutions (Deb et al., 2005)

Of particular importance to the Pareto Optimal Front are the nadir and ideal points. The nadir point is represented by an objective vector constructed from the worst values of each objective function corresponding to X_{PO} (note that the nadir point does not necessarily correspond to the worst objective vector). The ideal point is an objective vector constructed from the optimal solutions of each single-objective LP involving the components of $\boldsymbol{F}(\boldsymbol{x})$. It is equivalent to vector $\overline{\boldsymbol{x}}$ that was previously introduced. The nadir and ideal points have several uses in decision-making. They are for instance used to provide the range of the objective functions (Deb, Miettinen, & Chaudhuri, 2010). Figure 3.2.2.3-4 (Deb et al, 2010) shows the nadir and ideal points in relation to the Pareto Optimal Front.

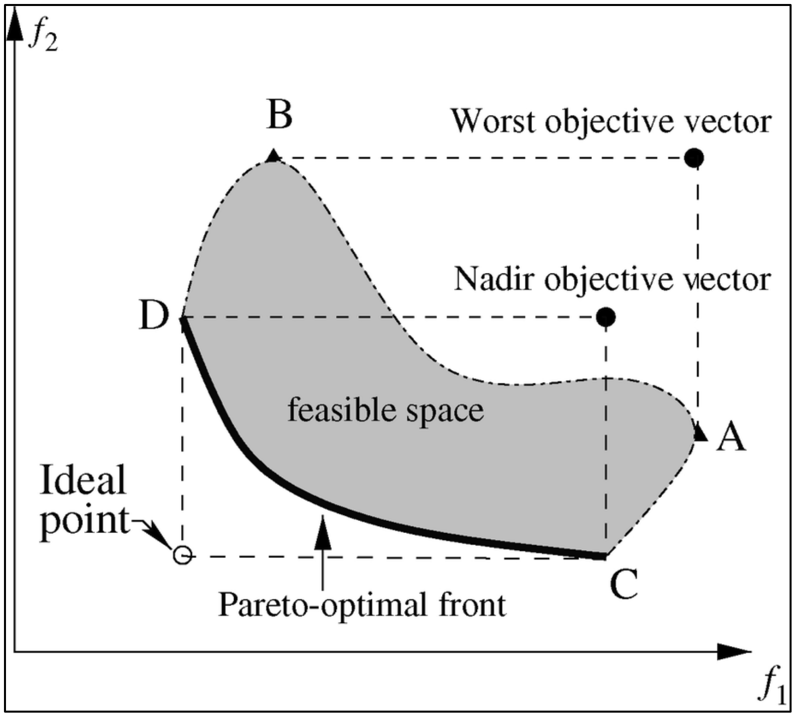

Figure 3.2.2.3-4 Nadir and Ideal Points (Deb et al., 2010)

3.2.3 Solving Methods

Hwang and Masud (2012) distinguish between three different approaches to multi-objective optimization problem-solving, based on the time of decision-making.

A priori methods require the decision-maker to state their preferences before solving the problem. This is often done by ranking objectives in order of importance to the decision-maker. For example, a lexicographic minimization problem in standard form can be posed as

$$lex\ max \quad (\boldsymbol{c}^1)^T\boldsymbol{x}, \dots, (\boldsymbol{c}^k)^T\boldsymbol{x}$$

$$Subject\ to \qquad \boldsymbol{A}\boldsymbol{x} = \boldsymbol{b}, \qquad \boldsymbol{A} : m \times n,\ \ m \le n \qquad\qquad (3.2.3-1)$$

It is assumed here that a small decrease to objective $(\boldsymbol{c}^1)^T\boldsymbol{x}$ is preferrable to very large decrease in $(\boldsymbol{c}^2)^T\boldsymbol{x}, \dots, (\boldsymbol{c}^k)^T\boldsymbol{x}$. Another common and arguably the most popular method for expressing preferences in achieving objectives is to reduce the multi-objective optimization problem (MOOP) to a single-objective linear programming (LP) problem by forming a weighted linear combination of the objectives. The disadvantage of these methods is the inherent need to have preferences for the objectives, which might not always be the case. Interactive methods involve phases of information exchange between the decision-maker and the optimization model. Using intermediate calculations, the decision-maker guides the search towards a preferred solution. The STEM method in an example of an interactive method (Benayoun, Montgolfier, Tergny, & Laritchev, 1971). A posteriori methods are focused on the generation of Pareto Optimal solutions to present to the decision-maker, who then selects trade-offs. This usually involves the plotting of the Pareto Optimal Front for two-objective and three-objective problems. Figure 3.2.2.3-1 illustrates the distinction between the two most commonly used methods: the a priori and a posteriori approaches.

The next section discusses general methods for solving multi-objective linear programming (MOLP) problems. The applications presented in this work are limited to an a posteriori approach.

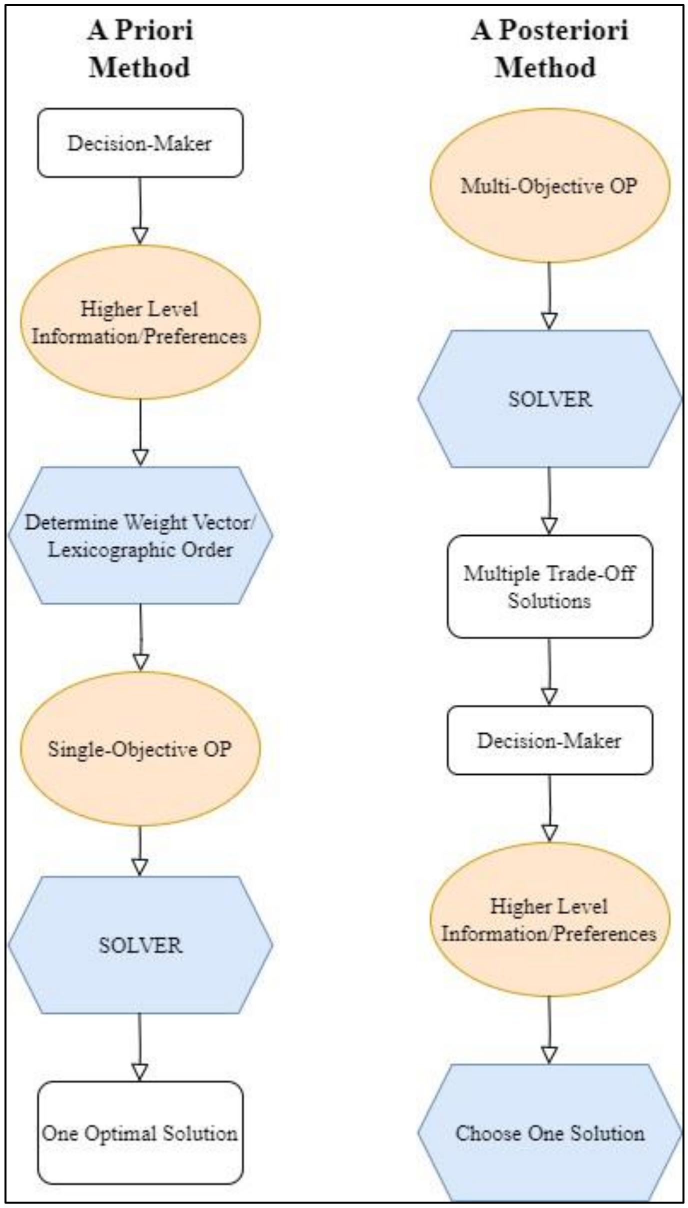

Figure 3.2.2.3-1 Comparison Between A Priori and A Posteriori Methods

3.2.3.1 Weighted-Sum Method

Arguably the most popular method for solving MOOPs is the weighted-sum method. It has been applied to various domains, including materials science (Kalita, Ragavendran, Ramachandran, & Bhoi, 2019), process system engineering (Li, & Zhao, 2023), chemical product design (Ng, Chemmangattuvalappil, Dev, & Eden, 2016), and aircrew rostering (Lučić, & Teodorović, 2007). The weighted-sum method for the MOLP problem involves minimizing the single-objective composite function $\boldsymbol{Q}$, where

$$\boldsymbol{Q} = \sum_{i=1}^{k} w_i \left(\left(\boldsymbol{c}^i \right)^T \boldsymbol{x} \right) \qquad (3.2.3.1 - 1)$$

and $w_i \geq 0$ are scalar weights. Some literature recommends setting $\sum_{i=1}^{k} w_i = 1$ to ensure a convex combination of weighted functions, although Marler and Arora (2010) argue that this is only required for a posteriori articulation of preferences, whereas a priori articulation benefits from unrestricted weights since it helps in determining appropriate weight values. The minimum of the weighted-sum in equation (3.20) is always Pareto optimal. Moreover, by systematically varying the weights, minimizing the weighted sum can produce all Pareto Optimal solutions if the multi-objective optimization problem is convex (Miettinen, 1999). The drawback of the method is that it is unable to generate points on non-convex sections of a Pareto Optimal hypersurface, which makes it unsuitable for non-linear programming. Furthermore, the weighted-sum method is not necessarily efficient at exploring the Pareto Optimal set since the points on the Pareto optimal front are not necessarily uniformly distributed when choosing uniformly distributed weights w_i (Kusch, 2020).

3.2.3.2 Weighted-Metric Method

The weighted-metric method generalizes the weighted-sum method by computing the weighted distance metric $\boldsymbol{Q_m}$ of any solution from the ideal point $\overline{\boldsymbol{x}}$ using norm p, as shown in equation (3.2.3.2-1).

$$\boldsymbol{Q_m} = \left(\sum_{i=1}^{k} w_i \left| \left(\boldsymbol{c}^i\right)^T \boldsymbol{x} - \overline{\boldsymbol{x}}_{\boldsymbol{i}} \right|^p \right)^{1/p} \qquad (3.2.3.2-1)$$

$p = 1$ corresponds to the Manhattan metric, $p = 2$ is the Euclidean metric and $p = \infty$ is known as the Tchebycheff metric. When $p = 1$ is used, all deviations from the ideal point $\overline{\boldsymbol{x}}$ are taken into account, while the Tchebycheff metric ensures that only the largest deviation from the ideal point is considered (Jaimes, Martinez, & Coello, 2009). In other words, the Tchebycheff metric assumes that the decision-maker's fundamental priority is to improve the worst performing objective as much as possible. Figure 3.2.3.2-1 shows the difference between commonly used metrics (Purdue University).

For $p \neq \infty$, the convexity of the feasible region is required to guarantee that all Pareto Optimal solutions can be found, whereas for the Tchebycheff metric, all Pareto Optimal solutions can always be found. If the optimal solution of $\boldsymbol{Q_m}$ is unique, or if all weights are non-negative, then the solution is Pareto Optimal.

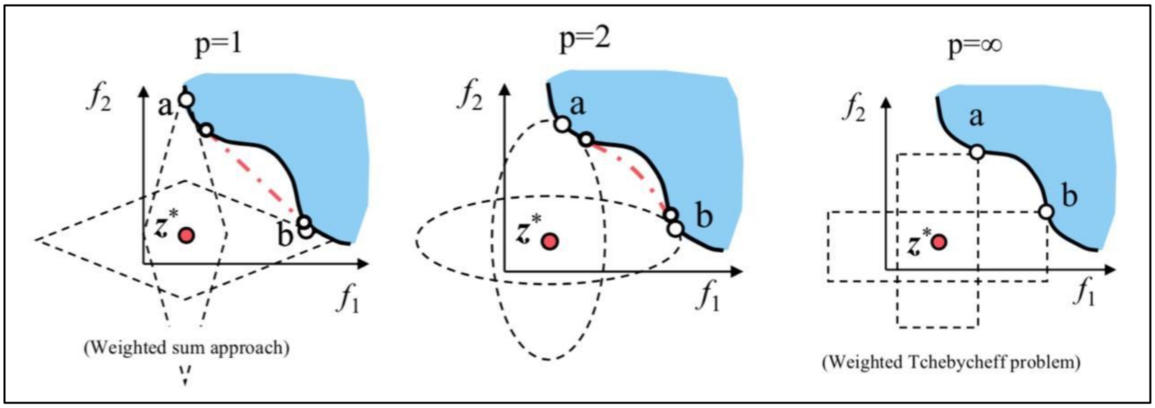

Figure 3.2.3.2-1 Different Metrics Applied to Weighted-Metric Method (Purdue University)

3.2.3.3 ε-Constraint Method

The ε −constraint method was first introduced by Marglin in 1967. It involves minimizing a single objective function while imposing inequality constraints on the other objective functions at different time steps g. The modified LP is posed as follows

$$\begin{aligned} &Minimize \quad (\boldsymbol{c}^1)^T\boldsymbol{x} = z \\ &Subject\ to \quad \boldsymbol{Ax} = \boldsymbol{b}, \quad \boldsymbol{A} : m \times n, \ \ m \le n \\ &\left(\boldsymbol{c}^i\right)^T\boldsymbol{x} \le \varepsilon_{\boldsymbol{g}}^{\boldsymbol{i}}, \\ &\boldsymbol{x} \ge 0. \end{aligned} \tag{3.2.3.3 − 1}$$

The upper bounds $\varepsilon_{\boldsymbol{g}}^{\boldsymbol{i}}$ are varied at every iteration g to produce unique Pareto Optimal solutions. The ε −constraint method is usually preferred to the weighted-sum method since it produces more robust Pareto Fronts and can also capture all Pareto Optimal solution in the case of a non-convex feasible region (Kusch, 2020). However, the method requires prior knowledge on the range of the objective functions to narrow down which $\varepsilon_{\boldsymbol{g}}^{\boldsymbol{i}}$ upper bounds to test. The nadir and ideal points can inform the decision-maker on the range of the Pareto Optimal Front. The nadir point can be used as a starting value for prescribing upper bounds. Figure 3.2.3.3-1 (Teichert, Currie, Küfer, Miguel-Chumacero, Süss, Walczak, & Currie, 2019) illustrates the construction of a Pareto Optimal Front using the ε −constraint method.

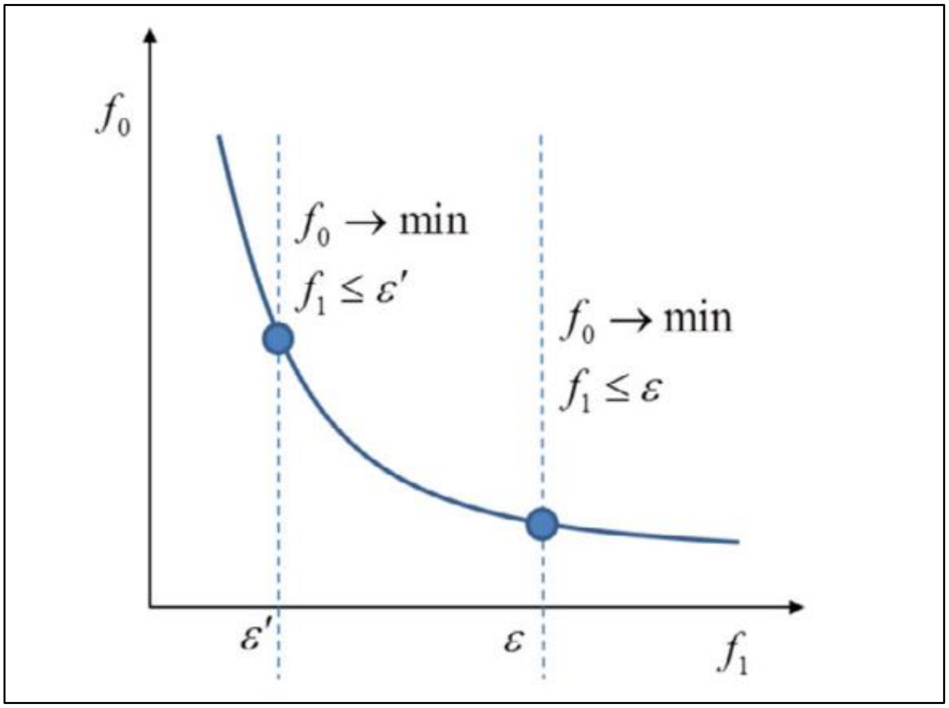

Figure 3.2.3.3-1 Construction of a Pareto Optimal Front with the $\boldsymbol{\varepsilon}$ −Constraint Method (Teichert et al., 2019)

The present works makes use of *the* ε −constraint method due to it's a posteriori approach which does not require pre-specifying preference parameters for the objective functions. Furthermore, industry knowledge can guide the decision-maker in selection appropriate upper bounds for the different objectives.

3.2.3.4 Evolutionary Algorithms (EAs)

Multi-objective evolutionary algorithms (MOEAs) are metaheuristics that progressively approximate sets of Pareto optimal solutions. Unlike traditional optimization techniques that typically collapse the MOOP into a single-objective problem, MOEAs maintain a population of potential solutions, facilitating the exploration of diverse regions of the solution space.

The most popular MOEA is NSGA-II (Non-Dominated Sorting Genetic Algorithm-version 2), introduced by Deb, Pratap, Agarwal, and Meyarivan in 2002. The algorithm is initialized by generating potential solutions to the MOOP that form a population. In a step referred to as non-dominated sorting, the population is sorted into different levels of non-domination. The first level consists of solutions that are not dominated by any other solution in the population, the second level consists of solutions that are only dominated by the first level, and so on. Each solution is assigned a rank based on its level of non-domination, where a lower rank indicates a better level of non-domination. The non-dominated fronts are identified, and the crowding distance, which measures how close a solution is to its neighbors is computed. Next, the selection process is carried out using a combination of rank and crowding distance. Solutions are chosen through tournament selection, favoring those with lower ranks and, among those with equal ranks, those with larger crowding distances to maintain diversity. The selected solutions then undergo crossover and mutation operations to produce a new offspring population, which introduces variability and explores new areas of the solution space. The parent and offspring populations are combined to form an intermediate population, ensuring that the best solutions from both are considered. This combined population is sorted again based on non-domination and crowding distance. The best individuals are selected to form the next generation’s population. If the number of solutions exceeds the population size, solutions from the last front are selected based on their crowding distance until the population size limit is reached. This iterative process of selection, crossover, mutation, and combination continues for a predefined number of generations or until a convergence criterion is met. The result is a set of diverse and high-quality Pareto optimal solutions that approximate the Pareto front.

CHAPTER 4. SAMPLE COMPUTATIONS: DISCRETE RATE SIMULATION AND MULTI-OBJECTIVE OPTIMIZATION FOR AN IRON ORE CONCENTRATOR

4.1 Background

In this chapter, a Discrete Rate Simulation framework using the two-mode approach presented in Chapter 3 is applied to a case study involving a Canadian iron ore concentrator producer, to stabilize plant performance and obtain saleable product tonnage. With the help of simulation-based optimization, a set of control variables is selected to balance operational Key Performance Indicators (KPIs). Subsequently, a mathematical model of the global iron ore market incorporates output data from the simulation for the optimization of product sales.

4.2 Stockpile Control Strategies with DES/DRS

4.2.1 Modelling Context

The Labrador Trough, also known as the New Quebec Orogen, is a geologically significant region in northeastern Canada, spanning from Ungava Bay in the north, through Québec and Labrador, and extending southwest into central Québec. This 1,600 km long and 160 km wide structure, formed around 2 billion years ago during the Paleoproterozoic era, is characterized by its rich deposits of iron ore which have been mined since 1954 (Schiller, 2011). The Trough is particularly noted for its banded iron formations constituted of sedimentary and volcanic rocks. Today, it is one of the world's largest iron ore districts with defined resources exceeding 78 billion tonnes. The map of the Labrador Trough is shown on Figure 4.2.1-1 (Century Global, 2012). The Labrador Trough consists of three main deposit types:

1. *Taconites.* Found predominantly in the Schefferville area, taconites are fine-grained and weakly metamorphosed iron formations with high magnetite (Fe_3O_4) content, typically grading around 30% Fe.
2. *Metataconites.* Metataconite deposits, located in the Southern Trough, are more intensely metamorphosed and coarser-grained, containing specular hematite (Fe_2O_3) and magnetite (Fe_3O_4). These deposits vary significantly in mineralogy and composition across the

Labrador City/Wabush and Fermont areas and can have drastically different magnetite to hematite ratios.

3. *Direct Shipping Ore (DSO) Deposits.* The direct shipping ore (DSO) deposits were the first to be mined in the Trough and are primarily located in the Schefferville area. They fall into two categories: soft high-grade hematite deposits formed by supergene leaching and enrichment of primary taconites, composed mainly of friable fine-grained secondary iron oxides, and hard high-grade hematite deposits without evidence of leaching or supergene processes.

Figure 4.2.1-1 Map of the Labrador Trough (Century Global, 2012)

Today, some mines still exploit DSO deposits in the Schefferville area containing ore grading 56-58% Fe of hematite ore (Schiller, 2011). However, the iron ore mined in the Trough predominantly grades between 30% and 44% iron. To increase the iron content, mines in the Southern Trough crush and grind the ore, then apply gravitational and magnetic concentration methods, producing concentrates with about 65% iron. Depending on the grain size, the concentrate is either shipped as is or agglomerated into centimeter-sized balls and fired to produce hard iron ore pellets (Dumont, 2008).

In this context, the case study presented herein focuses on a prominent mining company operating an open pit mine and an iron concentrator within the Southern Labrador Trough. This company has established itself as a major player in the industry by exploiting the area's substantial iron ore resources. Geostatistical orebody modeling predicted a relatively uniform mill feed head-grade and consistent levels of deleterious elements. As a result, the mill has been optimized for ore from the main pit. Figure 4.2.1-2 shows the flowsheet of the processing plant.

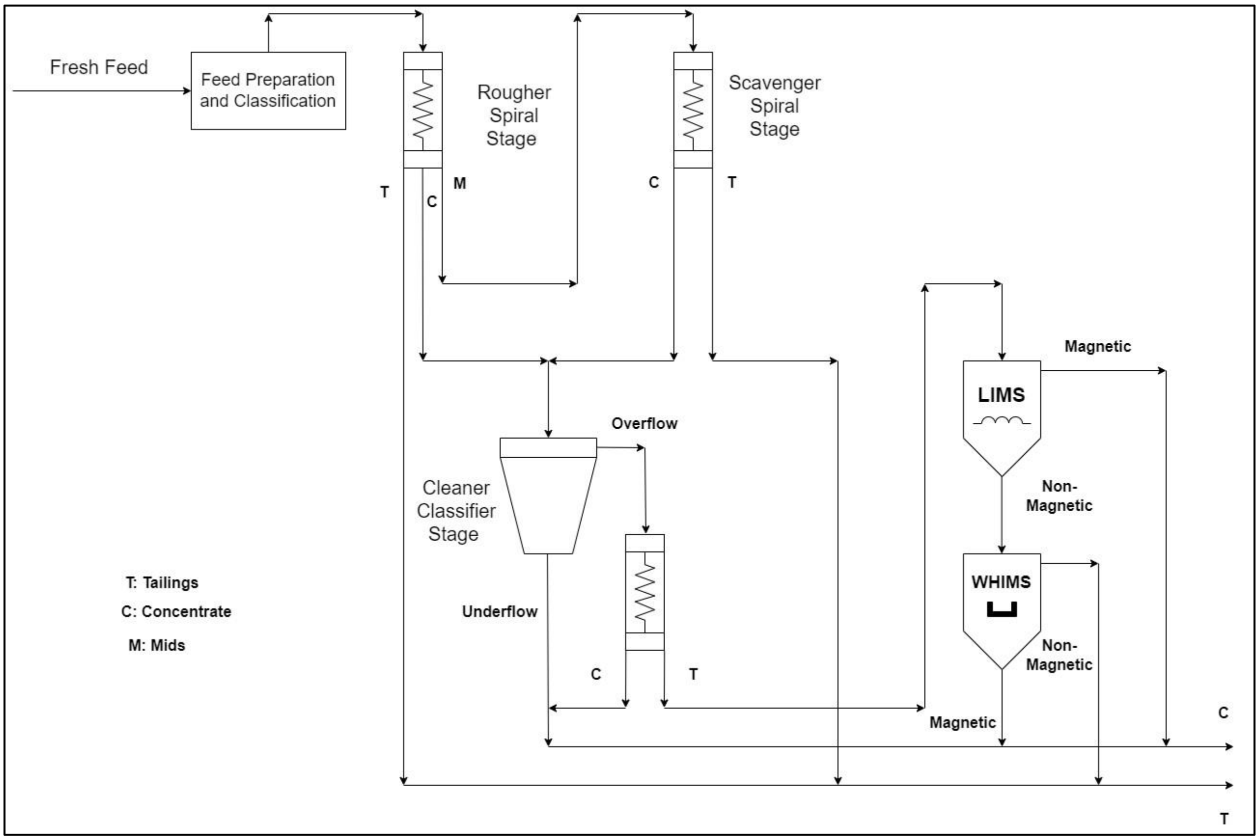

Figure 4.2.1-2 Processing Plant Flowsheet

The flowsheet contains a gravity circuit where spirals at the rougher stage and the cleaner classifier stage work together to remove silica of all sizes. The rougher stage maximizes iron recovery while preventing coarse silica from advancing to the cleaner stage. The cleaner stage then removes fine and mid-sized silica, ensuring the final concentrate meets the target silica grade of less than 4.5%. Additionally, the scavenger spirals recover misplaced iron from the rougher stage middlings and remove mid-size to coarse silica. Sending the mids concentrate to the magnetic separation circuit prevents the reintroduction of coarse silica into the cleaner classifier stage. A combination of LIMS, WHIMS, and spirals constitute the magnetic circuit of the flowsheet. This circuit is used to extract iron from the overflow of the cleaner classifier stage and the mids-scavenger stage. The LIMS stage primarily recovers magnetite (Fe_3O_4), while the subsequent WHIMS stage focuses on the remaining hematite (Fe_2O_3), adjusting the magnetic intensity to maximize hematite recovery from paramagnetic minerals.

Recent exploration efforts have uncovered new mineralized zones proximate to the main pit, which prompted the company to develop a new pit, therefore forming an integrated mining complex consisting of the two pits and a centralized mill. The new pit promises to significantly extend the mining complex's operational life and enhance its production capacity; however, chemical analyses have highlighted differences in ore types from the main pit. As shown in Table 4.2.1-1, iron ore from the new pit has a relatively higher sulfur content. This is detrimental to steelmaking, as steel with high sulfur content loses strength at high temperatures (Yu, Sun, Li, Han, Li & Han, 2023).

Table 4.2.1-1 Chemical Composition of the Main Pit and New Pit Ores

	Fe (%)	*SiO_2 (%)*	*Al_2O_3 (%)*	*MgO (%)*	*CaO (%)*	*P (%)*	*S (%)*
Main Pit Ore	31.6	52.4	0.8	0.4	0.35	0.02	0.01
New Pit Ore	29.8	54.1	0.6	0.3	0.4	0.02	0.3

In response, the company has initiated geometallurgical studies to devise suitable control strategies aimed at mitigating the high sulfur levels. These studies have highlighted the importance of the grinding process and ore fineness in influencing the efficiency of flotation desulfurization, underscoring the need to optimize these factors to ensure that ore from the new pit meets quality standards (Qiu, Wu, Ai, Zhao, & Yu, 2015). The company upgraded its mill with a multi-stage grinding circuit, particularly designed for processing blended feed primarily sourced from the new pit. Figure 4.1.2-3 shows the upgraded flowsheet.

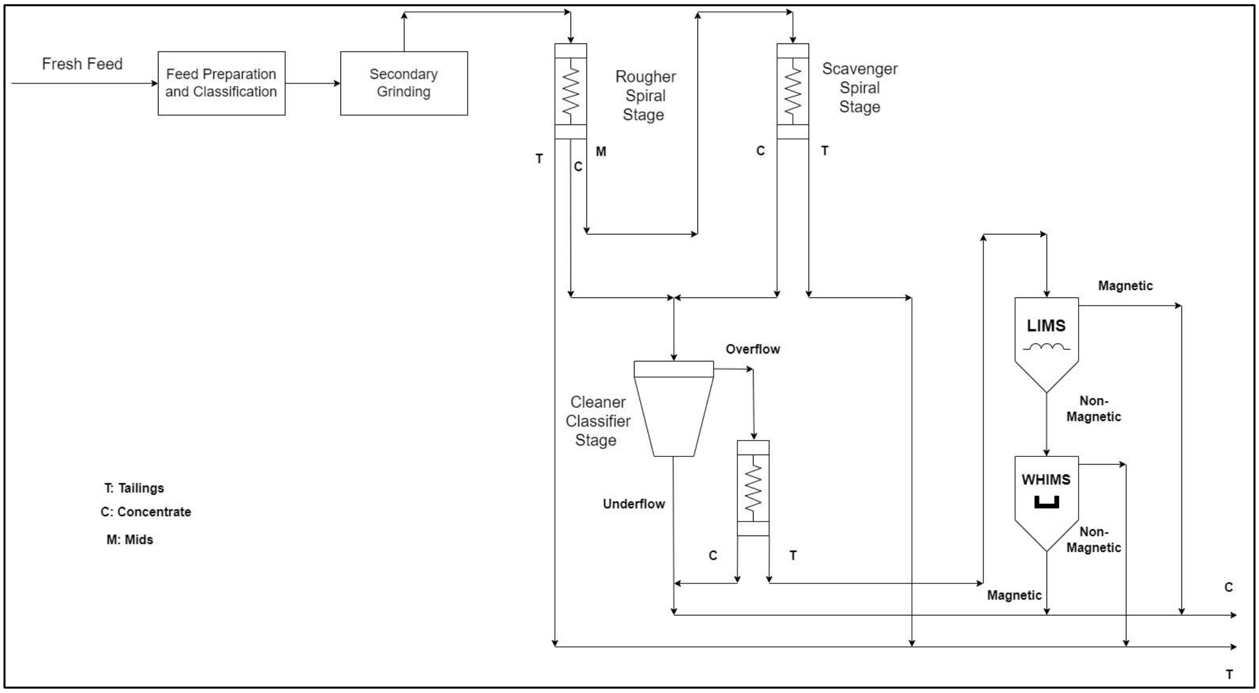

Figure 4.2.1-3 Upgraded Processing Plant Flowsheet

Due to the depletion of the main pit, which is currently in a ramping down period, it is forecasted that 70% of the mill feed will originate from the new mine. For simplicity, ore extracted from the new pit is denoted as Ore 2, while ore from the main pit is designated as Ore 1. The company is looking to optimize its mine-to-mill integration by managing uncertain plant feeds, maximizing mill throughput, and therefore concentrate production, and minimizing auxiliary costs related to stockpile holding and storage. While using fixed mass balances to evaluate potential plant performance is standard practice in the mineral processing sector (Wilson, 2021), the present work incorporates data-driven fluctuations in mass and composition of flows, which are typical of a multi-mine complex, through dynamic mass balances via Discrete Event Simulation parametrized with industry and relevant public data from iron producers.

4.2.2 DRS Model

The DRS framework utilized in this work adapts Navarra et al.'s (2019) two-mode model with multiple configuration rates to optimize mass balancing of heterogeneous ore feed types and stabilize plant throughput. It incorporates operational buffers, such as stockpiling and ore blending practices, with adjustments made in response to geological uncertainties in the ore feeds. The mining-and-milling operation is simulated until a target ore extraction level of 4,681,648 t is achieved, which roughly corresponds to 365 days, with 30-day production campaigns followed by 1-day planned shutdowns. The ore from both mines is blended and stockpiled prior to processing. The centralized mill has an averaged iron metallurgical recovery of 80% relative to average plant feed grades of 30.2%. A simplified geostatistical model is considered in this work, although geological variability has been successfully incorporated in the framework using state-of-the-art simulation techniques (Wilson, 2021). Ore is mined one parcel at a time, where each parcel is a collection of mining blocks. The size of each parcel X_k for $k = 1, \dots, n_{parcels}$ is a random variable with units of kiloton following a uniform distribution $X_k \sim U(30,50)$. Furthermore, the proportion $p_{2,k}$ of Ore 2 in a parcel is a random variable following a normal distribution $p_{2,k} \sim N(0.3,0.05)$. In this simplified geostatistical model, geological uncertainty is controlled by the standard deviation of $p_{2,k}$, which is called the geostatistical standard deviation σ_{geo} (Navarra et al., 2019).

The current adaptation considers that Ore 2 is more desirable to the centralized iron concentrator, due to its low sulfur content. However, the recent expansion of the mining complex with the opening a new pit, has introduced variability in the mill feed, due to the high sulfur in Ore 1. To address the varied ore feeds, the DRS framework employs practices such as blending and stockpiling to mitigate the impacts of unforeseen changes in ore characteristics due to geological uncertainty. These control strategies operate within two distinct modes, Modes A and B, with different operational policies. Mode A is more productive than Mode B since the multi-stage grinding circuit is offline. This is due to the different blend of Ores 1 and 2 in each mode of operation. While 70% of the complex's production is expected to originate from mine 1, Mode A utilizes a 60%-40% blend for Ores 1 and 2 due to the higher desirability of low sulfur ore. However, a perpetual application of Mode A would lead to frequent Ore 2 stockouts since the proportion of Ore 2 in the blend of Mode A is higher than what is mined in the complex. As such, Mode B is considered a replenishment mode in which a 85%-15% blend of Ores 1 and 2 is utilized to allow a replenishment of the Ore 2 stockpile. Due to uncertainty in incoming feeds, there could be production campaigns in which either Ore 1 or Ore 2 are entirely depleted. As such, the two-mode model is extended to include recourse actions. If the total stockpile level, which is considered as the sum of the Ore 1 and Ore 2 stockpile levels, drops below a certain threshold before a planned shutdown, a contingency mode is triggered, based on the current system state. When the critical ore (Ore 2) is depleted under Mode A, a contingency mode is initiated, reducing the production rate and processing only the available ore type (Ore 1) for a 1-day period to allow Ore 2 to replenish. Similarly, Mode B incorporates the same recourse actions, but with reversed effects. The decision to switch between modes is made during planned shutdowns.

Table 4.2.2-1 summarizes the operating conditions for the adapted DRS framework.

Table 4.2.2-1 Operating Conditions for DRS framework

Mode	Configuration	Throughput (tpd)	Proportion of Ore 1 (%)	Proportion of Ore 2 (%)
Mode A	Regular	15,000	60	40
	Contingency	9,750	100	0
Mode B	Regular	12,000	85	15
	Contingency	6,000	0	100

As shown in the overall mass balance expected at the centralized mill in Table 4.2.2-2, Mode A is expected to consume Ore 2 while Mode B replenishes the Ore 2 stockpile. Contingency modes allow rapid recovery from stockouts by focusing the milling effort on a single ore type, however, these modes are not preferred due to their overall reduction in productivity (35% for Mode A contingency and 50% for Mode B contingency).

Table 4.2.2-2 Overall Mass Balance Expected at the Mill

Mode	Configuration	Ore 1 Throughput (tpd)	Ore 2 Throughput (tpd)	Into Mill (tpd)	Ore 1 Stockpile Balance (tpd)	Ore 2 Stockpile Balance (tpd)
Mode A	Regular	9,000	6,000	15,000	1,500	-1,500
	Contingency	9,750	0	9,750	-2,925	2,925
Mode B	Regular	10,200	1,800	12,000	-1,800	1,800
	Contingency	0	6,000	6,000	4,200	-4,200

Table 4.2.2-3 contains the time segment parameters for the DRS simulation.

Table 4.2.2-3 Time Segments for the DRS

Time Segment	Duration (days)
Production Campaign	30
Contingency Segment	1
Shutdown	1

The generalized flowchart of the DRS framework is shown in Figure 4.2.2-1 (adapted from Wilson, 2021).

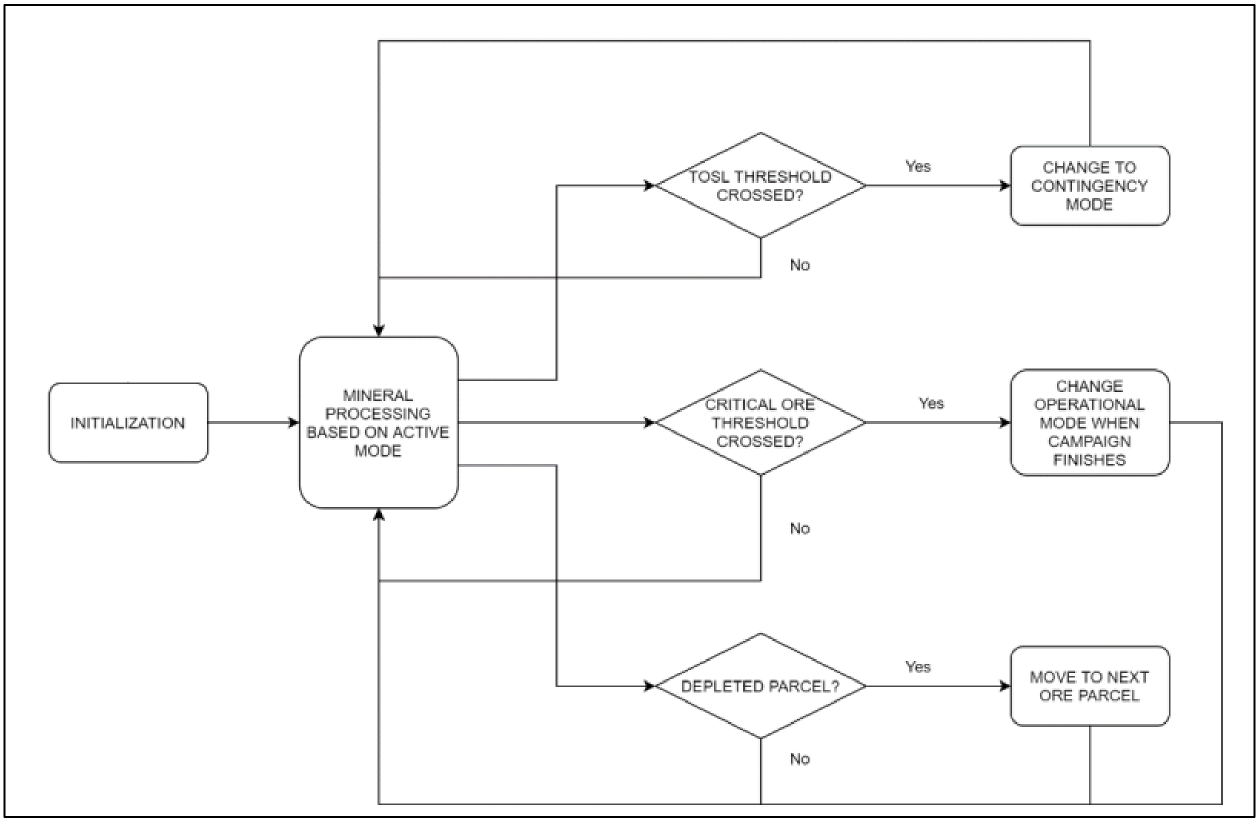

Figure 4.2.2-1 Generalized Flowchart of the DRS framework (adapted from Wilson, 2021)

The DRS framework is entirely implemented on Visual Basic for Applications, with associated macro-enabled Excel sheets for output data visualization.

The framework includes the following assumptions:

1. Both modes have a similar downstream performance (grade of concentrate, recovery…)
2. Mode B requires multi-stage grinding, therefore the production rate of Mode B is 80% that of Mode A, the multi-stage grinding circuit is off-line for Mode A
3. Mode A is more productive than Mode B hence the simulation starts in Mode A
4. Each combined ore feed block is entirely processed prior to loading the next parcel
5. Mining rates exceed plant capacity hence milling rates constitute the operational bottleneck

With the increased variability in ore types in the mill feed resulting from the open-pit expansion into new pushbacks, the DRS framework adapted here employs alternate operational modes A and B, as a control strategy for managing stockpiles. This framework balances the goal of minimizing stockout risk with other objectives, such as reducing stockpile size (and thereby lowering holding and storage costs) and maximizing mill throughput. Thus, the DRS framework serves as a context for multi-objective optimization. As detailed in Chapter 3, a Pareto Optimal solution—which represents a state where no objective can be improved without worsening another—can be identified, by varying state variables in the DRS and comparing KPIs. In the following, the critical level of Ore 2, which triggers a threshold crossing event, is varied, along with the maximum stockpile level to obtain Pareto Optimal solutions.

4.2.3 Pareto Optimal DRS Configuration

Recall from equation (3.1.3-1) of the EOQ problem, the re-order point is proportional to the lead time and the rate of consumption. Hence a deterministic analysis assists in selecting an initial starting point for the critical Ore 2 level of $l_{2,cr} = 1500\frac{t}{day} \times 30\ days = 45{,}000t$. Similarly, the target maximum stockpile level $l_{s,t}$ can be specified by technical services or upper-level management, as a buffer for unplanned shutdowns. The target stockpile size is taken as the sum of the Ore 1 and Ore 2 stockpiles. The company considered in this work recommends 10 days of mill operation, for an initial target stockpile level of 150,000, assuming no contingency.

A deterministic optimal ratio of time spent in Modes A and B can be computed as follows (Navarra et al., 2019)

$$\frac{t_A}{t_B} = \left(\frac{w_{2B}w_{1D} - w_{1B}w_{2D}}{-w_{2A}w_{1D} \pm w_{1A}w_{2D}}\right)\left(\frac{r_B}{r_A}\right) \qquad (4.2.3-1)$$

where t_A and t_B are the times spent in Modes A and B respectively in days, and r_A and r_B are the milling rates of Modes A and B respectively. All other variables were introduced in Chapter 3. In the current scenario, $\frac{t_A}{t_B} = 1.20$.

Similarly, a deterministic optimal average throughput r can be calculated as

$$r = \left(\frac{w_{1A}w_{2B} - w_{2A}w_{1B}}{\left(w_{2B}\left(\frac{r_B}{r_A}\right) - w_{2A}\right)w_{1D} - \left(w_{1B}\left(\frac{r_B}{r_A}\right) - w_{1A}\right)w_{2D}} \right) r_B \qquad (4.2.3-2)$$

In the case study, $r = 13{,}636\ tpd$. These values serve as benchmarks when selecting an optimal $(l_{2,cr}, l_{s,t})$ pair for the simultaneous maximization of throughput and minimization of total stockpile size under uncertainty (similarly to how the ideal vector introduced in Chapter 3 informs the decision-maker on the range of the objective functions). In the following, 25 different scenarios are considered by varying $l_{s,t}$ and $l_{2,cr}$ around their central values, which were obtained deterministically. The KPI to balance against stockpile size is plant throughput, calculated as

$$DRS\ Average\ Throughput\ (tpd) = \frac{Total\ Tonnage\ Milled}{Final\ Simulation\ Time} \qquad (4.2.3-3)$$

Table 4.2.3-1 summarizes the average throughputs for all considered scenarios in tons per day.

Table 4.2.3-1 Average Simulation Throughputs (tpd)

$l_{s,t}$ (kt)	$l_{2,cr}$ (kt)				
	25	**35**	**45**	**55**	**65**
130	13,128	13,174	13,135	13,135	13,129
140	13,136	13,260	13,152	13,135	13,135
150	13,178	13,215	13,155	13,155	13,145
160	13,178	13,229	13,151	13,151	13,141
170	13,230	13,265	13,151	13,151	13,141

From the simulation results, it appears that a target stockpile level of 140,000 t and a critical Ore 2 level of 35,000 t yields a satisfying solution to the multi-objective optimization problem of selecting the maximum throughput configuration with the minimum stockpile size. While the throughputs exhibited by the scenarios are quite close to the deterministic optimal average throughput, the simulations yield consistently lower values. These discrepancies can be explained by the application of contingency segments in the simulation during stockouts, which are inherently less productive and ignored in the deterministic formula.

Table 4.2.3-2 shows the ratio of time $\frac{t_A}{t_B}$ spent in each mode for each considered scenario. There appears to be drastic differences between scenarios that use lower and higher values than the deterministically computed critical Ore 2 level of 45,000 t. A higher critical level of Ore 2 causes the DRS framework to favor lower consumption of Ore 2. This results in more time spent in Mode B, which is the replenishment mode for Ore 2. The configurations with higher critical Ore 2 levels are also less productive since Mode A does not require multi-stage grinding for sulfur control. The ratio of time for the chosen configuration is comparable to the optimally calculated ratio from equation (4.2.3-1) (1.20 vs 1.27).

Table 4.2.3-2 Ratio of Simulation Time Spent in Each Mode

$l_{s,t}$ (kt)	$l_{2,cr}$ (kt)				
	25	**35**	**45**	**55**	**65**
130,000	1.20	1.25	1.09	1.09	1.09
140,000	1.20	1.27	1.09	1.08	1.08
150,000	1.25	1.28	1.08	1.08	1.07
160,000	1.25	1.29	1.07	1.07	1.07

170,000	1.29	1.29	1.07	1.07	1.07

4.2.4 Visualizations

This section presents the visualizations included in the framework implementation's macro-enabled sheets. These visualizations are generated in real-time with the click of a start button and update at each discrete time step corresponding to a threshold crossing event. The DRS is run with the chosen configuration of section 4.2.3 ($l_{s,t} = 140{,}000\ t$ and $l_{2,cr} = 35{,}000\ t$). Figure 4.2.4-1 shows the discrete jumps between the different modes of operation at each simulation clock advance. The figure shows that the decision to switch between modes is made during shutdown segments.

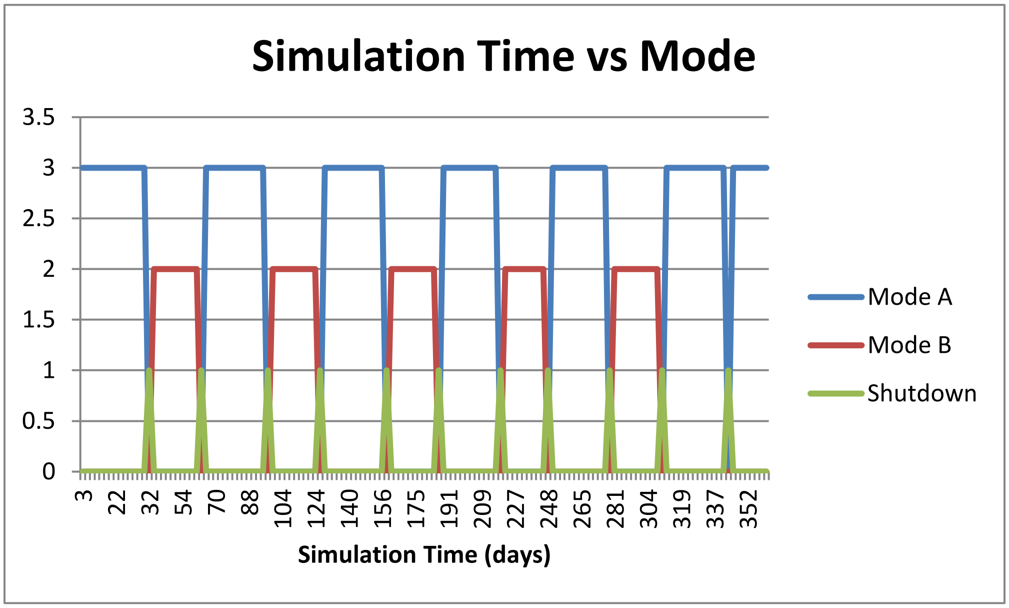

Figure 4.2.4-1 Simulation Time vs Mode for Chosen Configuration

The fluctuations in the levels of Ore 1 and 2 stockpiles are shown in Figure 4.2.4-2. The more productive Mode A is favored here with the total stockpile level consisting mostly of Ore 1 due to the faster consumption of Ore 2, until the last days of the operation where the proportion of Ore 2 exceeds Ore 1. Finally, the DRS framework also outputs the tonnage of iron concentrate produced throughout the simulation, as illustrated in Figure 4.2.4-3. After 1 year of operation, the final concentrate tonnage to be sold on the market is on average 1,240,723 t, after running the DRS framework 100 times with the chosen configuration and different RNG seeds.

As seen on Figure 4.2.4-2, the system enters a contingency segment after around a month of operation due to a lack of Ore 2. This occurs due to the initialization of the total stockpile with the proportions of Ore 2 from the deposit, which is lower than in Mode A. However, this is the only contingency segment encountered and the operation remains productive. On the other hand, a critical Ore 2 level of 15,000 with the target stockpile level kept constant yields multiple contingency segments throughout the year, as shown in Figure 4.2.4-4 resulting in an overall lower throughput of 13,156 tpd.

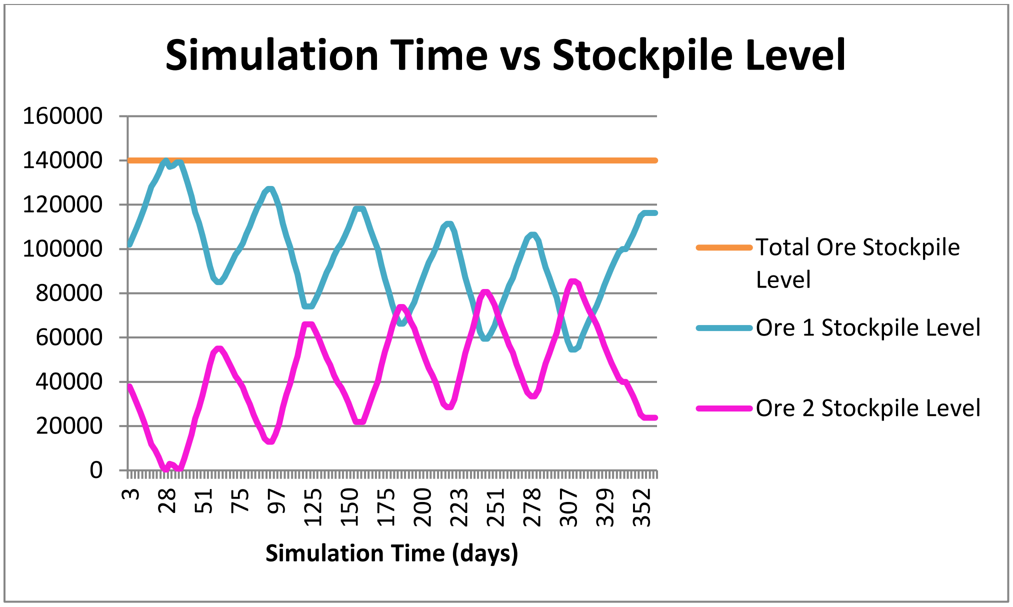

Figure 4.2.4-2 Simulation Time vs Stockpile Level for Chosen Configuration

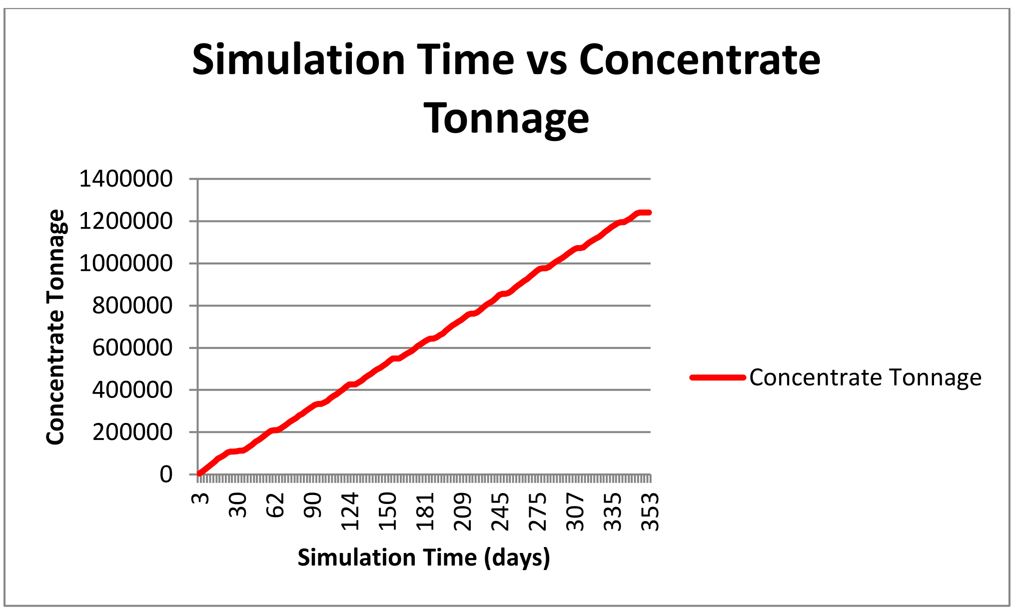

Figure 4.2.4-3 Simulation Time vs Concentrate Tonnage

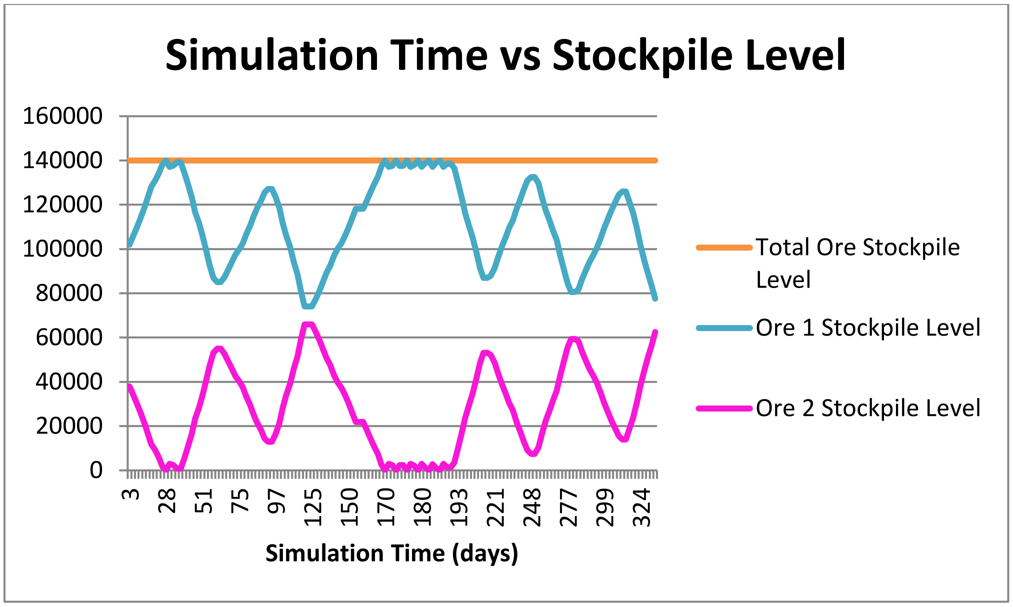

Figure 4.2.4-4 Multiple Contingency Segments with Low Critical Ore 2 Level

A throughput that approaches the deterministic optimum can be found by increasing the target stockpile level to 190,000 t and the critical Ore 2 level to 45,000 t, as shown in Figure 4.2.4-5. For such configuration the throughput is 13,304 tpd, however the larger total stockpile size implies additional operational costs.

The DRS framework presented in this work is of particular interest to the company, since it relates control strategies to mitigate geological risk at the input to output saleable concentrate tonnages. In the next section, a multi-objective optimization (MOOP) model is introduced to optimize concentrate sales to steelmakers, while minimizing production costs across the ironmaking value chain.

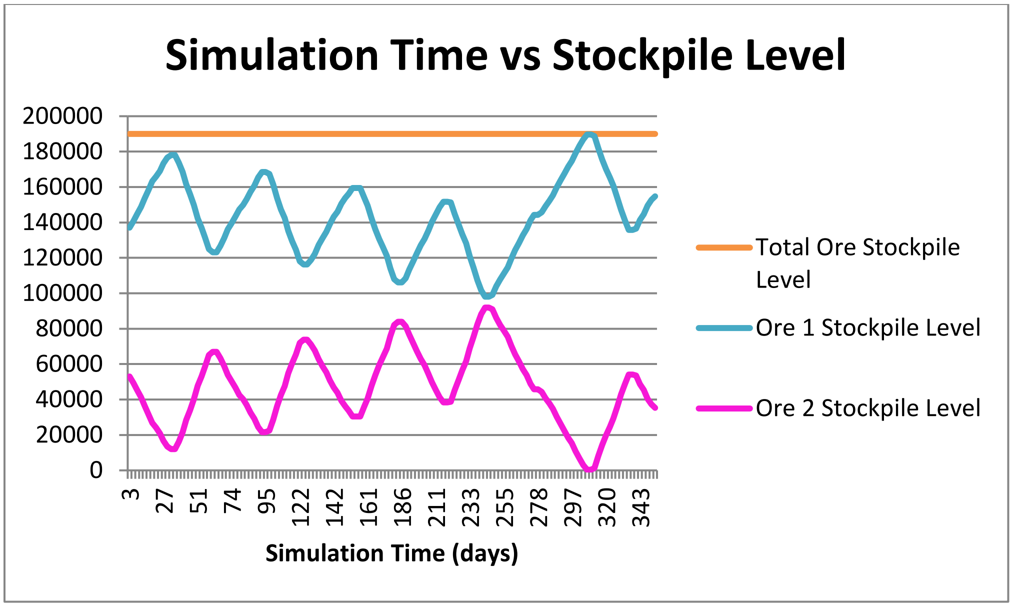

Figure 4.2.4-5 Higher Average Throughput with Larger Stockpiles

4.3 Optimizing Concentrate Sales

The company prides itself on producing high-grade iron concentrate with a 66% Fe content and very low impurities, making it an attractive asset for ironmakers worldwide, as impurities incur penalties on the price of end-product steel (Pownceby, Hapugoda, Manuel, Webster, & MacRae, 2019), and lead to excessive slag volumes. This high-quality product positions the company favorably within the global iron ore market, where the demand for premium quality iron ore is increasing due to diminishing high-grade low impurity deposits. With rising environmental standards, the global iron ore market gained a new dimension of complexity due to stringent emission standards imposed by governments. These environmental regulations add to the existing market influences such as geological variability, market demand, and supply chain logistics. High-quality products are favored under these regulations because they lead to lower emissions during the steelmaking process. For instance, if the iron content of the feedstock to a blast furnace improves by 1%, coke use decreases by 1.5–2%, leading to lower CO_2 emissions (Carpenter, 2012). Consequently, the company is well-placed to capitalize on the growing premium for high-quality iron ore products, ensuring its competitiveness and relevance in a market increasingly driven by quality and sustainability. In this context, the company aims to build an optimization model to determine the most profitable markets for its contracts. By identifying which potential contracts will yield the highest revenue, the company can strategically allocate its high-grade concentrate, maximizing its financial returns while meeting global demand for iron ore products. The company makes use of its industry knowledge to build a blending model including its concentrate production, but also products from its competitors to meet ironmaker output demands and quality requirements. Logistical considerations are included in the model through product pricing that incorporates dynamic freight indices, on top of iron ore spot price assessments and quality differentials, in a free-on-board (FOB) or Cost of Freight to China (CFR China) basis. The objective of maximizing revenue is balanced along with other auxiliary KPIs such as the minimization of either total customer expenditure or CO_2-equivalent emissions.

4.3.1 Global Iron Ore Market Model

The global iron market can be represented as a mathematical model where metallurgical processes such as sintering, blast furnace operations, and direct reduction are described by material balances within a linear programming framework. In the following, the decision variables and parameters used in the model are defined. Subsequently, the objective functions are formulated.

4.3.1.1 Decision Variables and Parameters

Let P be the set of products, F be the set of flux and coke materials for sintering, F' be the set of flux and coke materials for sintering, J be the set of producers, K be the set of blast furnaces and L be the set of direct reduction plants in the model. For all $prod \in P, j \in J, k \in K, f \in F, f' \in F'$ and $l \in L$, the decision variables are defined as:

$prod_{jk}$: Tonnage of product i from supplier j sent to blast furnace k

Y_{fk}: Tonnage of flux, coke added to sinter feed for blast furnace k

$Z_{f'k}$: Tonnage of flux, coke added to blast furnace k burden

The required parameters are:

Products

$\%Fe_{prod\,j}$: Weight proportion of Fe for product $prod$ from supplier j

$\%CaO_{prodj}$: Weight proportion of CaO for product $prod$ from supplier j

$\%MnO_{prodj}$: Weight proportion of MnO for product $prod$ from supplier j

$\%MgO_{prodj}$: Weight proportion of MgO for product $prod$ from supplier j

$\%SiO_{2_{prodj}}$: Weight proportion of SiO_2 for product $prod$ from supplier j

$\%Al_2O_{3_{prodj}}$: Weight proportion of Al_2O_3 for product $prod$ from supplier j

$\%P_{prodj}$: Weight proportion of P for product $prod$ from supplier j

$\%LOI_{prodj}$: Loss on ignition for product $prod$ from supplier j

PI_{prodj}: Value of current price index for product $prod$ from supplier j ($/t CFR China)

$Capacity_{prodj}$: Capacity of product $prod$ from supplier j in the model (t)

Sintering

$\%Fe_{fk}$: Weight proportion of Fe for sintering material f from blast furnace k

$\%CaO_{fk}$: Weight proportion of CaO for sintering material f from blast furnace k

$\%MnO_{fk}$: Weight proportion of MnO for sintering material f from blast furnace k

$\%MgO_{fk}$: Weight proportion of MgO for sintering material f from blast furnace k

$\%SiO_{2_{fk}}$: Weight proportion of SiO_2 for sintering material f from blast furnace k

$\%Al_2O_{3_{fk}}$: Weight proportion of Al_2O_3 for sintering material f from blast furnace k

$\%P_{fk}$: Weight proportion of P for sintering material f from blast furnace k

$\%C_{fk}$: Weight proportion of C for sintering material f from blast furnace k

$\%LOI_{fk}$: Loss on ignition for sintering material f from blast furnace k

$\%Cost_{fk}$: Cost of sintering material f from blast furnace k ($/t)

$pmax_{PFk}$:Maximum proportion of pellet-feed in sinter for blast furnace k

$pmax_{Ck}$:Maximum proportion of concentrate in sinter for blast furnace k

$pmax_{Fk}$:Maximum proportion of flux in sinter for blast furnace k

$pmax_{COk}$:Maximum proportion of coke in sinter for blast furnace k

$\%SD_{max,sk}$/$\%SD_{min,sk}$: Maximum/minimum sinter demand for blast furnace k

$\%Fe_{max,sk}$/$\%Fe_{min,sk}$: Maximum/minimum Fe content in sinter for blast furnace k

$\%CaO_{max,sk}$/$\%CaO_{min,sk}$: Maximum/minimum CaO content in sinter for blast furnace k

$\%MgO_{max,sk}$/$\%MgO_{min,sk}$: Maximum/minimum MgO content in sinter for blast furnace k

$\%SiO_{2_{max,sk}}$/$\%SiO_{2_{min,sk}}$: Maximum/minimum SiO_2 content in sinter for blast furnace k

$\%Al_2O_{3_{max,sk}}$/$\%Al_2O_{3_{min,sk}}$: Maximum/minimum Al_2O_3 content in sinter for blast furnace k

$\%B_{max,sk}$/$\%B_{min,sk}$: Maximum/minimum basicity in sinter for blast furnace k

Blast Furnace

$\%Fe_{f\prime k}$: Weight proportion of Fe for BF material f' from blast furnace k

$\%CaO_{f\prime k}$: Weight proportion of CaO for BF material f' from blast furnace k

$\%MnO_{f\prime k}$: Weight proportion of MnO for BF material f' from blast furnace k

$\%MgO_{f\prime k}$: Weight proportion of MgO for BF material f' from blast furnace k

$\%SiO_{2_{f\prime k}}$: Weight proportion of SiO_2 for BF material f' from blast furnace k

$\%Al_2O_{3_{f\prime k}}$: Weight proportion of Al_2O_3 for BF material f' from blast furnace k

$\%P_{f'k}$: Weight proportion of P for BF material f' from blast furnace k

$\%C_{f'k}$: Weight proportion of C for BF material f' from blast furnace k

$\%LOI_{f'k}$: Loss on ignition for BF material f' from blast furnace k

$\%Cost_{f'k}$: Cost of BF material f' from blast furnace k ($/t)

$\%HMD_{max,k}$/$\%HMD_{min,k}$: Maximum/minimum hot metal demand for blast furnace k

$\%P_{max,k}$/$\%P_{min,k}$: Maximum/minimum P content in BF burden for blast furnace k

$\%Mn_{max,k}$/$\%P_{min,k}$: Maximum/minimum Mn content in BF burden for blast furnace k

$\%Fe_{max,k}$/$\%Fe_{min,k}$: Maximum/minimum Fe content in BF burden for blast furnace k

$\%CaO_{max,k}$/$\%CaO_{min,k}$: Maximum/minimum CaO content in BF burden for blast furnace k

$\%MgO_{max,k}$/$\%MgO_{min,k}$: Maximum/minimum MgO content in BF burden for blast furnace k

$\%SiO_{2_{max,k}}$/$\%SiO_{2_{min,k}}$: Maximum/minimum SiO_2 content in BF burden for blast furnace k

$\%Al_2O_{3_{max,k}}$/$\%Al_2O_{3_{min,k}}$: Maximum/minimum Al_2O_3 content in BF burden for blast furnace k

$\%B_{max,k}$/$\%B_{min,k}$: Maximum/minimum basicity in in BF burden for blast furnace k

$f_{MHM,k}$: Fraction of total Mn in hot metal for blast furnace k

fd_{prodjk}: Fraction of product in descending burden (the rest ends in the flue dust)

Direct Reduction

$\%DRI_{max,l}$/$\%DRI_{min,l}$: Maximum/minimum DRI demand for DR plant l

$\%Fe_{max,l}$/$\%Fe_{min,l}$: Maximum/minimum Fe content in DRI for DR plant l

$\%CaO_{max,l}$/$\%CaO_{min,l}$: Maximum/minimum CaO content in DRI for DR plant l

$\%MgO_{max,l}$/$\%MgO_{min,l}$: Maximum/minimum MgO content in DRI for DR plant l

$\%SiO_{2_{max,l}}$/$\%SiO_{2_{min,l}}$: Maximum/minimum SiO_2 content in DRI for DR plant l

$\%Al_2O_{3_{max,l}}$/$\%Al_2O_{3_{min,l}}$: Maximum/minimum Al_2O_3 content in DRI for DR plant l

Emissions

$CO2_s$: Sintering CO_2 emission factor (t CO_2 /t sinter)

$CH4_s$: Sintering CH_4 emission factor (t CH_4 /t sinter)

$CO2_{BF}$: BF CO_2 emission factor (t CO_2 /t HM)

$CH4_{BF}$: BF CH_4 emission factor (t CH_4 /t sinter)

$CO2_{DR}$: DR CO_2 emission factor (t CO_2 /t HM)

$CH4_{DR}$: DR CH_4 emission factor (t CH_4 /t sinter)

4.3.1.2 <u>Objective functions</u>

Objective 1. Maximize the company's revenue from concentrate sales

$$
\begin{aligned}
Max \sum_{k=1}^{K} price_{Concentrate,Company,k} \times Concentrate_{Company,k} \\
+ \sum_{l=1}^{L} price_{Concentrate,Company,k} \times Concentrate_{Company,l} \\
+ \sum_{k=1}^{K} price_{S_{Concentrate},Company,k} \times S_{Concentrate}{}_{Company,k}
\end{aligned}
$$

$$
\forall\, k \in K \qquad (4.3.1.2-1)
$$

where $S\_Concentrate \in P$ is the portion of total produced concentrate sold to sinter plants.

Objective 2. Minimize total ironmaker expenditures

$$Min \sum_{prod \in P} \sum_{j \in J} cost_{prod,j,k} \times prod_{j,k} + \sum_{f \in F} cost_{Yf,k} \times Y_{f,k} + \sum_{f' \in F'} cost_{Zf',k} \times Z_{f',k} \quad (4.3.1.2-2)$$

Objective 3. Minimize CO2-equivalent emissions

$$Min \sum_{k \in K} CO2_s \times S_k + \sum_{k \in K} \frac{(CH4_s \times S_k) \times 21}{1000} + \sum_{k \in K} CO2_{BF} \times HM_k + \sum_{k \in K} \frac{(CH4_{BF} \times HM_k) \times 21}{1000}$$

$$+ \sum_{l \in L} CO2_{DR} \times DRI_l + \sum_{l \in L} \frac{(CH4_{DR} \times DRI_l) \times 21}{1000} \quad (4.3.1.2-3)$$

where S_k and HM_k are the tonnage of sinter and hot metal produced at blast furnace k respectively and DRI_l the tonnage of DRI produced at DR plant l. A conversion factor of $\frac{21}{1000}$ is used to transform CH_4 emissions to their CO_2 equivalent.

4.3.1.3 Constraints

The model constraints can be divided in four parts: one for product capacities and one for each metallurgical process. It is assumed in the model that each blast furnace k contains an integrated sinter plant, so that agglomerated ore constitutes a portion of the BF descending burden.

Capacity

Using the company's production rate and knowledge on competitors' yearly capacities, the following constraints are established

$$\sum_{k \in K} prod_{j,k} + \sum_{l \in L} prod_{j,l} \leq Capacity_{prod,j} \quad (4.3.1.3-1)$$

Sintering

Sintering Output

$$S_k = \sum_{j \in J} prod_{j,k}(1 - \%LOI_{prodj}) + \sum_{f \in F} Y_{f,k}(1 - \%LOI_{fk}) \qquad (4.3.1.3-2)$$

Fe Output

$$\%Fe_{min_{sk}} S_k \leq \sum_{j \in J} prod_{j,k}(1 - \%LOI_{prodj})\%Fe_{prodj} + \sum_{f \in F} Y_{f,k}(1 - \%LOI_{fk})\%Fe_{fk}$$

$$\leq \%Fe_{max_{sk}} S_k \qquad (4.3.1.3-3)$$

Maximum weight % of materials in sinter mix

$$\sum_{j=1}^{J} PFS_{jk}\left(1 - \%LOI_{PFS_j}\right) \leq pmax_{PFk} \times S_k \qquad (4.1.3-4)$$

$$\sum_{j=1}^{J} CS_{jk}\left(1 - \%LOI_{CS_j}\right) \leq pmax_{Ck} \times S_k \qquad (4.1.3-5)$$

$$\sum_{f=1}^{F} Y_{fk}\left(1 - \%LOI_{f_k}\right) \leq pmax_{fk} \times S_k \qquad (4.1.3-6)$$

Slag constraints

$$\%MgO_{min_{sk}} S_k \leq \sum_{j \in J} prod_{j,k}(1 - \%LOI_{prodj})\%MgO_{prodj} + \sum_{f \in F} Y_{f,k}(1 - \%LOI_{fk})\%MgO_{fk}$$

$$\leq \%MgO_{max_{sk}} S_k \qquad (4.3.1.3-7)$$

$$\%CaO_{min_{sk}} S_k \leq \sum_{j \in J} prod_{j,k}(1 - \%LOI_{prodj})\%CaO_{prodj} + \sum_{f \in F} Y_{f,k}(1 - \%LOI_{fk})\%CaO_{fk}$$

$$\leq \%CaO_{max_{sk}} S_k \qquad (4.3.1.3-8)$$

$$\%SiO_{2_{min_{sk}}}S_k \leq \sum_{j\in J} prod_{j,k}\left(1-\%LOI_{prodj}\right)\%SiO_{2_{prodj}} + \sum_{f\in F} Y_{f,k}\left(1-\%LOI_{fk}\right)\%SiO_{2_{fk}}$$

$$\leq \%SiO_{2_{max_{sk}}}S_k \qquad (4.3.1.3-9)$$

$$\%Al_2O_{3_{min_{sk}}}S_k$$

$$\leq \sum_{j\in J} prod_{j,k}\left(1-\%LOI_{prodj}\right)\%Al_2O_{3_{prodj}} + \sum_{f\in F} Y_{f,k}\left(1-\%LOI_{fk}\right)\%Al_2O_{3_{fk}}$$

$$\leq \%Al_2O_{3_{max_{sk}}}S_k \qquad (4.3.1.3-10)$$

Basicity

$$B_{min,sk} \leq \frac{\sum_{j\in J} prod_{j,k}\left(1-\%LOI_{prodj}\right)\%CaO_{prodj} + \sum_{f\in F} Y_{f,k}\left(1-\%LOI_{fk}\right)\%CaO_{fk}}{\sum_{j\in J} prod_{j,k}\left(1-\%LOI_{prodj}\right)\%SiO_{2_{prodj}} + \sum_{f\in F} Y_{f,k}\left(1-\%LOI_{fk}\right)\%SiO_{2_{fk}}}$$

$$\leq B_{max,sk} \qquad (4.3.1.3-11)$$

Coke Rate

$$Y_{coke,k} = 0.04 \times S_k \qquad (4.3.1.3-12)$$

The rule of thumb of equation (4.3.1.3-12) is used to calculate sintering coke rate and derives from the company's industry knowledge.

Blast furnace

Fe Output

$$\%Fe_{min_{BFk}}DHM_k$$

$$\leq \sum_{prod\in P}\sum_{j\in J} \%Fe_{prodj}fd_{prodjk}prod_{jk} + \%Fe_{sk}fd_{sk}S_k$$

$$+ \sum_{f\prime\in F\prime} \%Fe_{f\prime jk}fd_{f\prime k}Z_{f\prime k}$$

$$\leq \%Fe_{max_{BFk}} DHM_k \qquad (4.3.1.3-13)$$

Phosphorus Output

$$\%P_{min_{BFk}} DHM_k \leq \sum_{prod \in P} \sum_{j \in J} \%P_{prodj} fd_{prodjk} prod_{jk} + \%P_{sk} fd_{sk} S_k + \sum_{f' \in F'} \%P_{f'jk} fd_{f'k} Z_{f'k}$$

$$\leq \%P_{max_{BFk}} DHM_k \qquad (4.3.1.3-14)$$

Manganese Output

$$\begin{aligned} &\%Mn_{min_{BFk}} DHM_k \\ &\qquad \leq \sum_{prod \in P} \sum_{j \in J} \%Mn_{prodj} fd_{prodjk} prod_{jk} + \%Mn_{sk} fd_{sk} S_k \\ &\qquad + \sum_{f' \in F'} \%Mn_{f'jk} fd_{f'k} Z_{f'k} \end{aligned}$$

$$\leq \%Mn_{max_{BFk}} DHM_k \qquad (4.3.1.3-15)$$

where DHM_k is the hot metal demand for blast furnace k. The output hot metals calculated as

$$\begin{aligned} HM_k = \Bigg(&\sum_{prod \in P} \sum_{j \in J} \%Fe_{prodj} fd_{prodjk} prod_{jk} + \%Fe_{sk} fd_{sk} S_k + \sum_{f' \in F'} \%Fe_{f'jk} fd_{f'k} Z_{f'k} \\ &+ \sum_{prod \in P} \sum_{j \in J} \%P_{prodj} fd_{prodjk} prod_{jk} + \%P_{sk} fd_{sk} S_k + \sum_{f' \in F'} \%P_{f'jk} fd_{f'k} Z_{f'k} \\ &+ \sum_{prod \in P} \sum_{j \in J} \%Mn_{prodj} fd_{prodjk} prod_{jk} + \%Mn_{sk} fd_{sk} S_k \\ &+ \sum_{f' \in F'} \%Mn_{f'jk} fd_{f'k} Z_{f'k} \Bigg) \times 1.047 \end{aligned}$$

where 1.047 is to account for 4.5% of output carbon in the hot metal.

Slag constraints

The slag constraints for the BF portion are similar to equations (4.3.1.3-7) to (4.3.1.3-11).

Coke

$$Z_{coke,k} = 0.247 \times B + 415 \qquad (4.3.1.3-16)$$

Equation (4.3.1.3-16) relates the coke rate of blast furnace k to the descending burden B (Bhagat, Ray, & Gupta, 1991).

Direct reduction

DRI Output

Since the Direct Reduction process involves solid-solid reactions, there is no slag formation and the mass balance equations presented above for Fe, CaO, MgO, SiO_2 and Al_2O_3 are adapted to obtain the output DRI tonnage DRI_l.

Natural Gas

The quantity of natural gas (NG) in m^3 can be computed using an energy factor of 10 GJ/ t DRI and a conversion factor of 25.5 m^3/GJ NG.

$$NG_l = 255.5 \times DRI_l \qquad (4.3.1.3-17)$$

4.3.2 Example

In the following sections, the model presented above is fully applied to a case study involving the company and two of its main competitors, located in Australia and Brazil. These producers sell to three primary customers: two integrated blast furnaces with coke and sintering plants in China and Europe, and a direct reduction plant in the Middle East. Table 4.3.2-1 summarizes all saleable products for each producer with their associated yearly capacities. Recall that the yearly capacity for the company's concentrate was obtained from the DRS framework.

Table 4.3.2-1 Product Capacities

Producer	Product	Capacity (Mtpy)
Company	Concentrate (66%)	1.2
Brazil	Sinter Fines (66.5%)	0.2
	Pellet-feed Fines (66.5%)	0.3
	BF Pellets (65%)	0.4
	DR Pellets (67.5%)	0.75
	Lump Ore (63%)	0.2
Australia	Sinter Fines (58%)	0.35
	Pellet-feed Fines (66.5%)	0.1
	BF Pellets (65%)	0.35
	DR Pellets (67.5%)	0.5
	Lump Ore (63%)	0.12

The chemical composition of the products is given in Table 4.3.2-2.

Table 4.3.2-2 Chemical Composition of the Products

Producer	Product	Fe (%)	SiO_2 (%)	Al_2O_3 (%)	P (%)	S (%)	MnO (%)	CaO (%)	MgO (%)	LOI (%)
Company	Concentrate (66%)	66	4.42	0.27	0.014	0.007	0.08	0.1	0.1	0.18
Brazil	Sinter Fines (66.5%)	65	1.4	1.3	0.055	0.02	0.65	0.1	0.1	6.7
	Pellet-feed Fines (66.5%)	66.5	1.4	1.7	0.04	0.02	0.95	0.1	0.1	6.7
	BF Pellets (65%)	65	2.2	2	0.045	0.02	0.23	0.1	0.1	1.8
	DR Pellets (67.5%)	67.5	1.6	0.4	0.05	0.02	0.18	1	0.1	1.8
	Lump Ore (63%)	63	2.3	2.2	0.06	0.025	0.95	0.1	0.1	1.8
Australia	Sinter Fines (58%)	58	6	1.5	0.05	0.02	0.24	0.1	0.1	7
	Pellet-feed Fines (66.5%)	66.5	3.8	0.8	0.08	0.004	0.18	0.1	0.1	7
	BF Pellets (65%)	65	5	0.35	0.02	0.003	0.2	0.1	0.1	3
	DR Pellets (67.5%)	67.5	3.5	0.38	0.015	0.0035	0.15	1	0.1	3
	Lump Ore (63%)	63	4.8	1.5	0.04	0.004	0.95	0.1	0.1	3

The chemical composition of the sintering and blast furnace fluxes and coke is given in Table 4.3.2-3.

Table 4.3.2-3 Chemical Composition of the Fluxes and Fuels

Customer	Material	Cost ($/t)	Fe (%)	LOI (%)	MgO (%)	CaO (%)	SiO_2 (%)	Al_2O_3 (%)	C (%)
Europe	Sintering Coke	280	1.18	77.52	0	0.71	6.58	3.23	83.84
	Sintering Lime	110	0.78	40.42	0.42	50.85	4.05	0.76	0
	Sintering Dolomite	110	0	44.11	25	31.25	1.02	0.45	0
	BF Coke	300	2.5	84.5	0	0	8.2	1.4	85.47
	BF Lime	110	0.25	45.43	0.9	52.53	3	1.5	0
	BF Dolomite	100	0	48	25	34	0.5	0.1	0
China	Sintering Coke	200	1.5	79	0	0.2	7.9	2.9	79
	Sintering Lime	78	0.76	43.9	0.41	47.85	3.9	0.96	0
	Sintering Dolomite	98	0	44.11	25	31.25	1.02	0.45	0
	BF Coke	205	2.5	84.5	0	0	8.2	1.4	85.47
	BF Lime	85	0.25	45.3	0.9	54	3	1.5	0

	BF Dolomite	80	0	48	25	34	0.5	0.1	0
Middle East	Natural Gas	0.1 $/m^3	0	0	0	0	0	0	75

Using the formulas presented in Chapter 1, the price of each product is computed and detailed in Tables 4.3.2-4, 4.3.2-5 and 4.3.2-6. The freight cost from Canada to China is calculated using an adjusted c_3 (Tubarão-Qingdao) factor multiplied by 1.2 to cover for the nautical distance difference from Tubarão to Sept-Iles, where iron ore shipments depart. Freight costs for shipments from Australia to China use the c_5 index (Dampier-Qingdao). Similarly, shipments to Europe use a c_2 index (Tubarão-Rotterdam) that is adjusted based on distance differences. Price premiums are included for pellets and lump ore.

Table 4.3.2-4 Product Prices to China

Producer	Product	Fe (%)	FOB Price Index ($/t)	Fe Adjustment ($/t)	Premium /Discount ($/t)	Freight ($/t)	Sellings costs ($/t)	CFR Price ($/t)
Company	Concentrate (66%)	66.2	110.1	112.1	1	29.7	6	148.8
Brazil	Sinter Fines (66.5%)	65	110.1	110.1	0	24.79	10	144.89
	Pellet-feed Fines (66.5%)	66.5	113	Included	0	24.79	10	147.79
	BF Pellets (65%)	65	154.4	Included	0	24.79	10	189.19
	DR Pellets (67.5%)	67.5	165.6	Included	0	24.79	10	200.4

	Lump Ore (63%)	63	122.0	Included	0	24.79	10	156.8
Australia	Sinter Fines (58%)	58	98.3	98.3	0	8.7	4	111
	Pellet-feed Fines (66.5%)	66.5	113	Included	0	8.7	4	125.7
	BF Pellets (65%)	65	154.4	Included	0	8.7	4	167.1
	DR Pellets (67.5%)	67.5	165.6	Included	0	8.7	4	178.3
	Lump Ore (63%)	63	122.0	Included	0	8.7	4	134.7

Table 4.3.2-5 Product Prices to Europe

Producer	**Product**	**Fe (%)**	**FOB Price Index ($/t)**	**Fe Adjustment ($/t)**	**Premium /Discount ($/t)**	**Freight ($/t)**	**Sellings costs ($/t)**	**CFR Price ($/t)**
Company	Concentrate (66%)	66.2	110.1	112.13	-2	5.13	5	120.2
Brazil	Sinter Fines (66.5%)	65	110.1	110.1	0	10.3	6	126.4
	Pellet-feed Fines (66.5%)	66.5	113	Included	0	10.3	6	129.3
	BF Pellets (65%)	65	154.4	Included	0	10.3	6	170.7

	DR Pellets (67.5%)	67.5	165.6	Included	0	10.3	6	181.9
	Lump Ore (63%)	63	122.1	Included	0	10.3	6	138.3
Australia	Sinter Fines (58%)	58	98.3	98.3	1	22.02	11	132.32
	Pellet-feed Fines (66.5%)	66.5	113.0	Included	1.0	22.0	11.0	147.0
	BF Pellets (65%)	65.0	154.4	Included	1.0	22.0	11.0	188.4
	DR Pellets (67.5%)	67.5	165.6	Included	1.0	22.0	11.0	199.7
	Lump Ore (63%)	63.0	122.1	Included	1.0	22.0	11.0	156.1

Table 4.3.2-6 Product Prices to the Middle East

Producer	Product	Fe (%)	FOB Price Index ($/t)	Fe Adjustment ($/t)	Premium /Discount ($/t)	Freight ($/t)	Sellings costs ($/t)	CFR Price ($/t)
Company	Concentrate (66%)	66.2	110.1	112.1	0.0	24.8	10.0	146.9
Brazil	Sinter Fines (66.5%)	65.0	110.1	110.1	0.0	17.2	9.0	136.3
	Pellet-feed Fines (66.5%)	66.5	113.0	Included	0.0	17.2	9.0	139.2
	BF Pellets (65%)	65.0	154.4	Included	0.0	17.2	9.0	180.6

	DR Pellets (67.5%)	67.5	165.6	Included	0.0	17.2	9.0	191.8
	Lump Ore (63%)	63.0	122.1	Included	0.0	17.2	9.0	148.3
Australia	Sinter Fines (58%)	58.0	98.3	98.3	-1.0	12.1	7.0	116.4
	Pellet-feed Fines (66.5%)	66.5	113.0	Included	-1.0	12.1	7.0	131.1
	BF Pellets (65%)	65.0	154.4	Included	-1.0	12.1	7.0	172.5
	DR Pellets (67.5%)	67.5	165.6	Included	-1.0	12.1	7.0	183.7
	Lump Ore (63%)	63.0	122.1	Included	-1.0	12.1	7.0	140.2

Finally, Table 4.3.2-7 summarizes the customer's demand and product quality requirements.

Table 4.3.2-7 Summary of Output Product Requirements

Customer	Process	Fe (%)	MgO (%)	CaO (%)	SiO_2 (%)	Al_2O_3 (%)	Basicity	Output (kt)
Europe	Sintering	51-61	0.7-2.2	8.9-7.4	5.1-4	2.2-1	3.0-1.4	200-300
	BF (HM+Slag)	93.5-95.5 (HM)	2-4 (slag)	35-45 (slag)	38-25 (slag)	15-7 (slag)	2.9-1.7	750
China	Sintering	50-62	0.6-3.3	8.5-7.5	9.1-2	5.4-1.7	2.8-1.4	100-300

	BF (HM+Slag)	93.5-95.5 (HM)	2.3-4.5 (slag)	37-45 (slag)	33-27 (slag)	15-7 (slag)	3.2-1.7	850
Middle East	DR	89.5-92.5	0.2-0.1	2-1	3-1	0.6-0	-	650

4.3.2.1 Multi-Objective Optimization

The mathematical model presented in this work is flexible in that it can accommodate multiple objectives depending on the company's strategy and needs. In the following, the results of different configurations of objective functions are presented and discussed. For all implementations, the ε-constraint is used by transforming secondary objectives to constraints. Five upper bounds are established using the company's industry knowledge and are used to trace a trade-off curve for decision-making. For simplicity's sake, the following examples use two objectives at most, so that the Pareto Optimal front is analyzed in 2D, although all three objectives presented in section 4.3.1 can be optimized simultaneously using the same methods.

Minimizing Customer Expenditure

The mathematical model is optimized with the objective of minimizing customer expenditures when the decision maker wants to compare the performance and attractivity of its products in the market compared to its competitors. Under this configuration, the customers negotiate ore prices with all producers close to, or on a common contract-of-affreightment (COA) date. The customers' strategy is to select the ore proportioning that minimizes both purchasing costs and the impact on metallurgical plant performance. Since the example involves three customers, three objective functions corresponding to the total expenditure of each customer could be formulated and the MOOP could be solved using the ε-constraint method. However, since in this example the minimization of each customer's expenditure is equally important, a linear combination of the objective functions with equal weights is formulated (equation 4.3.1.2-2), and the multi-objective optimization problem (MOOP) is solved using the single-objective Simplex method. The model is formulated on Excel and the Solver add-in is used to solve it. Table 4.3.2.1-1 shows the tonnage of products sold and revenue generated by each company. The expenditure of each customer is detailed in Table 4.3.2.1-2.

Table 4.3.2.1-8 Realized Product Sales per Producer (Minimum Expenditure)

Producer	**Product**	**Tonnage Sold to China (kt)**	**Tonnage Sold to Europe (kt)**	**Tonnage Sold to Middle East (kt)**	**Revenue (M$)**
Company	Concentrate (66%)	523	688	0	165
Brazil	Sinter Fines (66.5%)	146	54	0	180
	Pellet-feed Fines (66.5%)	27	272	0	
	BF Pellets (65%)	0	0	0	
	DR Pellets (67.5%)	0	0	589	
	Lump Ore (63%)	0	0	0	
Australia	Sinter Fines (58%)	108	72	0	156
	Pellet-feed Fines (66.5%)	16	32	0	
	BF Pellets (65%)	314	0	0	

	DR Pellets (67.5%)	0	0	302	
	Lump Ore (63%)	120	0	0	

Under a minimum customer expenditure scenario, the company's sales are balanced between the two integrated blast furnaces in China and Europe. The Chinese customer relies on a mix of ores predominantly from the company and the Australian producer. The Middle Eastern direct reduction plant imports DR pellets exclusively from Brazil and Australia.

Table 4.3.2.1-9 Customer Expenditure (Minimum Expenditure)

Customer	**Total Expenditure (M$)**
Europe	295
China	313
Middle East	185
Total	793

The revenue generated by the company from this optimization model gives a lower bound on potential revenue.

Maximizing the Company's Revenue

Assuming the company has prior knowledge of its competitors forecasted yearly saleable product tonnages and that worldwide contracts can be negotiated by the technical marketing team with company leverage at a prior date to other competitors, the model is optimized to maximize the company's revenue by selecting the most lucrative contracts. In this implementation, competitors realize sales solely on the basis of fulfilling the customer's output product quality requirements. The customers' budgets are assumed to be infinite. The revenue generated from this configuration provides an upper bound on the company's potential profits. Table 4.3.2.1-3 shows the realized product sales per producer under the maximum company revenue scenario.

Table 4.3.2.1-10 Realized Product Sales per Producer (Maximum Company Revenue)

Producer	Product	Tonnage Sold to China (kt)	Tonnage Sold to Europe (kt)	Tonnage Sold to Middle East (kt)	Revenue (M$)
Company	Concentrate (66%)	942	299	0	176
Brazil	Sinter Fines (66.5%)	26	92	0	210
	Pellet-feed Fines (66.5%)	16	229	0	
	BF Pellets (65%)	0	0	0	
	DR Pellets (67.5%)	0	0	750	
	Lump Ore (63%)	122	0	0	
Australia	Sinter Fines (58%)	162	130	0	143
	Pellet-feed Fines (66.5%)	0	48	0	
	BF Pellets (65%)	0	350	0	
	DR Pellets (67.5%)	0	0	143	

	Lump Ore (63%)	0	0	0	

In this scenario, the company's sales are heavily skewed towards China due to higher profits per ton of concentrate sold. The Australian producer, unable to compete in China, meets the unfulfilled demand in Europe because of the company's reduced sales in that region. The reduced DR pellet imports from Australia are attributed to the higher allowed expenses for the Middle Eastern customer, that favors Brazilian pellets.

The expenditure of each customer is detailed in Table 4.3.2.1-4.

Table 4.3.2.1-11 Customer Expenditure (Maximum Company Revenue)

Customer	Total Expenditure (M$)
Europe	335
China	305
Middle East	187
Total	793

European expenditure is significantly higher than the previous scenario due to increased Australian imports. It is interesting to note that for the company, a heavily skewed concentrate sale balance towards China only results in a slight increase of Chinese expenditure (293M$ vs 305M$).

Maximizing the Company's Revenue and Minimizing Customer Expenditure

A more realistic implementation of the previous single-objective optimization problem benefits from economic considerations from the end of the customers, that simultaneously want to minimize their overall expenditure. The two above implementations provided a lower bound, and an upper bound, on the company's potential revenue respectively. In this example, each customer is assigned 5 different ε values that act as upper bounds on expenditures. The range of ε values is defined by $\varepsilon_{min,cus}$, corresponding to the expenditure of each customer under the minimum expenditure scenario, and $\varepsilon_{max,cus}$, which is the expenditure under the maximum revenue scenario. The ε values for China are in decreasing order since lowering European expenditure leads to increased Chinese expenditure.

Table 4.3.2.1-5 details the chosen ε values (M$) to trace the Pareto front.

Table 4.3.2.1-12 Chosen ε values (M$) (MOOP 1)

Customer	ε_{min}	ε_1	ε_2	ε_3	ε_{max}
Europe	295	305	315	325	335
China	314	312	310	308	306
Middle East	185	185.5	186	186.7	187
Total	794	802.5	811	819.7	828

The single-objective linear program of maximizing the company’s revenue is solved 5 times, once for each set of ε constraints. Table 4.3.2.1-6 summarizes the results after solving. Figure 4.3.2.1-1 shows the Pareto front obtained by the ε-constraint method. The solutions on the Pareto front are non-dominated and provide optimal trade-offs between maximizing the company’s revenue and minimizing total customer expenditure. The decision-maker can choose a scenario based on market conditions and past information on customer behavior.

Table 4.3.2.1-13 Company Revenue (M$) (MOOP 1)

Customer	ε_{min}	ε_1	ε_2	ε_3	ε_{max}
Company Revenue	164.9	170	173	175.8	176.1

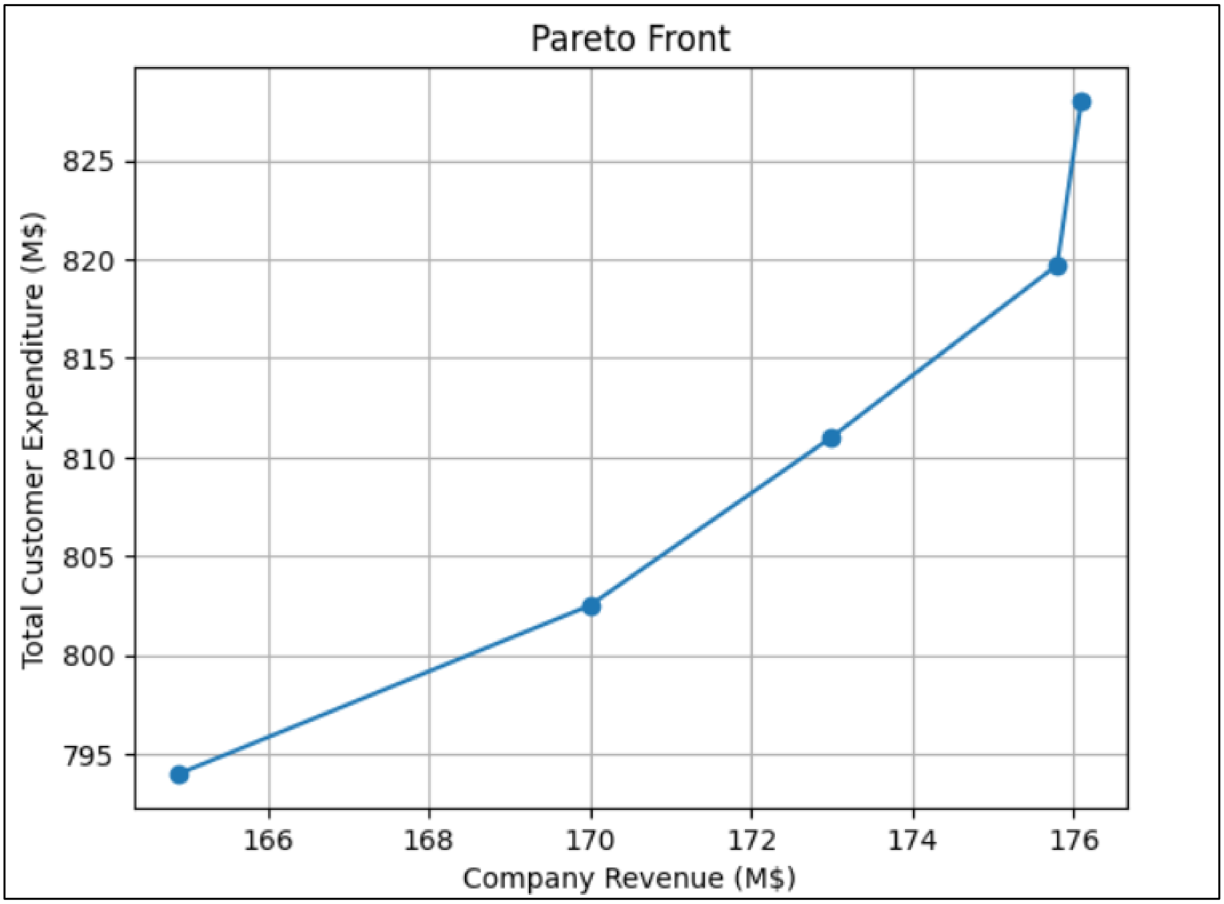

Figure 4.3.2.1-1 Pareto Front (MOOP 1)

The Pareto front is convex, which shows that marginal increases in the company's revenue require substantial increases in total customer expenditure. Table 4.3.2.1-7 shows product sales for scenario ε_{max} which yields the highest company revenue.

Table 4.3.2.1-14 Realized Product Sales per Producer (MOOP 1)

Producer	Product	Tonnage Sold to China (kt)	Tonnage Sold to Europe (kt)	Tonnage Sold to Middle East (kt)	Revenue (M$)
Company	Concentrate (66%)	942	299	0	176.1
Brazil	Sinter Fines (66.5%)	95	92	0	174
	Pellet-feed Fines (66.5%)	0	228	0	
	BF Pellets (65%)	0	0	0	
	DR Pellets (67.5%)	0	0	589	
	Lump Ore (63%)	39	0	0	
Australia	Sinter Fines (58%)	47	130	0	172
	Pellet-feed Fines (66.5%)	12	48	0	
	BF Pellets (65%)	0	350	0	
	DR Pellets (67.5%)	0	0	302	
	Lump Ore (63%)	120	0	0	

Maximizing the Company's Revenue and Minimizing CO2 equivalent emissions

In this section, the multi-objective optimization model is used to maximize the company's revenue while minimizing CO_2 emissions (equation 4.3.1.2-3). CH_4 emissions are also accounted for and transformed to their CO_2-equivalent tonnage. Table 4.3.2.1-8 shows the chosen ε values.

Table 4.3.2.1-15 Chosen ε values (Mt CO_2) (MOOP 2)

Customer	ε_{min}	ε_1	ε_2	ε_3	ε_{max}
Europe	1.055	1.06	1.065	1.07	1.075
China	1.21	1.205	1.2	1.195	1.19
Middle East	0.29	0.30	0.31	0.32	0.33
Total	2.555	2.565	2.575	2.585	2.595

Table 4.3.2.1-9 details the results after solving. It is to be noted that there is lower variability in the feasible range of carbon emissions since these are highly tied to the coke rate for the integrated blast furnaces, and the DRI output for the DR plant.

Table 4.3.2.1- 16 Company Revenue (M$) (MOOP 2)

Customer	ε_{min}	ε_1	ε_2	ε_3	ε_{max}
Company Revenue	173	173.6	174.4	175.3	176.1

Figure 4.3.2.1-2 shows the Pareto front obtained by the ε-constraint method. The Pareto front is almost linear, due to the proportional relationship between coke rates and blast furnace burden.

Furthermore, CO_2 equivalent emissions for the DR plant are computed using an emission coefficient and are thus proportional to the output DRI tonnage.

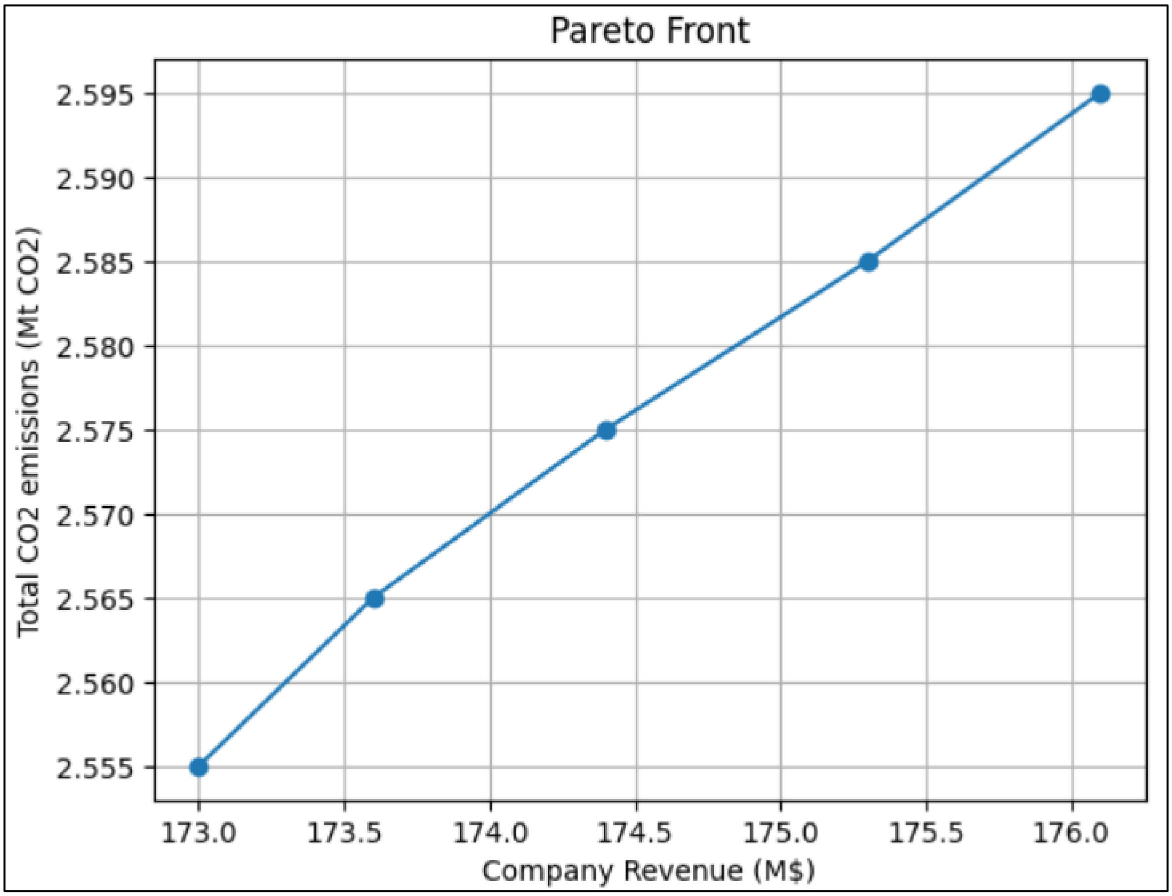

Figure 4.3.2.1-2 Pareto Front (MOOP 2)

This section introduced an ore proportioning model that integrates logistical considerations for the global iron ore market. The model encompasses various metallurgical processes, including blast furnace operation, sintering, and direct reduction. Its flexibility allows for application in multi-objective optimization scenarios to derive different sets of Pareto optimal solutions representing trade-offs between competing objectives. By providing the distribution of saleable products from iron producers in the market, decision-makers can gain a clearer picture of optimal global trades and compare the model's output to real-world data. Discrepancies could reveal trade agreements between competitors and customers offering preferential prices.

CHAPTER 5. CONCLUSIONS AND FUTURE WORK

5.1 Conclusions

The objective of this thesis was to extend the multi-mode Discrete Rate Simulation (DRS) framework, introduced by Navarra et al. (2019) to test control strategies along the mine-to-mill profile amidst geological uncertainty, by integrating a mill-to-market multi-objective optimization model. This approach effectively combines two areas of Operations Research: simulation and mathematical optimization. This thesis specifically comes in response to a need for decision-making tools in the mining industry that bridge the gap between mineral processing output tonnages and global commodity markets. In the DRS portion of this work, an iron concentrator's performance is stabilized amidst uncertain heterogeneous feeds, resulting from geological and geometallurgical factors, by employing operational policies that integrate ore stockpiling and blending with alternate modes of operation. In Chapter 4, a case study illustrates the yearly production of an iron mill to obtain the total concentrate tonnage to be sold on the global market. The case study introduces the simulation-based optimization of the DRS framework's control variables to balance Key Performance Indicators (KPIs) such as stockpile size and throughput. Using this output concentrate tonnage and industry knowledge on competitor's saleable product capacities, a decision-maker can benefit from a blending model, with logistical considerations related to bulk ore carrying, to understand market dynamics and product movements between producers and customers. As this work specifically addresses the iron industry, a mathematical model of the primary metallurgical processes responsible for the overwhelming majority of worldwide iron production is formulated. These processes, which are thoroughly reviewed in Chapter 2, include integrated blast furnace (BF) plants, which encompass feed preparation through fine ore amalgamation, also known as sintering, and direct reduction (DR). As discussed, the mathematical model is a large-scale material balance model to control end product quality requirements and output tonnages. It includes logistical considerations with the inclusion of the Baltic Exchange's Capesize Indices, introduced in Chapter 1, for freight cost calculations as well as greenhouse gas emissions accounting. The model informs the decision-maker on product flows between producers and customers. The mathematical model is flexible in that it can accommodate multiple potentially conflicting objectives and generate so-called Pareto Optimal solutions which offer non-inferior trade-offs for the decision-maker. Chapter 4 explores different formulations of the model as single-objective linear programs, either to minimize customer expenditure or to maximize a company's revenue, and extensions to multi-objective linear programs that consider both objectives simultaneously.

While the DRS framework has proven effective in stabilizing iron concentrator performance and optimizing mine-to-market operations, it is valuable to consider how alternative modeling approaches, such as Agent-Based Modeling (ABM) and System Dynamics (SD), might approach similar problems differently. DRS focuses on simulating the performance of continuous processes, such as the iron concentrator, by discretizing time and capturing variations in feed material and operational states. It is particularly strong in scenarios where the timing of events and the sequence of operations are critical, as it can model the dynamic response of the system to changes in input variables like ore characteristics. In contrast, ABM would model the iron concentrator and its associated market environment by representing each component (e.g., the concentrator, suppliers, logistics providers, and customers) as autonomous agents with their own decision-making processes and goals. ABM would emphasize the interactions and strategies of these agents, potentially revealing emergent behaviors such as competitive dynamics that DRS might not capture (machine failure, integration of additional processes or machines in the analysis…). On the other hand, SD would model the feedback loops and time delays that govern the long-term behavior of the mine-to-market system. Instead of simulating individual events in detail like DRS, SD would model the accumulation and depletion of stockpiles, the impact of production decisions on market prices, and the long-term sustainability of operations, offering insights into the long-term consequences of decisions that might not be immediately apparent.

Despite the strengths of the proposed method, implementing the integrated DRS and multi-objective optimization model presents several challenges. One significant challenge is the computational complexity involved in simulating and optimizing large-scale, continuous processes over extended periods, particularly when integrating geological uncertainty and market dynamics. The need for high-resolution data on feed characteristics, processing conditions, and market parameters also poses a challenge, as such data may be difficult to obtain or subject to significant variability. Additionally, aligning the proposed method with the decision-making processes of different stakeholders in the mining supply chain requires careful consideration of their varying objectives and constraints, which may conflict or evolve over time. The development of user-friendly interfaces and visualization tools to interpret the results of the model is crucial to ensure its practical adoption by industry practitioners. Finally, the integration of environmental and logistical considerations, such as greenhouse gas emissions (Tier 1, Tier 2 and Tier 3 data) and freight costs (Baltic indices), adds another layer of complexity that must be carefully managed to ensure the model's outputs are both accurate and actionable. Addressing these challenges will be critical to the successful implementation and broader adoption of the proposed method in the mining industry.

5.2 Future Work

A key aspect of the mathematical model for the global iron market presented in this thesis is the determination of saleable product costs. When solving the model under a particular scenario of producers and customers, it is assumed that the decision-maker is knowledgeable about current iron ore price indices and is confident that these prices will remain relatively stable at the time of sales. This stability is crucial to ensure that the analysis of the distribution of product flows remains relevant and accurate. However, price indices, as well as quality differentials, are dynamic in nature, which would require higher-level knowledge on market trends to set iron prices. To make the model an effective forecasting tool over long planning periods, reinforcement learning (RL) enabled tools, such as Long Short-Term Memory (LSTM) networks, could be employed to forecast prices. LSTM networks are particularly adept at handling time series data and capturing long-term dependencies, making them suitable for predicting fluctuating iron ore prices.

In the present work, an average output tonnage calculated from 100 simulations using a Pareto Optimal configuration of stockpile size and critical Ore 2 level was used as the input for the deterministic mathematical model of the global iron ore market, for simplicity’s sake. However, this raises concerns about the ability of the model to capture risk propagation into the market, since the distribution of outputs is collapsed into a single average output. To consider the entire distribution of concentrate tonnage outputs from the DRS framework, the mathematical model could be extended to a stochastic linear program since the incorporation of stochastic elements would allow the model to account for the variability and uncertainty inherent in the production process. If the range of variability in the concentrate tonnage output is of interest, the deterministic linear program could be formulated as a robust optimization problem by considering both the worst-case and best-case scenarios in terms of yearly saleable product capacity. Two problems with constraints $a^T x \leq b_{min}$ and $a^T x \leq b_{max}$ could be solved respectively, and an uncertainty range $[b_{min}, b_{max}]$ could be defined. Otherwise, since the output tonnage probability distribution can readily be defined by fitting techniques, chance-constrained optimization techniques can be used where the objective is to ensure the feasibility of the solutions for a pre-defined probability level.

The mathematical model presented in this work includes material balance considerations but could be extended with thermochemical constraints that ensure the conservation of energy for all metallurgical processed covered. Furthermore, metallurgical properties such as Reduction Degradation Index (RDI) and Reducibility Index (RI) of ores could be added in the form of constraints.

REFERENCES

2023 World Steel in Figures. (2023). https://worldsteel.org/wp-content/uploads/World-Steel-in-Figures-2023-4.pdf

Agalianos, K., Ponis, S. T., Aretoulaki, E., Plakas, G., & Efthymiou, O. (2020). Discrete event simulation and digital twins: review and challenges for logistics. *Procedia Manufacturing*, *51*, 1636-1641.

Battle, T., Srivastava, U., Kopfle, J., Hunter, R., & McClelland, J. (2024). The direct reduction of iron. In *Treatise on process metallurgy* (pp. 89-149). Elsevier.

Béchara, R., Hamadeh, H., Mirgaux, O., & Patisson, F. (2018). Optimization of the iron ore direct reduction process through multiscale process modeling. *Materials*, *11*(7), 1094.

Benayoun, R., De Montgolfier, J., Tergny, J., & Laritchev, O. (1971). Linear programming with multiple objective functions: Step method (STEM). *Mathematical programming*, *1*(1), 366-375.

Bhagat, R. P., Ray, H. S., & Gupta, S. K. (1991). Improvement in Performance of the Blast Furnace at Bhilai through Statistical Analysis and lmprovement in Burden Preparation. ISIJ International, 31(7), 669-676.

Canada, N. R. (2024, March 12). *Iron ore facts*. Natural Resources Canada. https://natural-resources.canada.ca/our-natural-resources/minerals-mining/mining-data-statistics-and-analysis/minerals-metals-facts/iron-ore-facts/20517

Carpenter, A. (2012). CO2 abatement in the iron and steel industry. *IEA Clean Coal Centre*, *25*, 193.

Chakrabarti, A. K. (2006). *Steel making*. PHI Learning Pvt. Ltd..

Chen, X., Molina-Cristóbal, A., Guenov, M. D., Datta, V. C., & Riaz, A. (2019). A novel method for inverse uncertainty propagation. *Advances in Evolutionary and Deterministic Methods for Design, Optimization and Control in Engineering and Sciences*, 353-370.

Chong, E. K., & Żak, S. H. (2013). *An introduction to optimization* (Vol. 75). John Wiley & Sons.

Clout, J. M. F., & Manuel, J. R. (2015). Mineralogical, chemical, and physical characteristics of iron ore. In *Iron Ore* (pp. 45-84). Woodhead Publishing.

da Silva Guimarães, P. G., Borges, C. C. H., & Arbex, W. A. (2020). MULTIOBJECTIVE PIG IRON COST OPTIMIZATION USING SIMPLEX PROJECTION. Revista Mundi Engenharia, Tecnologia e Gestão (ISSN: 2525-4782), 5(6).

Dai, Z. (2021, June). Sintering Proportioning Optimization: Use LP and GA-CSO. In *2021 3rd World Symposium on Artificial Intelligence (WSAI)* (pp. 34-40). IEEE.

Damiron, C., & Krahl, D. (2014, December). A global approach for discrete rate simulation. In *Proceedings of the Winter Simulation Conference 2014* (pp. 2966-2977). IEEE.

De Vos, L., Bellemans, I., Vercruyssen, C., & Verbeken, K. (2019). Basic Oxygen Furnace: assessment of recent physicochemical models. *Metallurgical and Materials Transactions B*, *50*, 2647-2666.

Deb, K., & Gupta, H. (2005, March). Searching for robust Pareto-optimal solutions in multi-objective optimization. In *International conference on evolutionary multi-criterion optimization* (pp. 150-164). Berlin, Heidelberg: Springer Berlin Heidelberg.

Deb, K., Miettinen, K., & Chaudhuri, S. (2010). Toward an estimation of nadir objective vector using a hybrid of evolutionary and local search approaches. *IEEE Transactions on Evolutionary Computation*, *14*(6), 821-841.

Deb, K., Pratap, A., Agarwal, S., & Meyarivan, T. A. M. T. (2002). A fast and elitist multiobjective genetic algorithm: NSGA-II. *IEEE transactions on evolutionary computation*, *6*(2), 182-197.

Denysiuk, R. (2013). *Evolutionary multiobjective optimization: review, algorithms, and applications* (Doctoral dissertation, Universidade do Minho (Portugal)).

Dimitrakopoulos, R., & Ramazan, S. (2008). Stochastic integer programming for optimising long term production schedules of open pit mines: methods, application and value of stochastic solutions. *Mining Technology*, *117*(4), 155-160.

Dumont, M. (2008). Iron ore. *Canadian Minerals Yearbook*

Eduard, B., & Ming, W. (2010). Discrete event simulation: State of the art. *Discrete event simulations*.

Energy Information Admisitration (EIA). (2016). Industrial Sector Energy Consumption. https://www.eia.gov/outlooks/ieo/pdf/industrial.pdf

Eyring, A., Hoyt, N., Tenny, J., Domike, R., & Hovanski, Y. (2022). Analysis of a closed-loop digital twin using discrete event simulation. *The International Journal of Advanced Manufacturing Technology*, *123*(1), 245-258.

Fabian, T. (1967). Blast furnace production planning—a linear programming example. *Management Science*, *14*(2), B-1.

Geerdes, M., Chaigneau, R., & Lingiardi, O. (2020). *Modern blast furnace ironmaking: an introduction (2020)*. Ios Press.

Ghosh, A., & Chatterjee, A. (2008). *Iron making and steelmaking: theory and practice*. PHI Learning Pvt. Ltd..

Gkiotsalitis, K. (2023). Multi-objective optimization. In *Public Transport Optimization* (pp. 355-373). Cham: Springer International Publishing.

Gunantara, N. (2018). A review of multi-objective optimization: Methods and its applications. *Cogent Engineering*, *5*(1), 1502242.

Hašek, J., & Schenk, H. (1991). Distribution Fitting Methods. *Direct Methods of Solving Crystal Structures*, 401-402.

Huitu, K., Helle, H., Helle, M., Kekkonen, M., & Saxén, H. (2013). Optimization of steelmaking using fastmet direct reduced iron in the blast furnace. *ISIJ international*, *53*(12), 2038-2046.

Hwang, C. L., & Masud, A. S. M. (2012). *Multiple objective decision making—methods and applications: a state-of-the-art survey* (Vol. 164). Springer Science & Business Media.

Isnugroho, K., & Birawidha, D. C. (2018). The production of pig iron from crushing plant waste using hot blast cupola. *Alexandria Engineering Journal*, *57*(1), 427-433.

Ivanov, D., Dolgui, A., Das, A., & Sokolov, B. (2019). Digital supply chain twins: Managing the ripple effect, resilience, and disruption risks by data-driven optimization, simulation, and visibility. *Handbook of ripple effects in the supply chain*, 309-332.

Jaimes, A. L., Martınez, S. Z., & Coello, C. A. C. (2009). An introduction to multiobjective optimization techniques. *Optimization in Polymer Processing*, *1*, 29.

Jégourel, Y. (2020). The global iron ore market: From cyclical developments to potential structural changes. *The Extractive Industries and Society*, *7*(3), 1128-1134.

Jupp, K., Howard, T. J., & Everett, J. E. (2013). Role of pre-crusher stockpiling for grade control in iron ore mining. *Applied Earth Science*, *122*(4), 242-255.

Kalita, K., Ragavendran, U., Ramachandran, M., & Bhoi, A. K. (2019). Weighted sum multi-objective optimization of skew composite laminates. *Structural Engineering and Mechanics*, *69*(1), 21-31.

Khan, A., & Asad, M. W. A. (2020). A mathematical programming model for optimal cut-off grade policy in open pit mining operations with multiple processing streams. *International Journal of Mining, Reclamation and Environment*, *34*(3), 149-158.

Kumar, A., Agrawal, A., Kumar, A., & Kumar, S. (2023). Prediction of hot metal temperature in a blast furnace iron making process using multivariate data analysis and machine learning methodology. *Metallurgical Research & Technology*, *120*(6), 605.

Kusch, L. (2020). *Robustness Measures and Optimization Strategies for Multi-Objective Robust Design*. Technische Universität Kaiserslautern.

L'Ecuyer, P. (2012). *Random number generation* (pp. 35-71). Springer Berlin Heidelberg.

Lawson, B., & Leemis, L. (2008, December). Monte Carlo and discrete-event simulations in C and R. In *2008 Winter Simulation Conference* (pp. 11-16). IEEE.

Leal-Taixé, L. (2014). Multiple object tracking with context awareness. *arXiv preprint arXiv:1411.7935*.

Lecture 9: Multi-objective optimization. (n.d.). https://engineering.purdue.edu/~sudhoff/ee630/Lecture09.pdf

Li, H., & Zhao, L. (2023). Data-driven distributionally robust joint chance-constrained optimization for industrial utility systems under uncertainty. In *Computer aided chemical engineering* (Vol. 52, pp. 935-941). Elsevier.

Liu, C., Xie, Z., Sun, F., & Chen, L. (2016). Optimization for sintering proportioning based on energy value. *Applied Thermal Engineering, 103,* 1087-1094.

Lučić, P., & Teodorović, D. (2007). Metaheuristics approach to the aircrew rostering problem. *Annals of Operations Research, 155,* 311-338.

Lüngen, H. B., & Schmöle, P. (2022, May). History, development and processes of direct reduction of iron ores. In *Proceedings of the 8th European Coke and Ironmaking*

Congress and the 9th International Conference on Science and Technology of Ironmaking, Bremen, Germany (Vol. 29).

Madhavan, N., Brooks, G., Rhamdhani, M. A., & Bordignon, A. (2022). Contribution of CO2 Emissions from Basic Oxygen Steelmaking Process. *Metals*, *12*(5), 797.

Madias, J. (2024). Electric furnace steelmaking. In *Treatise on process metallurgy* (pp. 243-265). Elsevier.

Make, L., Bo, Z., Kuangdi, X. (2023). Ironmaking Blast Furnace. In: Xu, K. (eds) The ECPH Encyclopedia of Mining and Metallurgy. Springer, Singapore. https://doi.org/10.1007/978-981-19-0740-1_1035-1

Marglin, S. A. (1967). Public Investment Criteria, MIT Press.

Marler, R. T., & Arora, J. S. (2010). The weighted sum method for multi-objective optimization: new insights. *Structural and multidisciplinary optimization*, *41*, 853-862.

Matsumoto, M., & Nishimura, T. (1998). Mersenne twister: a 623-dimensionally equidistributed uniform pseudo-random number generator. *ACM Transactions on Modeling and Computer Simulation (TOMACS)*, *8*(1), 3-30.

Miettinen, K. (1999). *Nonlinear multiobjective optimization* (Vol. 12). Springer Science & Business Media.

Muwanguzi, A. J. B., Wy, Y., Karasev, A. V., Byaruhanga, J. K., & Jönsson, P. (2013). Investigation of direct reduction of lumps from natural hematite iron ore.

Navarra, A., Alvarez, M., Rojas, K., Menzies, A., Pax, R., & Waters, K. (2019). Concentrator operational modes in response to geological variation. *Minerals Engineering*, *134*, 356-364.

Navarra, A., Grammatikopoulos, T., & Waters, K. (2018). Incorporation of geometallurgical modelling into long-term production planning. *Minerals Engineering*, *120*, 118-126.

Navarra, A., Rafiei, A. A., & Waters, K. (2017). A systems approach to mineral processing based on mathematical programming. *Canadian Metallurgical Quarterly*, *56*(1), 35-44.

Nduagu, E. I., Yadav, D., Bhardwaj, N., Elango, S., Biswas, T., Banerjee, R., & Rajagopalan, S. (2022). Comparative life cycle assessment of natural gas and coal-based directly reduced iron (DRI) production: A case study for India. *Journal of Cleaner Production*, *347*, 131196.

Ng, L. Y., Chemmangattuvalappil, N. G., Dev, V. A., & Eden, M. R. (2016). Mathematical principles of chemical product design and strategies. In *Computer Aided Chemical Engineering* (Vol. 39, pp. 3-43). Elsevier.

Ocean Equities (2013). Iron Ore: The Labrador Trough. *London: Ocean Equities*, *18*(1).

Órdenes, J., Toro, N., Quelopana, A., & Navarra, A. (2022). Data-driven Dynamic simulations of gold extraction which incorporate head grade distribution statistics. *Metals*, *12*(8), 1372.

Pownceby, M. I., Hapugoda, S., Manuel, J., Webster, N. A., & MacRae, C. M. (2019). Characterisation of phosphorus and other impurities in goethite-rich iron ores–Possible P incorporation mechanisms. *Minerals Engineering*, *143*, 106022.

Pustejovska, P., Jursova, S., Brozova, S., & Sousek, J. (2013). Effect of waste and alternative fuels on blast-furnace operation. *Metallurgist*, *56*(11), 908-911.

Qian, Y., Li, Y., Hao, Y., Yu, T., & Hu, H. (2024). Greenhouse gas control in steel manufacturing: inventory, assurance, and strategic reduction review. *Carbon Research*, *3*(1), 27.

Qiu, T., Wu, C., Ai, G., Zhao, G., & Yu, X. (2015). Effects of multi-stage grinding process and grinding fineness on desulfurization separation of high-sulfurous iron ore. *Procedia engineering*, *102*, 722-730.

Ramakgala, C., & Danha, G. (2019). A review of ironmaking by direct reduction processes: quality requirements and sustainability. *Procedia Manufacturing*, *35*, 242-245.

Raychaudhuri, S. (2008, December). Introduction to monte carlo simulation. In *2008 Winter simulation conference* (pp. 91-100). IEEE.

Rogers, W. P., Kahraman, M. M., Drews, F. A., Powell, K., Haight, J. M., Wang, Y., ... & Sobalkar, M. (2019). Automation in the mining industry: Review of technology, systems, human factors, and political risk. *Mining, metallurgy & exploration*, *36*, 607-631.

Runciman, N., Vagenas, N., & Baiden, G. (1999). Evaluation of underground development mining systems using discrete-event simulation. *Simulation*, *72*(1), 4-11.

Salama, A., Greberg, J., & Schunnesson, H. (2014). The use of discrete event simulation for underground haulage mining equipment selection. *International Journal of Mining and Mineral Engineering*, *5*(3), 256-271.

Santelices, G., Pascual, R., Lüer-Villagra, A., Mac Cawley, A., & Galar, D. (2017). Integrating mining loading and hauling equipment selection and replacement decisions using stochastic linear programming. *International Journal of Mining, Reclamation and Environment*, *31*(1), 52-65.

Savolainen, J., & Urbani, M. (2021). Maintenance optimization for a multi-unit system with digital twin simulation: Example from the mining industry. *Journal of Intelligent Manufacturing*, *32*(7), 1953-1973.

Schiller, E. (2011). Canada’s Labrador & Newfoundland/Québec iron ore mines expand production. *Resource World Magazine*, 74-77.

Shen, Y. S., Yu, A. B., Austin, P. R., & Zulli, P. (2012). CFD study of in-furnace phenomena of pulverised coal injection in blast furnace: Effects of operating conditions. *Powder Technology*, *223*, 27-38.

Sohn, H. Y. (2019). Energy consumption and CO2 emissions in ironmaking and development of a novel flash technology. *Metals*, *10*(1), 54.

Tabesh, M., Azimi, E., & Askari-Nasab, H. Discrete Event Simulation of an Iron Ore Milling Process.

Teichert, K., Currie, G., Küfer, K. H., Miguel-Chumacero, E., Süss, P., Walczak, M., & Currie, S. (2019). Targeted multi-criteria optimisation in IMRT planning supplemented by knowledge based model creation. *Operations Research for Health Care*, *23*, 100185.

Valery, W., Duffy, K., & Jankovic, A. (2019). Mine to Mill optimization. SME mineral processing and extractive metallurgy handbook, 335-343.

Williams, R. V. (1983). *Control and analysis in iron and steelmaking*. Elsevier.

Wilson, R., Mercier, P. H., Patarachao, B., & Navarra, A. (2021). Partial least squares regression of oil sands processing variables within discrete event simulation digital twin. *Minerals*, *11*(7), 689.

Wilson, R., Toro, N., Naranjo, O., Emery, X., & Navarra, A. (2021). Integration of geostatistical modeling into discrete event simulation for development of tailings dam retreatment applications. *Minerals Engineering*, *164*, 106814.

Winstin, W., & Goldberg, J. (2004). The EOQ with uncertain demand: The (r, q) and (s, S) models. *Operations Research: Applications and Algorithms (Section 16.6); Cengage Learning: Boston, MA, USA*, 895-902.

Yang, Y., Raipala, K., & Holappa, L. (2014). Ironmaking. In *Treatise on Process Metallurgy* (Vol. 3, pp. 2-88). Elsevier Ltd. https://doi.org/10.1016/B978-0-08-096988-6.00017-1

Yellishetty, M., Ranjith, P. G., & Tharumarajah, A. (2010). Iron ore and steel production trends and material flows in the world: Is this really sustainable?. *Resources, conservation and recycling*, *54*(12), 1084-1094.

Yildirim, I. Z., & Prezzi, M. (2011). Chemical, mineralogical, and morphological properties of steel slag. *Advances in civil engineering*, *2011*.

Yongyi, Y., Hegui, D., Keng, W., Jianliang, Z., Kuangdi, X. (2023). Blast Furnace Ironmaking. In: Xu, K. (eds) The ECPH Encyclopedia of Mining and Metallurgy. Springer, Singapore. https://doi.org/10.1007/978-981-19-0740-1_1006-1

Yu, J., Sun, H., Li, P., Han, W., Li, Y., & Han, Y. (2023). A pilot study on recovery of iron from sulfur-bearing hematite ore using hydrogen-based mineral phase transformation followed by magnetic separation. *Journal of Environmental Chemical Engineering*, *11*(5), 110630.